MANIPULATING PHOTOSYNTHESIS FOR ENERGY CONVERSION IN AN ELECTROCHEMICAL CELL

by

JESSICA ONG CALKINS

(Under the Direction of Ramaraja Ramasamy)

ABSTRACT

With the constant strain on the environment by fossil fuels, finding an alternate source of renewable energy is vital. Among a myriad of renewable energy sources, solar stands out. As of today, solar energy panels operate at ~15 % conversion efficiency. Alternate means of harvesting energy from sunlight is critical for maximum utilization of this 'free' energy source. In plant photosynthesis, the quantum efficiency of light conversion is nearly 100 %.[1] Photosynthetic membranes inside plant cells use light energy to generate charge separation. The process can be manipulated to generate electrical power in an electrochemical cell. The process uses light and water to produce electricity. In this study, thylakoids extracted from spinach leaves were explored as photo-biological catalysts for light induced water oxidation reaction on an electrode surface. The extracted thylakoids were immobilized onto multi-walled carbon nanotubes (MWNTs) modified gold electrode using a molecular tethering agent[2]. The resulting thylakoid-MWNT composite electrodes were used as anode in a photo-electrochemical cell to study light driven electricity generation. The steady state current density generated by the system was 22 μA cm^{-2}. This is the first

attempt to demonstrate a direct light to electricity conversion in a photosynthetic electrochemical cell using plant thylakoids as photo-biological catalysts.

INDEX WORDS: photo-electrochemical cell, artificial photosynthesis, thylakoids, photosystem II, biological fuel cell.

MANIPULATING PHOTOSYNTHESIS FOR ENERGY CONVERSION IN AN ELECTROCHEMICAL CELL

by

JESSICA ONG CALKINS

BS, Georgia Institute of Technology, 2011

A Thesis Submitted to the Graduate Faculty of The University of Georgia in Partial Fulfillment of the Requirements for the Degree

MASTER OF SCIENCE

ATHENS, GEORGIA

2012

MANIPULATING PHOTOSYNTHESIS FOR ENERGY CONVERSION IN AN ELECTROCHEMICAL CELL

by

JESSICA ONG CALKINS

Major Professor:	Ramaraja P. Ramasamy
Committee:	William Kisaalita
	Mark Eiteman

Electronic Version Approved:

Maureen Grasso
Dean of the Graduate School
The University of Georgia
December 2012

DEDICATION

I lovingly dedicate this thesis to my parents, who supported me throughout my educational journey. Thank you Mom and Dad for your love and support which helped me to be where I am today.

ACKNOWLEDGEMENTS

I would like to first acknowledge God, for his love and support to allow me to work through the tough times, and laugh through the fun times. Secondly, I would like to acknowledge my Major Professor, Dr. Ramasamy, for his ideas and creativity to help me learn and accomplish this work. Lastly I would like to acknowledge the College of Engineering at the University of Georgia and its faculty, including my committee members Dr. Eiteman and Dr. Kisaalita. Although a newly established College, the people that make up this environment gave me support to try new things and explore possibilities that I could never imagine possible. Thank you.

TABLE OF CONTENTS

Page

LIST OF FIGURES

Page

CHAPTER 1

INTRODUCTION

The byproducts of fossil fuels have lead to multiple environmental problems including the green house effect, acidification, damage to the ozone layer, and increased air and water pollution [2]. Currently, 85% of the total fuel consumption is from fossil fuels, which are made up of coal, oil, and natural gas.

One amazing aspect of nature is the ability to convert light or solar energy into chemical energy via photosynthesis. This unmatched ability is the only process known on earth to form oxygen from water. There has been a great deal of research involving the use of photosynthetic materials in the implementation of an environmentally friendly source of energy. As of today, solar energy panels operate at ~15 % conversion efficiency. In photosynthesis, the quantum efficiency of the energy conversion is nearly 100 % [3]. Also, the only input for a photosynthetic energy source is water and sunlight while the only byproduct of the energy conversion is oxygen. This makes photosynthesis a more environmentally friendly source of energy conversion compared to fossil fuels.

Photosynthetic membranes use light energy to generate a charge separation that is ultimately converts light energy into chemical energy. When a photon of light reaches the special P680 chlorophyll *a* molecule (reaction center), resonance energy is produced. From this, a charge separation is generated that releases an electron and passes it to the plastoquinone molecules (Q_A and Q_B) and then to the cytochrome b_6f complex. Then the electron is used to reduce plastocyanin which is the immediate electron donor for Photosystem I (PSI). At

PSI, the electron is excited again to a higher energy state by a photon, and transferred to ferredoxin which in turn reduces ferredoxin-$NADP^+$ reductase which forms NADPH from $NADP^+$. Meanwhile, the oxygen evolving complex (OEC) divides water into an oxygen singlet, an electron and a proton. The proton is later used for a proton gradient to help drive the ATP synthase complex using a proton motive force. The electron, on the other hand is used to replace the initial electron that was split from the special P680 chlorophyll *a* molecule during the photon interaction.

The ability for the oxygen evolving complex in photosynthetic organelles to split water and generate a charge separation has led to multiple attempts to find a way to use photosynthetic materials as source of energy. This is due to the fact that photosynthetic materials can use water and solar energy to generate electrons, which in turn can be used to generate current. Numerous organelles of the photosynthetic thylakoid membrane have been investigated for photocurrent activity, including intact thylakoids, individual chlorophyll particles, photosystem II, photosystem I and the oxygen-evolving complex.[4-8]. Specific photosystems have been examined and tested to try to optimize photocurrent generation, the current that flows through a photosensitive device as a result of radiant power exposure. Photosystem I is an organelle that partners with multiple redox couples during the electron transfer process through its 700nm excited chlorophyll molecule. The electrons generated at the PSI are transferred to reduce ferrodoxin. Ferrodoxin, in its native environment, reduces the enzyme ferredoxin-$NADP^+$ reductase which in turn reduces $NADP^+$ to

NADPH, and hence its name. Fourmond et al. attempted to redirect this electron transfer chain to a hydrogenase for the production of hydrogen as the byproduct [9].

Protein density is a huge factor in to help enhance overall photocurrent generation per area. It has been found that a higher surface concentration as well as a facilitated electron transfer pathway to the electrode is necessary for high current generation [10]. Carbon nanotubes (CNT) greatly increase the surface area of a working electrode. Since a major factor that affects the photocurrent generation of photosynthetic particles is the density of immobilized organelles and the facilitated pathway of electron transfer, one solution is to use multi-walled carbon nanotubes (MWNTs) with 1-pyrenebutanoic acid, succinimidyl ester (PBSE) as a tethering reagent because it is found to have high bioelectrocatalytic activity and it increases the surface area of the electrode [11]. Carbon nanotubes (CNT) in combination with PBSE work by attaching proteins via a covalent amide bond and using π- π hydrophobic interactions between PBSE and the CNT aromatic wall.[3]

In this work, we studied the photo-electrochemical activity of spinach thylakoids immobilized on to multi-walled carbon nanotube (MWNT) modified electrodes. We also report the demonstration of direct light to energy conversion with water as the only input using a photosynthetic fuel cell composed of a thylakoid based anode and laccase based cathode.

CHAPTER 2

LITERATURE REVIEW

Plant photosynthesis has evolved over 2.5 billion years to convert solar (light) energy into chemical energy using only water, with an unmatched quantum efficiency of nearly 100 %.[12] In recent years, there has been an increasing interest in mimicking the natural photosynthetic process for energy conversion and photo fuel (ethanol, H_2 etc.) production. This is being done using metal oxides, semiconductors or synthetic chemical catalysts for carrying out the light-driven water splitting reaction.[5, 7, 13-16] Another approach to mimic photosynthesis is to directly extract and isolate natural photosynthetic pigments and use them as catalysts. This approach has been explored using both bacterial chlorophylls[17] and higher order plant pigments[18-21]. For example, the direct conversion of light into electricity based on photosynthesis in an electrochemical cell has been investigated in the past[22-25], using natural systems such as thylakoids, chlorophyll molecules, photosystems and oxygen evolving complexes[4, 8, 10, 26-29], or using whole cells as in the case of cyanobacterium[30]. Besides these sporadic attempts, major challenges remain that must be overcome in order to realize viable photosynthetic electrochemical power generation. The primary challenge is to achieve high photo-catalytic activity in immobilized photosynthetic catalysts. This is difficult because of the naturally low reactivity between the photosynthetic reaction centers and the electrode[5], which makes it harder to establish electrical communication between them. The second challenge is the difficulty in diverting the photo-generated electrons from their native electron transfer pathways

towards the electrode for photocurrent generation. This would require that the pathways be manipulated to use the electrode as the terminal electron acceptor. The third major challenge is to capture the electrons generated at the oxygen evolving complex (OEC), as early as possible in the photosynthetic linear electron transport pathway in order to operate at low anode potentials. For light energy harvesting applications, it is thermodynamically advantageous to collect electrons directly from the molecules at high-energy states along the photosynthetic electron transport pathway, such as an excited photosystem II (PSII).[10, 31] This can be accomplished by using isolated PSII complexes to catalyze the photo-induced water splitting reaction on the electrode, which may require that the PSII reaction centers be electrically wired to the nanomaterial modified electrode using cytochromes[3] or nickel-nitrilotriacetic acid[32] as cross-linkers. However these immobilization approaches limited to specific electrode material type (e.g. gold) and a direct electrical communication may not be always guaranteed. To overcome this limitation, quinone derivatives have been used as electron-transfer mediators to establish electrical communication in PSII-based electrodes in a recent work[33]. Nevertheless, due the low stability as well as very low electrochemical activity of isolated PSII, thus far it is not practical for PSII proteins to be considered useful for applications.

On the other hand, photosynthetic organelles possess many advantages over isolated reaction center complexes for electrochemical applications such as: high individual protein stability, require fairly simpler immobilization procedures and offer multiple electron transfer routes. For example, if thylakoid membranes

are used in the place of isolated PSII, the electron transfer from OEC to the electrode can be achieved via plastoquinone, cytochrome (cyt) b_6f or plastocyanin in addition to a direct transfer from PSII[3]. Moreover retention of their natural partners will result in enhanced stability of the individual proteins in thylakoids in comparison to their isolated counterparts[34]. Therefore using thylakoids as photo-biocatalysts offer the potential for high photo-electrochemical activity as well as high stability for both energy conversion and fuel production applications.

2.1 Photosynthesis

Photosynthesis converts atmospheric carbon dioxide and water into carbohydrates via light energy. Wide ranges of organisms possess phototrophic behavior including cyanobacteria – blue green algae, certain bacteria, and both nonvascular and vascular plants. Photosynthesis, in most species, occurs along the thylakoid membrane of chloroplast organelles. The chloroplasts are bound by a highly permeable outer membrane and a nearly non-permeable inner membrane. Inside the inner membrane is the stroma which consists of the enzymes needed to convert CO_2 to carbohydrates. Enclosed in the stroma is an extensive network of more membranes that make up the thylakoid membrane. These photosynthetic membranes use light energy to generate a charge separation that is converted into chemical energy.

2.2 Linear Electron Transport

During the light reactions, a photon of light excites the special P680 chlorophyll a molecule (Light Harvesting Reaction Center II) and resonance

energy is produced. From this, a charge separation is generated and an electron is released and passed to plastoquinone (PQ) molecules (first Q_A and then Q_B) followed by the cytochrome b_6/cytochrome f complex (cyt b_6f). Then the electron is used to reduce plastocyanin, which is the immediate electron donor for Photosystem I (PSI). The electron is excited again by a photon at the P700 chlorophyll a molecule to a higher energy state, and then transferred to ferredoxin (FD), which in turn reduces ferredoxin-$NADP^+$ reductase. This enzyme is used to reduce $NADP^+$ to NADPH, which is used later in the dark reactions to form carbohydrates from CO_2. Meanwhile, the oxygen-evolving complex (OEC) located at the PSII complex divides water into an oxygen singlet, an electron, and a proton. The proton is pumped into the lumen side of the membrane to form a proton gradient to help drive the ATP synthase complex using a proton motive force. The electron, on the other hand is used to replace the initial electron that was split from the special P680 chlorophyll a dimer during the first photon interaction.

PSII is the site of both electron excitation via photons and water oxidation. It is the only natural system known to split water at nearly 100% efficiency. Taking a deeper look into this extraordinary complex, we see the system is composed of multiple chlorophylls and carotenoids. PSII in higher order plants contain the PSII complex as well as peripheral light-harvesting complexes, unlike cyanobacteria which only contain the core complex. PSII is homo-dimeric and the membrane-intrinsic section in cyanobacteria contains CP47 and CP43 antenna proteins, which bind to chlorophyll a 13 and 16 respectively. The

antenna proteins help funnel excited electrons to the reaction center subunits D1 and D2 where charge separation occurs. This causes an oxidation of P_{680}. PSII has been shown to contain 36 transmembrane helices, 35 chlorophyll a, 12 β-carotene, 2 pheophytin a, $cytb_{559}$ and $cytc_{550}$ hemes, two plastoquinones, 25 integral lipids and the Mn_4Ca-cluster from a crystallized structure of PSII from *Thermosynechococcus elongates* analyzed up to 2.9Å. [35]

The reaction center of PSII from higher order plants and purple bacteria are very similar with the only discrepancy being at the luminal dimer of chl_a molecules or the special pair. In purple bacteria the special pair forms an eclipse conformation around the pyrrole rings, however in plants the special pair is staggered and forms a slight tilt.[36] This results in very different optical properties, with the absorbance spectrum of the purple bacteria special pair having discrete separate bands [37] and the spectrum of the plant special pair having a congested overlapping display. [38, 39] The difference indicates that the plant special pair has a weaker excitonic coupling than that of purple bacteria. [40, 41]

2.3 Alternative Electron Transport Pathways

In nature, phototrophic organisms have ways of altering the common route of electron transport in the light reactions. One perfect example that is well understood is the cyclic electron flow pathway. This process is used to increase the pH gradient across the thylakoid membrane to help drive the proton motive force. During the linear electron transport pathway, for every four electrons transported, two $NADP^+$ molecules are reduced to two NADPH. Simultaneously, two molecules of ATP are generated during photophosphorylation. During the

following dark reactions, two molecules of NADPH and three molecules of ATP are needed to reduce one molecule of CO_2 to CH_2O. This results in a higher demand for ATP molecules. The cyclic electron transport pathway is used in this case to redirect electrons from FD back to cyt b_6f through the PQ pool where it can direct back to PSI. This process allows hydrogen to be transported into the lumen side of the membrane during the reduction of PQH_2, increasing the proton gradient. The complete pathway of the cyclic electron flow is believed to be facilitated by ferredoxin-plastoquinone reductase[42], however it is still unclear. Recent studies show that two proteins, PGR5 (Proton Gradient Regulation 5) and an integral protein PGRL1, are involved with the transfer of electrons from FD to PQ in *Arabidopsis Chlamydomonas reinhardtii*. [43]

FD does not only transfer electrons in either the linear or cyclic pathways, recent studies suggest that FD can transfer electrons to at least six other enzymes to facilitate with enzyme regulation and other biosynthetic pathways. The deviation from the normal route along the electron transport pathway is usually induced by a change in the surrounding environment of the enzyme. The major isoform of FD in C. reinhardtii, PetF, has been shown to transfer electrons to various enzymes including sulfite reductase [44], glutamate synthase [45] and fatty acid desaturases. [46] Other isoforms of FD are encoded as new electron acceptors from PSI to work as redox enzymes for other pathways under certain extreme environmental conditions. The isoform FDX5 gene in *Chlamydomonas* cells increased expression under anaerobic or hypoxia conditions. [47, 48] The

isoform Fd2 is suggested to be mainly involved with the linear electron flow and Fd1 helps regulate the photosynthetic electron transfer chain. [49]

2.4 Herbicides and Inhibitors

Herbicides are chemical compounds used to kill or prevent growth of certain higher order plants. One of the ways a herbicide works is by blocking the proteins functions in the electron transport chain through an inhibitory function. An example is the PSII herbicide, triazine. In PSII, the QA and QB plastoquinones are attached to specialized sites on the D2 and D1 proteins respectively. The D1 and QB proteins are linked by two hydrogen bonds (serine 264 and histidine 215). After QB accepts the two electrons from QA, the protein detaches from the D1 protein to continue the electron transport chain. From there, an oxidized QB will attach to the vacant site of D1. The triazine herbicide, however, has a higher binding affinity to the D1 site and therefore will block the site from QB.[50] Triazine is unable to be reduced which results in an inability for the chlorophyll molecule to dissipate its excited energy forming a triplet chlorophyll molecule. The triplet chlorophyll reacts with oxygen to form oxygen singlets which results in lipid peroxidation. [51]

Another herbicide technique is to implant a molecule that works as a competitive electron acceptor. In the case of the PSI inhibitor bipyridillum (paraquat), paraquat acts as a competitor to FD for the electron flow from the PSI F_a/F_b protein. F_a/F_b has a redox potential of -560 mV so it can easily pass electrons to FD at a redox potential of approximately -510 mV. Paraquat has a redox potential of -446 mv so it becomes more favorable for electron transfer.

The reduced for of paraquat is very reactive and will reduce oxygen to superoxide to regenerate the paraquat oxidized form. [51]

3-(3,4-Dichlorophenyl)-1,1-Dimethylurea (DCMU) is a herbicide that is known to block the electron transport pathway in photosynthesis. It has been reported to inhibit linear electron transfer at as low as 1Um. [52] DCMU blocks the Q_B binding site; therefore it competes with Q_B to bind and accept electrons. DCMU cannot be reduced, so electrons are unable to leave Q_A, the prerequisite quinone electron acceptor.

KCN has shown to inhibit electron transport from diaminodurene to methylvoilogen and phosphorylation. It also inihibits cyclic photophosphorylation, which can be restored with PMS. High concentrations of KCN (> 10mM) at high pH values (>7.5) is believed to inhibit the copper palstocyanin protein during linear photosynthesis.[53]

2,5-dibromo-3-methyl-6-isopropylbenzoquinone (DBMIB) has been shown to occupy the Q_o site of the cyt b_6f complex. Two molecules from the inhibitor can bind to each monomer of the spinach cyt b_6f complex in both isolated and intact thylakoid membranes.[54] With the use of electron paramagnetic resonance spectra, the orientation of the cyt b_6f Rieske iron-sulfur protein has distinct orientation depending on the stochiometry of the inhibitor.[55] This suggests that DBMIB alters the Rieske iron-sulfur protein to stop electron flow.

2.5 Redox-Active Compounds

Recent studies have shown the ability to redirect electrons from Q_A^- in PSII of cyanobactera to engineered collection sites approximately 13Å away on

the stromal side of the membrane.[56] This redirection along with the addition of an herbicide to block Q_B resulted in reduced oxidative damage due to a decrease in Q_A/Q_B intermediate transfer time. Recently, cationic redox-active metal complexes were use to redirect electrons from Q_A^- at a 9Å distance from the site. [57] The authors used Co^{III} complexes small enough to fit in a 5Å diameter negatively charged patch along the stromal side of the membrane. The complexs needed a well poised E^o for efficient ET from Q_A^-; the redox potential for herbicide-bound PSII is approximately -90 mV vs. NHE. [58, 59]

2.6 Mediators

Mediators are used to help facilitate electron transfer from the source to the electrode surface. Electron transfer to an electrode is difficult attributable to many redox-sites being buried within the organelle or due to irreversible redox behavior due to slow heterogeneous electron transfer. [60] Ideal mediators should exhibit well-defined electron stoichiometry, have a known $E^{o'}$, quick heterogeneous and homogeneous electron transfer, be soluble in aqueous media near a pH of 7, stable in both oxidized and reduced forms and have no interaction with the biological part of interest.[61] Also, the formal potential of the mediator should be close to the biological organism of study. [62]

Mediators have a slightly lower redox potential then the electron source, which is needed to help drive the reduction of the compound. Mediators are usually small enough to fit in the binding pockets of the biological components to collect excited electrons. The mediator will compete with normal electron transport pathways for the excited electrons. Once reduced, mediators redirect

the electron route to an electrode surface. In electrochemical cells, mediators are normally applied to the electrolyte of the system and commonly cause a dramatic increase in current. The increased current is the result of more electrons making it to the electrode surface. In non-mediated bioelectrical systems, it is very difficult for electrons to transfer from the biological electron source to the electrode surface due to the electron transfer sites being buried within the protein or enzyme and having very site specific donors, which is the case for the PSII electron donor site which is most likely Chl_{D1}. [63]

2.7 Fuel Cells

Fuel cells are devices that have the ability to convert chemical energy from a fuel supply into electrical energy via a chemical reaction with an oxidizing agent. Some examples of energy carriers include hydrogen, methanol, and ethanol. All of these fuels are CO_2 neutral and can be produced by solar energy; therefore they are environmentally friendly. The term biofuel is used when the fuel is derived from biological means. This includes biomass conversion, solid biomass, liquid fuels and biogases. Well known biofuels are bioethanol, an alcohol produced during fermentation of carbohydrates from sugar or starch from crops, and biodiesel which is derived from trans-esterification of vegetable oils and animal fats. Both forms of energy can be used to fuel vehicles however they are mainly used as additives.

2.8 Hydrogen Fuel Cells

Hydrogen is considered one of the most promising future energy sources due to the fact that it results in no harmful emissions. [64] A hydrogen fuel cell is

composed of two electrodes, an anode and a cathode, near bipolar plates on both sides of the cell. Hydrogen gas is pumped into the cell and a catalyst is used to split the hydrogen gas into a proton and an electron, similar to the photosynthetic method of splitting water molecules into oxygen gas, protons and electrons. A proton conducting membrane in the hydrogen fuel cell only allows the protons to pass through and the electrons are forced to travel though an external circuit that is connected to the cathode. This flow of electrons in the external circuit is captured as electricity. The protons are released on the other side of the membrane where they are reunited with the electrons and oxygen to form water at the cathode. Therefore water is the only byproduct of a hydrogen fuel cell. [65]

2.9 Hydrogenase and Nitrogenase

A hydrogenase is an enzyme or redox-active metalloprotein that catalyses hydrogen oxidation. They are key enzymes that catalyze the following reversible reaction ($2H + 2e^- \leftrightarrow H_2$). The direction of the reaction depends on the electrochemical potential of the components reacting with the hydrogenase, and they play a vital role in microbial metabolism. [66] Another source of renewable hydrogen in nature is through nitrogenases. Nitrogenases fix atmospheric nitrogen through an ATP-dependent process which results in hydrogen as a byproduct.

Hydrogenase enzymes are found in both anaerobic and aerobic environments, however the majority exists in anaerobic conditions with two main functions, to capture electrons to prevent over-reduction of the electron transport

chain and to provide alternative electron sources to aid in survival under non-ideal conditions.

There are three major types of hydrogenases, [Fe-only]-type, [NiFe]-type and Fe-S-cluster-free hydrogenase. [67] The [Fe-only]-type is known to have the simplest design and the highest activity level, recorded up to 2000 H_2 s^{-1}.[68, 69] However, these hydrogenases are extremely sensitive to oxygen. [5] The metallo-cluster of the hydrogenase is suggested to be the source of oxygen sensitivity and it is believed that oxygen binds to the open coordination site on the distal Fe which prevents protons from binding.[70] The [Fe-only] type includes green algae, strict anaerobes, fungi, and protists. Most hydrogenases in this category are monomeric with up to four subunits and have similar sequencing with three main motifs, L1, L2 and L3.[70, 71]) However, recently a clone of a putative hydrogenase from *Enterobacter cloacae* lacking motif L1 was cloned in *Escherichia coli* was able to successfully produce H_2.[70, 72]

Green algae have been used to produce hydrogen in two distinct light-driven pathways with ferredoxin as the primary electron-donor to hydrogenase. [70] The most common pathway is to use water as the substrate which employs both photosystems and the second pathway involves the use of NADH from the glycolytic breakdown of carbohydrates where only PSI is implicated. Another less understood pathway is through the dark fermentative pathway that is believed to involve a pyruvate-ferredoxin-oxidoreductase (PFOR) enzyme. It is suggested that PFOR provides a link between fermentative carbon dissimilation and H_2 production. [73]

2.10 Ethanol and Methanol Production

Ethanol is already being used as a gasoline additive in fuel markets today. Ethanol provides a renewable energy resource to help meet growing demands for this liquid energy. Ethanol mainly comes from corn and other starch-based crops. However, this poses a threat to the rise in grain and food prices as ethanol demands skyrocket. Because of this, the Department of Energy (DOE) is concentrating their efforts on alternative ethanol sources including woody plants, forest and agriculture residue and both municipal solid waste and industrial waste streams. The process of biomass collection and transportation to refineries are very expensive. The conversion of sugar to biofuel via expensive cellulose enzymes also makes ethanol production pricey. Therefore photosynthesis could be used to convert CO_2 into simple carbon fuels like formic acid and methanol which can be refined further into ethanol. This would create a more efficient energy conversion pathway that was also environmentally friendly by reducing CO_2 emissions. During the dark reactions of photosynthesis, CO_2 is taken up from the atmosphere to form higher energy products. This allows the plant to store energy in the form of chemical energy like sugars. During respiration, the chemical energy is released to do useful work. The idea of mimicking CO_2 conversion in plants to useful fuels will help reduce atmospheric CO_2, one of the major green house gases, as well as produce usable fuels.

In order to mimic CO_2 reduction in plants, catalysts are needed. Ideally, catalysts should have high energy efficiency and high turnover rates or current densities. [74] Dubois et al.[75] used a $[Pd(triphosphine)(solvent)]^{2+}$ platform based

electrocatalyst for CO_2 reduction to CO. Rosen et al.[74] developed a flow cell using a platinum anode in a compartment containing 100 mM aqueous sulfuric acid flowing at 0.5 ml min^{-1} and a silver cathode in a compartment containing 18 mol % EMIM-BF_4 in water again at a 0.5ml min^{-1} flow rate. The addition of ionic liquid between the cambers allowed a very low overpotential requirement of 0.17 V for CO formation. Due to poisoning of the platinum anode from CO produced on the cathode, a Nafion 117 membrane was placed between the anode and cathode to isolate the anode form the ionic liquid. [76]

2.11 Combining Photosynthesis and Hydrogenase

There are three components that are essential for a solar powered-hydrogen generator. According to Krassen et al.[64] the components are (1) a light sensitizer which is used to absorb photons to produce excited electrons through a charge separation. This drives a reductive force for the production of H_2. The electron source could be from other catalytic centers, from a sacrificial donor, or from an electrode. (2) A catalyst is needed to use the reductive force to produce molecular hydrogen and (3) a wire to allow electron transfer between the sensitizer and the catalyst. An example of sensitizers and catalysts would be photosystems and hydrogenases respectively.

Hydrogenase or nitrogenase enzymes have been suggested as good candidates to form hydrogen-producing devices via water oxidation. [77-81] This process would involve a full cell application with photosynthetic systems on the anode, or oxidizing side, and hydrogenase on the cathode, reducing side. A major obstacle for sustainable photosynthetic hydrogen producing systems is the

susceptible nature of hydrogen with oxygen gas. Oxygen irreversibly inactivates hydrogen producing systems which results in oxygen-dependent activity that consumes hydrogen.[81-83]

2.12 Recent Studies with Photosynthesis and Hydrogenase

Just recently, a study developed a photo-bioreactor to demonstrate the relationship between dinitrogenase-driven H_2 production and oxygenic photosynthesis in unicellular cyanobacterium *Cyanothece*. Under continuous illumination and a nitrogen-deprived environment, cells evolved H_2 at rates up to 400 µmol mg Chl^{-1} cm^{-1}. Simultaneously, photosynthetic O_2 evolution occurred without detrimental effects. Production of H_2 and O_2 was stable for over 100 h in the presence of CO_2. Stable rates reached 125 and 90 µmol mg Chl^{-1} cm^{-1} for H_2 and O_2 respectively. [84]

Other catalyst can also be used to generate hydrogen. Grimme et al. composed bioconjugates of rebuilt PSI containing the PsaC glycine variant with 1,6-hexanedithiol molecular wires. Pt 3 nm nanoparticles were used as the catalyst for hydrogen production and the system was assembled with sodium ascorbate as an electron donor to dicholorophenyl-indophenol, which donates to $P700^+$. The molecular wires served as both a covalent link between PSI and the nanoparticle and as a conduit for electron transfer. This system, upon illumination, generated hydrogen at a rate of 9.6 µmol H_2 mg Chl^{-1} h^{-1} for over 24 hours. Upon addition of cytochrome C_6, the system generated hydrogen at a rate of 49.3 µmol H_2 mg Chl^{-1} h^{-1}. [85]

Figure 2.1 depicts the combination of photosystem II of the photosynthetic pathway with [FeFe] hydrogenase for hydrogen production.

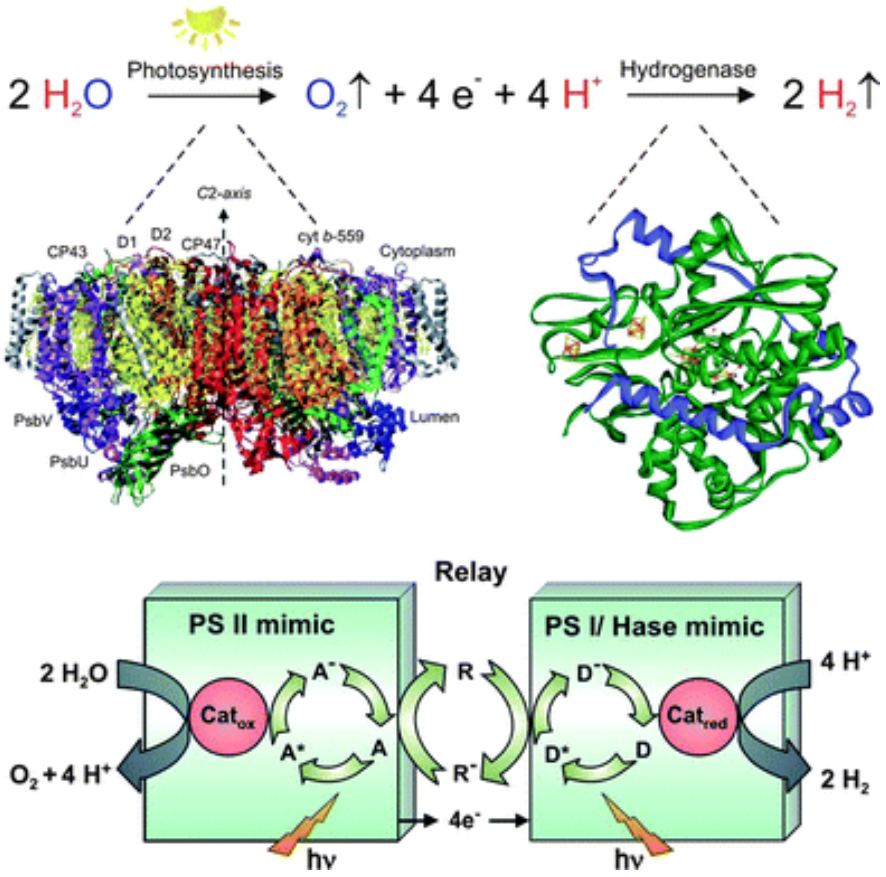

Figure 2.1. Hydrogen Production Pathway: Possible hydrogen production pathway via coupling of PSII and hydrogenase.[1] (Figure adopted from reference 53).

2.13 Photovoltaic Cells

Photovoltaic cells exhibit the ability to generate electrical energy from solar energy. This is accomplished by the photovoltaic effect, which occurs when a photon of light excites electrons from the valence band to higher energy states, the conduction band. At the excited state, electrons can move freely between atoms and these captured electrons work as charge carriers or excitons along an electric field. Usually a semiconductor, like crystalline silicon and cadmium

telluride, is treated to contain an electric field. When the photon releases the electron, exciton dissociation occurs and a free excited electron and a hole are produced. The electron is captured by a metal electrode at the negative contact and drawn to the positive end of the electric field and the movement of electrons produces electricity.

2.14 Silicon-based

Silicon-based photovoltaic cells are the most common of this type. Currently, the efficiency of silicon-based photovoltaic cells is in the range of 15-20%. Energy efficiencies have been shown as high as 47.7% with carrier multiplication absorbers used in both top and bottom cells.[86] Downsides of these conventional solar panels include the fragile nature of the material, the difficult development process and the large amount of energy needed for production.

2.15 Polymer-based

Polymer-based solar cells are a relatively new field of study. Advantages of using polymers instead of silicon include low cost of fabrication, mechanical flexibility and ease of processing. Unfortunately, polymer-based solar cells have very low efficiency rates. As of 2005, the most efficient reported polymer-based solar cell was composed of bulk heterojunctions of the polymer poly(3-hexylthiophene) and methanofullerene with a 4.4% efficiency. The polymer-based cell had increased absorption throughout the active layer and increased hole mobility. [87] In 2010, a tandem cell polymer reached conversion efficiencies of 5.84%. The interlayer of this device consisted of a n-type nanocrystalline TiO_2 layer and a p-type conducing polymer layer. The interlayer acts as a

metal/semiconductor contact instead of a tunnel junction which is seen in most inorganic tandem cells. [88] Just recently, a polymer photovoltaic cell using $SiO_2/WO_3/Ag/WO_3$ deposited on glass substrates achieved up to 6.05% conversion efficiency. [89] This was the highest efficiency seen for polymer based cells from this literature review.

2.16 Photosynthetic-based

Another new and rapidly developing field of research is photosynthetic photovoltaic cells. In these devices, energy from the sun is directly converted into electrical power via the natural charge separation in photosystems. This differs from fuel cells because photovoltaic cells capture excited electrons that can be used directly for current generation. In photosynthetic fuel cells, the energy captured is instead used to help reduce protons into hydrogen gas which is later used in a hydrogen-based fuel cell.

2.17 Photosynthetic Half-Cell Photovoltaics

The ability for the oxygen evolving complex in photosynthetic organelles to split water and generate a charge separation has led to multiple attempts to find a way to use photosynthetic material as a source of energy. This is due to the fact that photosynthetic materials can use water and solar energy to produce an electron transfer, which in turn can be used to generate current in an environment friendly fashion. Numerous organelles of the photosynthesis process have been purified and immobilized to discover an ideal mechanism for the collection of energy.

2.18 Stability

One of the major issues with using isolated proteins is there instability. Photoinhibition is the inhibition of photosynthesis caused by excessive radiance that may damage the photosynthetic apparatus which leads to destruction of the photosynthesizing pigments. [90] Photosystems are provided with a number of self-repair enzymes to help reduce the harmful effects of photoinhibition. Once the proteins are isolated, usually the self-repair organelles are no longer present. Therefore the systems are more susceptible to damage and short life expectancies. A major step in utilizing photosynthetic energy devices is determining a stability mechanism that is economical and effective.

One technique to stabilizing photosynthetic complexes is to mimic the native state. Peptide surfactants have been used to help stabilize photosynthetic complexes by simulating a lipid bilayer. The surfactants consist of amino acids with a hydrophilic head (example: aspartic acid or lysine) and a hydrophobic tail (example: consecutive alanines). Surfactants are a common designed molecular nanomaterial for membrane protein studies. [91, 92] Das et al. [8] used A_6K (AAAAAAK) and V_6D (VVVVVVD) as cationic and anionic peptide surfactants respectively to stabilize photosynthetic complexes during fabrication of a soild-state electronic device. The authors were able to product a short circuit current density of 0.12 Ma cm^{-2} under an excitation intensity of 10 W cm^{-2} at 808 nm.

Recently a very stable system using PSI from thermophilic bacterium and cytochrome-C_6 was used to generate hydrogen *in vitro* upon illumination. The system was stable for >85 days with no decrease in hydrogen production as

tested and a maximum yield of ~5.5 μmol H_2 h^{-1} mg^{-1} chl which is approximately 25-fold greater than current biomass based fuel production.[16]

2.19 Optimization

One technique that is commonly used to optimize photosynthetic sensitizers is to increase the surface area of the electrode. Usually the geometric area of the electrode is the area of the flat surface. This cannot be changed based on the electrode; however the electrode can be modified to increase the real surface area, which includes the topographical surface area built over the flat geometric surface area. This will allow more reaction centers per area of space. These approaches have included the use of gold nano particles (GNP) [32, 33, 93], nonoporous gold electrodes[94], carbon nanotubes[11, 95] and redox active hydrogels[10].

Another way to optimize energy collection from photosynthetic sensitizers is to create a system that allows for direct electron transfer from the organism to the electrode surface, or transfer without a mediator. As mentioned earlier, mediators have a lower redox potential then that of the electron source, which is needed for favorable electron transfer. From there, the electrode surface must have a lower redox potential to facilitate electron transfer from the mediator to the electrode where it can be used for energy generation. During the transfer process, the electron loses some of its excitonic energy. Removing the intermediate step of a mediator will allow an increase in the electrode potential which will permit the system to collected electrons at higher energy states. The critical issues in the direct electron transfer between a protein redox center and

the electrode are: low active site loading (geometric area basis) and insufficient electrical communication between the protein redox center and the electrode. The former is due to the large size of the protein compared to metallic catalyst centers, and the latter is due to the electrical insulation of the protein redox center by the surrounding amino acids[96]. Also, the distance of the catalyzing agent and the electrode must be decreased in order to establish electron transfer. This allows a decrease in the mass diffusion limitation. Figure 2.2 depicts mass transport limitations due to mediated systems. The disadvantage of direct electron transfer, however, is the difficulty in establishing undeviating contact with the electrode and the electron source site. If this is the case, another option for optimization would be to use mediators at higher redox potentials. Ideally the redox potential should only be slightly lower than the redox potential of the biological electrons source. Furukawa et al. [97] developed a photosynthetic/metabolic biofuel cell using polyaniline as an electro-catalysis instead of a mediated system. Polyaniline exhibits both electroconductive and biocompatible characteristics. The Polyaniline also enhanced the surface area with its nano-strucutre. From this, the authors obtained a peak current density of approximately 150μA cm^{-2} with a 100Ω load and a power density of 5.3μW cm^{-2}. Badura et al.[10] used osmium enclosed redox polymers from poly(vinyl)imidazol as a electrode modification that served as both an immobilization technique and a mediator. The authors immobilized PSII and were able to generate a current density of 45μA cm^{-2} at a light intensity of 2.65 mW cm^{-2}.

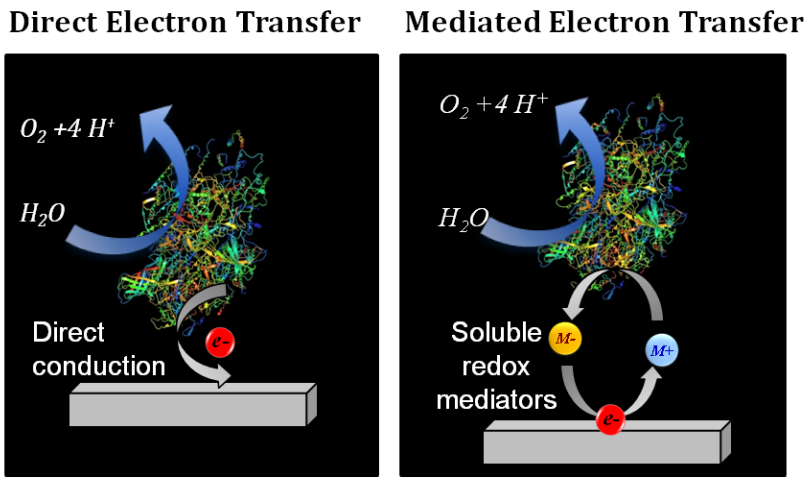

Figure 2.2. Direct vs. Mediated Electron Transfer: Direct electron transfer allows electrons to travel from biocatalyst to the electrode directly; mediated systems require an intermediate step to transfer electrons from biocatalyst to electrode.

A third way to optimize photosynthetic energy conversion in an electrochemical cell is the orientation of the photosynthetic organelles. Multiple studies indicate that orienting photosystems with the donor side facing the electrode results in facilitated electron transfer. [32, 98-100] This assembly is usually accomplished via nickel-nitrilotriacetic acid (Ni-NTA) chelators, which bind at site specific histidine 6-tagged proteins.

2.20 Immobilization

Most bio-electrochemical cells require enzymes or redox proteins to be immobilized on the electrode surface. Multiple techniques have been employed to immobilize photosynthetic complexes. Bioelectrocatalytic self-assembled monolayers (bio-SAMs)[7], mercapto benzoquinone via electropolymerization[33], Ni-NTA with histidine-tagged photosystems[31, 101, 102], redox hydrogels[10], 1-pyrenebutanoic acid succinimidyl ester (PBSE) on carbon nanotubes[11, 95], and the spontaneous growth of biofilms on electrode surfaces[103] have all been used

as successful immobilization techniques. Each technique provides different beneficial characteristics, including increasing surface area of the electrode, enhancing the electron transfer process, or/and allowing particular protein orientation.

Unfortunately on average, immobilization leads to slightly less protein activity compared to native proteins. Therefore the proper immobilization technique needs to first conserve protein activity for long stable energy conversion. One technique previously, entrapped thylakoids in a silica network which enhanced protein stability over native thylakoids in suspension, the organelles remained active for up to 30 days.[34] In addition the immobilization technique should allow facilitated electron transfer from the protein to the electrode, with minimum resistance and interference; this could be employed by redox mediators, protein orientation and protein relativity to the electrode surface. Lastly, the technique should allow electron transfer at high energy states, therefore the potential of the electrode surface should correspond accordingly with the potential of the donor electron of the protein.

CHAPTER 3

PHOTOSYNTHETIC ENERGY CONVERSION

3.1 Energy from Thylakoid Membranes

Thylakoids are membrane bound organelles that consist of the photosynthetic integral proteins and the redox mediated enzymes. They make up the grana found within the chloroplast and they are also present in cyanobacteria. The inner area bound by the thylakoid is called the lumen and it plays an important role during photophosphorylation. During the light reactions, the lumen becomes very acidic, close to pH 4, in order to drive the proton motive force to generate ATP via ATP synthase. The advantage of using full thylakoids for photo-electrochemical applications is that the thylakoids retain the native enzymes and biomolecular complexes allowing for enhanced stability and facilitated electron transfer.

3.2 Recent Studies

In order to generate usable energy from phototrophic organisms, the electrons from the electron transport pathway must be redirected into an energy storage device. Carpentier et al. [104] used thylakoid membranes isolated from spinach leaves as a photo-biocatalyst in a photoelectrochemical cell where electrons were diverted to reducing a platinum electrode; the native thylakoid membranes were studied under light and dark duty cycles with and without the presence of potassium ferricyanide as a mediator. Native thylakoids produced photocurrents as high as 6 to 9 mA without a mediator and up to 4 folds higher

current with the presence of potassium ferricyanide. The authors [104] conclude that photocurrent generation without mediator is attributed to either direct electron transfer from the thylakoid integral proteins to the electrode surface or to impurities present in the electrolyte that can act as a mediator. One example would be oxygen, which is known to accept electrons from PSI [105] to form a superoxide radical, which later creates hydrogen peroxide. Hydrogen peroxide has been shown to react with platinum electrodes. [106] The authors [104] also immobilized the thylakoid membranes onto the electrode surface with an albumin-glutaraldehyde crosslinked matrix and found that 40% of the apparent photosynthetic activity was lost after immobilization; however stability of the cell increased.

Trammell et al. [100] worked on focusing in on the direct electron transfer site of photosynthetic reaction centers by orienting the primary donor side of the proteins towards the electrode surface. Genetically modified reaction centers with polyhistidine tags at the C-terminal end of the M-subunit from Rhodobactor sphaeroides was immobilized on gold electrodes modified with Ni(II) nitrillotriacetic acid alkanethiol.[107] The immobilization process caused the primary electron donor site (special pair P) to be orientated toward the electrode surface[100, 108]. The authors used various sized linkers to determine the dependence of ET upon distance. They concluded that the distance dependence factor of electron tunneling from the immobilized reaction centers to the electrode surface to be 0.8 per methylene unit, indicating that close proximity of the electron source to the electrode surface is vital for photovoltaic cells. After

characterizing the electrode using techniques such as atomic force microscopy (AMF) and electrochemical calculations including fitting a Marcus' model integrated over the density of electronic states of the gold electrode, the results indicated that the orientation of the reaction centers change depending on the length of the linker chain, which direct impacts protein mobility. [99]

Bedford et al.[109] used electrospinning to immobilize thylakoids on conductive nanofibers consisting of poly(3,4-ethylenedioxythiophene)/ poly-(styrene sufonate) and poly(ethylene oxide) to encapsulate thylakoids from spinach. White light produced a power density of ~13 mW cm^{-2} while red (λ=625nm), green (λ=520nm), and purple (λ=470nm) produced power densities of ~24, ~7 and ~14 mW cm^{-2} respectively. Light-induced pH measurements were used to determine that the thylakoid vesicles could still produce proton gradients across the membrane after immobilization.

3.3 Energy from Photosystem I

In addition to whole thylakoid membranes, specific photosystems have been examined and tested to try to optimize the efficiency of photocurrent collection. The advantages of using photosystems include: less interference of redox enzymes and proteins from the electron donor site which reduces electron transfer competition, closer orientation of the donor site to the electrode to help establish direct electron transfer, and a better understanding of the necessary potential gap due to only one electron transfer pathway.

Photosystem I is an interesting organelle that partners with multiple redox couples during the electron transfer process from its 700nm reaction chlorophyll

molecule. In 2007, a multi-enzyme electron-transfer chain was developed with PSI as the photocatalytic unit. Cytochrome C_6 and ferredoxin were used as electron carriers and ferredoxin-NADPH reductase as the electron acceptor to demonstrate an efficient recycling system for NADPH. [9]

3.4 Recent Studies

PSI has also been immobilized on a gold nanoparticle (GNP) modified electrode and used for photocurrent generation. One study [93] fabricated an electrode by sedimenting GNP on the gold substrate followed by modification with 3-mercapto-1-propanesulfonic acid via gold–sulfur self-assembling. Finally the electrode was modified with PSI by electrostatic adsorption and the photocurrent density reached 290Na cm^{-2} on a planar electrode surface. An electrochemical cell modified with nanoporous gold leafs and PSI resulted increased real surface area due to enlarged pores via dealloying allowed an increase by 5-12-fold. This caused an enhancement of photocurrent by a factor of 3-6 with an optimized photocurrent density of ~300 nA cm^{-2}.[94] The highest energy output to date for PSI was just recently reported with a photocurrent density of 362 µA cm^{-2} and a power density of 81 µW cm^{-2}. The device contained a zinc oxide nanostructure semiconductor in which PSI was self assembled. The authors treated PSI with peptide surfactants for stability, increased the light absorption cross-section and used high affinity peptide motifs that promote selective adsorption to enhance the photovoltaic performance. [110]

3.5 Energy from Photosystem II

Another organelle of particular interest is the photosystem 2 complex (PSII). PSII complex consists of both chlorophyll p680 reaction center and the oxygen evolving complex (OEC), the sites for light energy collection and water oxidation respectively. During initial excitation, PSII is the site in which electrons induced by photons are in their highest potential energy state. The oxygen evolving complex subsequently replenishes the electron-hole pair that was prompted by the photon via the oxidation of water, which makes PSII a self-replenishing source of energy in theory. The excited electron from p680 is transferred via resonance energy to pheophytin (Phe) and then to the plastoquinone pool to follow the electron transport chain. [111] Ideally, replacing Phe with another equally reactive electron accepting electrode will allow the highest conversion of energy from the solar cell [112]. The electron transfer pathway is fueled by the electron's tendency to move towards a low energy state; therefore energy is lost during the electron transfer steps. Also, the rate-limiting step in PSII is the reduction of Q_B by two electrons from Q_A and the diffusion of the quinine into the membrane bilayer[113]. Therefore it is hypothesized that H_2O oxidation via PSII could be accelerated if electrons could be efficiently extracted from Q_A^-.[57] However, one downside of using PSII is its unstable nature outside of the thylakoid membrane.

In order to collect the photochemical energy from photosystem II, the organelle needs to come into contact with the electrode surface for direct electron transfer, or the electron transfer must be facilitated from the

photosystem II complex to the working electrode via a mediator. The direct electron transfer from photosystem II to the electrode is problematic because the phe-plastoquinone binding site is located deep within the organelle's outer layer [114]. Also, the life expectancy and stability of photosystem II is very limited when it is not present in its native location of the thylakoid membrane. Orientation of the immobilized photosystem II complex is also believed to play an important role in successful electron transfer, with the donating site facing the electrode surface [3].

3.6 Recent Studies

Multiple attempts have been made to increase photosystem II stability and activity as well as to optimize the electron transfer to a collection source. [31, 112, 114] The use of a polyHis tag and Ni-NTA gold substrate has successfully immobilized photosystem II complexes but with little stability and efficiency [8, 115]. Also, the techniques of using BSA-glutaraldehyde crosslinking agents have been used for years as a form of photosystem II immobilization for herbicide detection. [104] Recently the use of osmium containing redox hydrogels have proven to be an immobilization technique that help reserve stability as well as increase photosystem II concentration in contact with the electrode. It is thought that the redox hydrogels serve as both an immobilization technique as well as a mediator to help facilitate the electron transfers from the PSII complex to the electrode. This technique produced a current density of 45 μA cm^{-2} at a light intensity of 2.65 mW cm^{-2}. [10]

Vittadello et al. [31]attempted to use photosystem II complexes tethered to gold surfaces to produce photocurrent. They used a histidine-tagged

photosystem II from cyanobacterium Thermosynecococcus elongates to covalently bind the protein with a gold electrode modified with Ni^{2+} - nitrilotriacetic acid (Ni-NTA). Methods including crystallography, atomic force microscopy, and Rutherford backscattering spectroscopy measurements were used to define the quality of the immobilization technique as well as the number of layers and surface density. They calculated a theoretical photocurrent density of 43 mA cm^{-2} and a photon flux density of 2000 µmol quanta $m^{-2}s^{-1}$ between 365 and 750nm. They also measured photosystem II activity before and after immobilization and concluded that PSII complexes remain photochemically competent even after the immobilization process. Fluorescence relaxation kinetics was utilized to describe the electron transfer kinetics of the acceptor side of PSII in vivo, vitro, and on gold-coated surfaces. It was found that PSII in vivo decayed at a faster rate (4-6ms) compared to in vitro (25-35ms). In addition, fluorescence kinetics revealed that the mechanism of electron transfer on the acceptor side of PSII is the same before and after the isolation process.

Noji et al.[32]successfully bound PSII enzymes from thermophilic cyanobacterium *Thermosynechococcus* elongatus to gold nanoparticles (GNP) via a His-tag located at the C-terminus of CP47 and using nickel-nitrilotriacetic acid (Ni-NTA). This allowed the electron acceptor side of the PSII dimmer to orient towards the GNP surface. The GNPs were 20nm in diameter and could bind approximately four to five PSII dimers per particle confirmed by transmission electron microscopy. The oxygen evolution activity from free PSII complexes

was similar to the activity of the PSII-GNP conjugates at 580μmol O_2 (mg chl)$^{-1}$ h^{-1} and 575 $\pm$ 80 μmol O_2 (mg chl)$^{-1}$ h^{-1} respectively.

3.7 Photosynthetic Full-Cell Photovoltaics

Photosynthetic full cells utilize biocatalysts in both anode and cathode compartments within an electrochemical cell. The idea is to use photosynthetic organisms to oxidize water along the anode surface to induce a charge separation. The generated electrons flow through an external circuit while protons (hydrogen) and oxygen are redirected towards the cathodic end of the cell. Oxygen gas is reintroduced to electrons and water is produced via a reducing agent.

3.8 Recent Studies

Yehezkeli et al. [33] used electropolymerize mercapto benzoquinone (Pmbq) to immobilize isolated PSII from theromphilic cyanobacterium mastigocladus laminosus to the anode end of a full cell. An electrically wired bilirubin oxidase/carbon nanotube (BOD/CNTs) modified electrode was used for the cathode. Photo-induced quinine-mediated electron transfer was observed on the anode surface in the form of photocurrent with a power output of 0.10 W with a light intensity of 400 nm. Potentials above E=0.0 V vs. SCE reveled photocurrents greater than 300 nA, upon lowering the potential below E=0.0 V resulted in a decrease in photocurrent. The results relate well to the Pmbq redox potential of Eo' ~ 0.05 V vs. SCE, so Pmbq can only remain in an oxidized quinoid state to help facilitate electron transfer at positive potentials. The full with the Pmbq/PSII photoanode coupled to the BOD/CNTs cathode generated a

photocurrent with a quantum yield of 1.0 % at 675nm. In addition a new anode with a bis-aniline-crosslinked matix to bind gold nanoparticles and PSII was executed in a full cell manor. At 675 nm, a quantum yield of 0.7% was observed. The loss in quantum yield despite the increase in surface morphology is contributed to lower loading of PSII due to lack of the enhanced binding affinity of benzquinone at the Q_B site.

A microelectromechanical system (MEMS) based on photosynthetic electrochemical cells was developed using thylakoids from spinach. Electrons were harnessed from photosystems via a phenazine methosulfate redox mediator. The protons move through a proton exchange membrane from the anode to the cathode compartment. The electrons move through the external circuit to produce a current density of 1.1μA cm^{-2} with a light intensity of 2000 μmol photons m^{-2} s^{-1} and an applied voltage of 5.2 μV. The MEMS device produced an open circuit voltage of 470 mV. In the cathode chamber, the electrons either reduced a ferricyanide mediator or O_2 directly. [116]

3.9 Artificial Photosynthesis

In an attempt to deviate from instable living systems and to reduce the costs of isolation, immobilization, and quick repair; synthetic sensitizers and catalysts are considered. Porphyrinoids like phthalocyanines and porphyrins, are at the fore front of mimicking the excitation reaction centers within the same optical range. Crystallized structures of the light-harvesting antenna of PSII indicated circularly arranged chromophores [117]. Therefore cyclic porphyrin arrays are one of the main forms that are being studied. They are usually constructed

via covalent bonds, noncovalent bonds, or metal coordination bonds. The covalently bonded cyclic porphyrins are the most robust, but they are difficult to assemble, especially during macrocyclization. The noncovalently bonded porphyrins degrade easily due to sensitivity to the environment.[118, 119] The advantage of using porphyrinoids come from centers that are either made from cheap metal or no metal at all and the versatility of a synthetic product. However, disadvantages include low preparation yields and low life span for excited states. Poly-pyridines of transition metals have a longer life spans and high energy excitation states; however they normally use very costly metals. [64]

3.10 Recent Studies

Biomimetic materials to mimic the PSII OEC have been around since the early 1970's. Copying the function of the OEC will allow both a release of an electron that can be captured and used in a photovoltaic cell and the production of hydrogen that can be used for fuel cell applications. In 1972, Fujishima and Honda developed TiO_2 photoelectrodes that became the first device to split water via UV light. [120] Since then, arrays of water oxidizing systems have been developed to mimic the OEC of PSII to produce hydrogen gas. Multijunctional photoelectrodes containing illuminated AlGaAs/Si RuO_2/Pt_{black} have been used to evolve H_2 and O_2 gas with sustained water splitting at 18.3% conversion efficiencies [121]. Solids of gallium and zinc mitrogen oxide, modified with oxide of both rhodium and chromium have been shown to promote H_2 evolution at 2.5% quantum efficiency under visible light. [122] More recently, a tetra-ruthenate polyoxometalate catalyst that utilizes polynuclear dendrimeric Ru(II) polypyridine

sensitizers that activate colloidal IrO_2 nanoparticles have shown up to a 30% quantum yield.[123] These and many more water oxidation biomimetic materials have shown water splitting potential. [124-126]

Cobalt-containg polyoxotitanates (TiCo) were used to prepare Nocera-type CoO_x water-oxidation electrocatalysts where the TiCo served as cages to hold cobalt ions in a titania matrix on fluoride modified tin oxide electrodes. An initial current density of 0.8 mA cm^{-2} was obtained at an applied potential of 1.35 V vs. NHE with up to 80% of the density retained after one hour. [127] Esswein et al.[128] have reported current densities up to 100 mA cm^{-2} for water oxidation using a high surface area electrode functionalized with cobalt-based oxygen evolving catalysts. In order to maintain stable activity, achieving as high as ~90 h, the anodes needed an applied overpotential of 442 and 363 mV in pH 7 phosphate and pH 9.2 borate electrolyte respectively.

Currently for an ideal water electrolysis two gap tandem device, the maximum conversion efficiency is ~46% with a singlet fission top cell and a multiple exciton generation bottom cell.[86]

3.11 Biological Energy Comparison

Besides photosynthetic organelles, biological power sources have also been developed using enzymes and microbes as catalysts. Microbial fuel cells typically consist of anode and cathode chambers with bacteria growing on the anode. The bacteria oxidize organic matter which results in a release of electrons which get transferred to the electrode surface. Protons are simultaneously released into the solution and pass through a proton exchange

membrane (PEM) to the cathode chamber. Oxygen is dissolved into the cathode solution and the combination of protons, electrons and oxygen make water as a byproduct.

3.12 Microbial Fuel Cells

Many parameters affect the energy output of microbial fuel cells. Ionic strength of the solution and distance of the anode and cathode can dramatically affect power output. In 2005 a jump in power density was reported from of 720 to 1330 mW m^{-2} with a change in NaCl concentration from 100 to 400 mM. Power also increased from 720 to 1210 mW m^{-2} from the decrease in electrode distance from 4 to 2 cm. The power increase was attributed to the decrease in internal resistance.[129]

Ringeisen et al.[130] developed miniature microbial fuel cell using Shewanella oneidensis DSP10 in a lactate medium for the anolyte and a ferricyanide buffer for the catholyte. A maximum power density of 24 and 10 mW m^{-2} were obtained for the true surface areas of reticulated vitreous carbon (RVC) and graphite felt (GF) electrodes respectively without mediators in the anolyte. Short current densities reached 100 mA m^{-2} for RVC and 32 mA m^{-2} for GF anodes. Upon the addition of mediators, the current and power increased. The high densities were attributed to short diffusion lengths and high surface-area-to-chamber volume ratio. A similar mediatorless microbial fuel cell was optimized and developed by Moon et al.[131] with a power density of 0.56 W m^{-2}. The power per unit cell working volume was 102 mW L^{-1}, which was the highest reported at

the time for this fuel type. The power generate remained stable for over two years.

Liu and Logan[132] developed an air-cathode single chamber microbial fuel cell using carbon electrodes with the presence and absences of the PEM. The biocatalysts were bacteria grown from domestic waste water with glucose and wastewater as substrates. Power density reached a maximum of 262 ± 10 mW m^{-2} with glucose as a substrate. The power density increased to 494 ± 21 mW m^{-2} upon the removal of the PEM. The power density with waste water was 28 ± 3 mW m^{-2} with the PEM. A similar increase in power density to 146 ± 8 mW m^{-2} was seen with PEM removal. Liu later improved the cell configuration to enhance coulombic efficiency by applying a J-cloth layer on the water-facing side of the cathode, which allowed significant reduction of oxygen diffusion. This resulted in over 100% increased coulombic efficiency. Sandwiching the cloth between the anode and cathode allowed a large reduction in internal resistant which gave a power density of 627 W m^{-3} in fed-batch mode and 1010 W m^{-3} in continuous-flow mode. This is the highest reported power density for microbial fuel cells to date.[133] The advantages of using microbial fuel cells over photosynthetic fuel cells include high stability as well as high power outputs.

3.13 Advantages of Photosynthetic Power

Silicon-based solar panels only work like photovoltaic cells to directly collect electricity from solar energy. On the other hand, photosynthetic based solar cells have been shown to produce direct electricity as well as energy dense fuels like hydrogen and ethanol. Developing systems to produce energy dense

fuels will allow longer storage time and mobility. Compared to microbial fuel cells that require organic matter as an energy source, photosynthetic power only requires sunlight and water, giving photosynthetic power unlimited energy supplies.

CHAPTER 4

EXPERIMENTAL RESULTS

In this work, thylakoids were extracted from spinach and immobilized on a carbon nanotube matrix to carry out photo-electrochemical water splitting on a gold electrode surface. By immobilizing thylakoid membranes rather than individual proteins, we are able to study the direct redox responses of integral membrane proteins present in thylakoids as well as understand the electron transport pathways between photosynthetic reaction centers and the modified electrode. We also used $[Fe(CN)_6]^{3-/4-}$, which has been known to interact with thylakoid membrane proteins[134], as a mediator to enhance the observed photo-current activity. We adapted a previously demonstrated molecular tethering approach that has proven to exhibit excellent bio-electrochemical characteristics[135-137] to immobilize thylakoid membranes on the carbon nanotube matrix via amide bonds to the membrane proteins as depicted in Figure 4.1. Colored arrows in the schematic indicate the possible electron transfer pathways between the thylakoid membrane proteins and the electrode, which have been explored and discussed in this paper.

Thylakoid membranes were tethered to MWNTs using PBSE through a coupled covalent and non-covalent attachment. The aromatic ring-like structure of carbon nanotube (CNT) walls forms a π- π stacking bond with the pyrene ring of the PBSE. On the other hand the surface primary amines of the thylakoid membrane bound proteins react with the succinimidyl ester group of the PBSE leading to an amide bond. This results in the tethering of thylakoids to CNTs

through molecular wires of PBSE. A basic schematic of the immobilized thylakoid membranes on the electrode surface is depicted in Fig. 1. The possible electron transfer pathways are indicated by colored arrows in Fig. 1. Yellow arrows correspond to direct electron transfer from chytochrome b_6f (cyt b_6f), green arrows represent facilitated electron transfer to the modified electron by the addition of $[Fe_3(CN)_6]^{3-}$ mediator, and purple arrows represent direct electron transfer from plastocyanin. The immobilization process of usingMWNT-PBSE modified gold electrode in the presence $[Fe_3(CN)_6]^{3-}$ mediator provides an effective and time efficient approach to studying photocurrent generation using photosynthetic proteins. We studied the photo-electrochemical activity of spinach thylakoids immobilized on to multi-walled carbon nanotube (MWNT) modified electrodes. We also report the demonstration of direct light to energy conversion with water as the only input using a photosynthetic fuel cell composed of a thylakoid based anode and laccase based cathode.

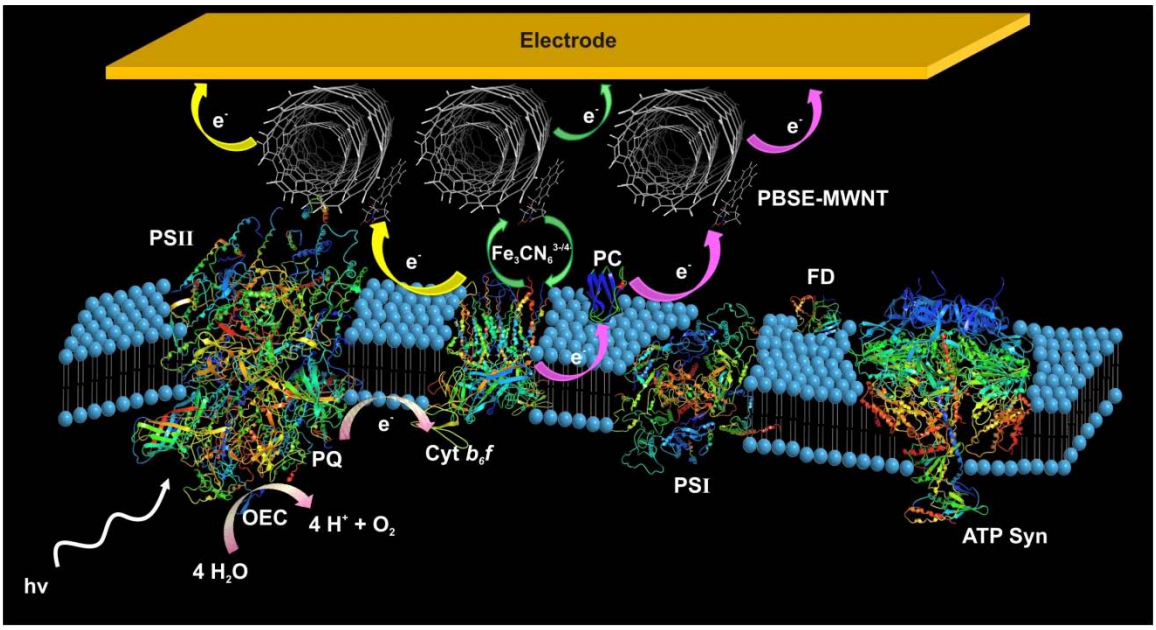

Figure 4.1. Schematic of Electron Transfer: Schematic representation of the electron transfer pathways in thylakoid-MWNT composite matrix. OEC, PQ, PC, FD, and ATP syn represent oxygen evolving complex, plastoquinone, plastocyanin, ferredoxin and ATP synthase respectively. (Note: Some crystallized protein structures are from bacterial origin).

4.1 Thylakoid Activity and Morphology

The oxygen evolution activity of isolated thylakoids was measured with a standard Clark O_2 electrode via a previously reported technique in a tricine pH 7.8 buffer. [138, 139] The average oxygen evolution rate was 253 µmol O_2 mg chl^{-1} h^{-1}. Tapping mode AFM and SEM were used to study the morphology of thylakoid-modified electrodes. The AFM topography, amplitude and phase images of the unmodified (control) and thylakoid-modified electrodes are shown in Figure 4.2. The unmodified control electrode with the bareMWNT matrix shows clear and identifiable nanotubes as seen in Figure 4.2a. The thylakoid modified-MWNT composite matrix shown in Figure 9b has a similar morphology as that of the control, but with distinct thylakoids on the surface.

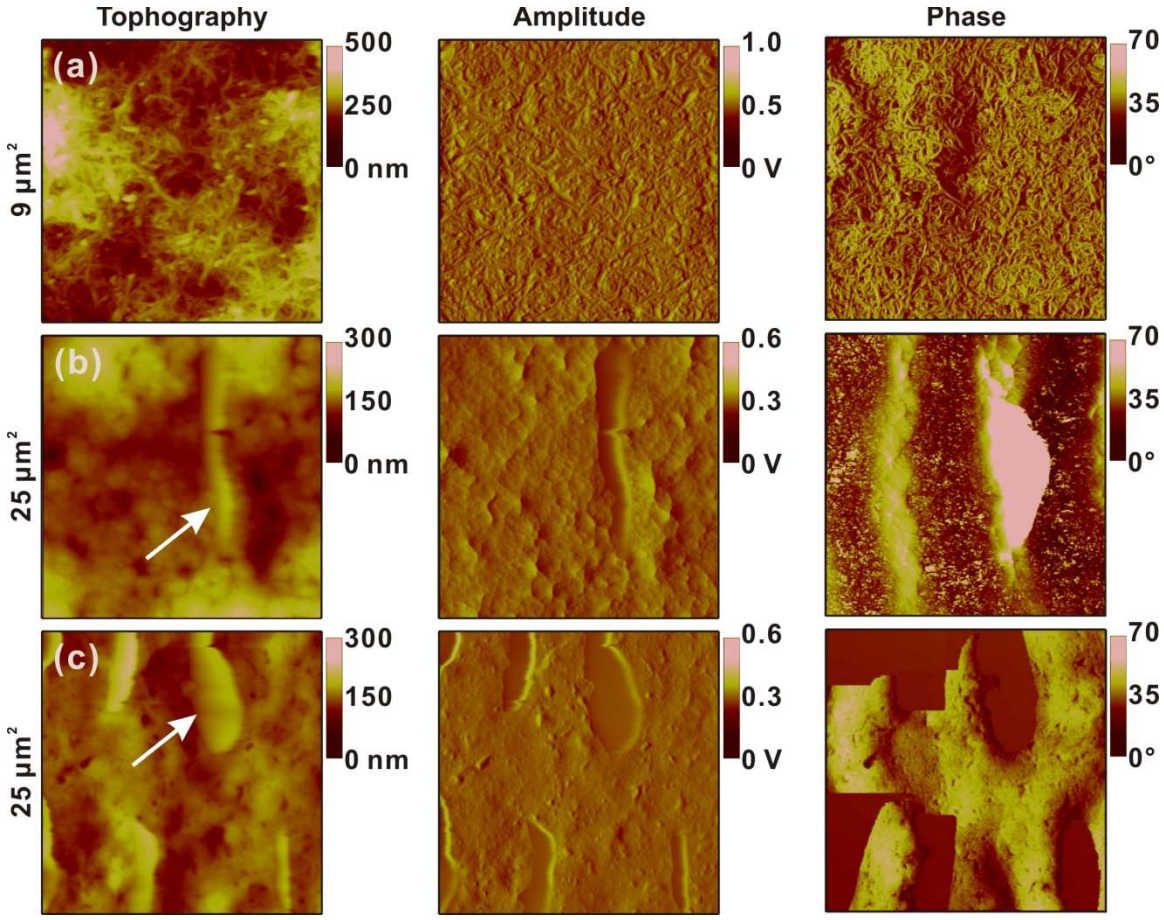

Figure 4.2. AFM Composite Morphology: AFM images of gold electrodes modified with (a)MWNT matrix without thylakoid (b) thylakoid-MWNT composite and (c) thylakoid withoutMWNT matrix. The topography, amplitude and phase images correspond to left, middle and right columns respectively. Thylakoids are marked by the arrows in the images.

Due to the blanketing effect of biological structures, the underlying MWNT fibrils in the composite are not obvious in the topography image, but are evident in amplitude and phase images in Figure 4.2. The presence of thylakoids is shown by the lighter extruding region in the composite (Figure 4.2b), sized approximately 3 µm ± 0.5 in length which agrees with the typical size of a thylakoid unit.[140] A thylakoid modified electrode surface in the absence of MWNT is also shown in Figure 4.2c for comparison. The surface roughness of the

thylakoid matrix is 9 nm ± 0.5, which is also similar for both thylakoids (Fig. 4.2c) and thylakoid-MWNT composite matrices (Fig. 4.2b). The morphology studied using SEM (Figure 4.3) also shows the length of thylakoids to be 3 µm ± 1.

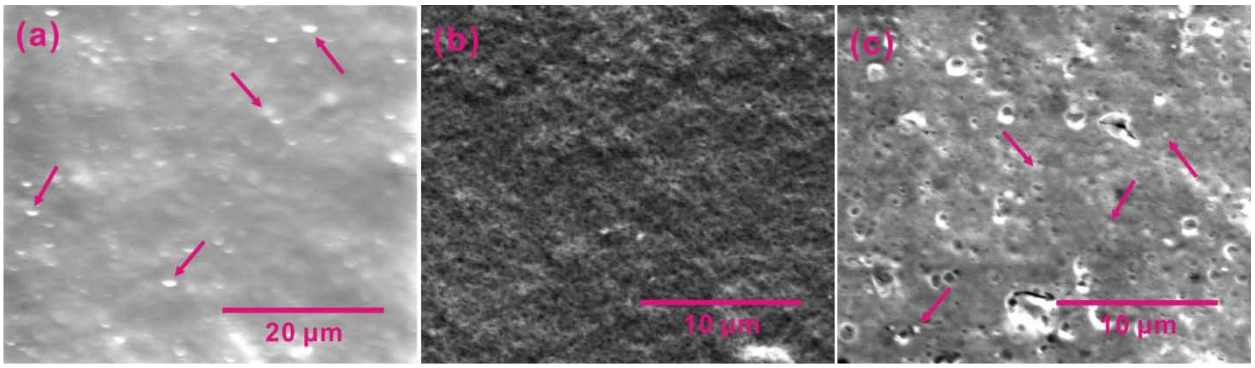

Figure 4.3. SEM Composite Morphology: SEM image of gold electrode immobilized with (a) thylakoids, (b) MWNT and (c) thylakoids-MWNT. Thylakoids are shown by the arrows.

4.2 Electron Transfer Pathways in Thylakoids

The thylakoid membrane consists of several membrane integral proteins that could participate in external electron transfer to the electrode. As schematically depicted in Figure 4.1, electrons generated as a result of water splitting in PSII, could eventually be transferred to the electrode in three possible routes as indicated by different colored arrows in Figure 4.1. This is in addition to the natural pathway of electrons during linear photosynthesis to reduce $NADP^+$. The yellow arrows indicate the first electron transfer pathway (ETP1): PSII → plastoquinone → *cyt* b_6f →MWNTMWNT → electrode. ETP1 is possible if the *cyt* b_6f is adsorbed or molecularly tethered toMWNTMWNT surface and its redox site is located close enough to theMWNT, which will result in a direct electron transfer from thylakoids to the electrode. The second possible electron transfer pathway (ETP2) is depicted by purple arrows: PSII → plastoquinone → *cyt* b_6f →

plastocyanin →MWNT → electrode. Here the electron gets routed to plastocyanin before reaching theMWNT matrix. Both ETP1 and ETP2 serve as direct electron transfer routes for electrochemical charge transfer. Upon the addition of a mediator such as ferricyanide, a third pathway as indicated by green arrows is also possible (ETP3): PSII → plastoquinone → *cyt* b_6f → ferricyanide →MWNT → electrode. In this case the ferricyanide mediator facilitates the electron transfer from multiple membrane proteins along the thylakoid to the electrode. Therefore the lack of electrical connectivity between membrane proteins and electrode is not of a concern. In our experiments, it is likely that all three routes, if not more through other integral membrane proteins, were being used for electrochemical communication between thylakoids and the electrode. Other electron transport pathways could occur due to impurities in the electrolyte including oxygen which is known to accept electrons from PSI [105] which then could oxidize ferrocyanide[116]. When oxygen accepts electrons from PSI, it forms a superoxide radical which later creates hydrogen peroxide which has been shown to react with electrodes. [106]

4.3 Electrochemical Redox Activity of Thylakoids

Cyclic voltammetry was used to study redox activity of the unmodified and thylakoid-MWNT composite electrodes and to identify the possible ETPs discussed above. The electrodes were cycled between -0.7 to 0.5 V vs. Ag/AgCl at a scan rate of 0.02 V s^{-1}. Figure 4.4a compares the cyclic voltammograms of thylakoid-MWNT composites in the presence and absence of the mediator. The formal potential (E^0) values for peaks 1_{peak} and 3_{peak} as observed in our results

were at 0.035 and 0.19 V (see Figure 4.4a), which fall closely with that of the literature values for *cyt* b_6f ($Fe^{II/III}$) and plastocyanin ($Cu^{I/II}$) respectively, when the pH difference is accounted.[141-144] This indicates that the thylakoids are not intact, but instead membrane particles due to the presence of plastocyanin which is located in the lumen. No redox peak directly attributable to plastoquinone was observed in our experiments, which is located inside the thylakoid lipid bilayer. Unlike plastoquinone, the *cyt* b_6f and plastocyanin redox sites are located on the inner surface of the thylakoid membrane (lumen side) and are relatively smaller than other thylakoid membrane bound proteins such as the photosystem complexes. Therefore it is likely that theMWNTs have easier access to the redox sites of *cyt* b_6f and plastocyanin. This could be the reason behind the redox activity of these proteins through direct transfer as observed in Figure 4.4a.

In the presence of 1.5 mM mediator, a single dominant oxidation peak (2_{peak} at E^0 0.157 V) was observed (see Figure 4.4a) and no clear redox peaks for *cyt* b_6f and plastocyanin were noticed. This indicates that the electron flux due to mediated transport was much higher than that of direct transport through the membrane bound proteins. The results suggest that the most favorable electron transfer pathway to the electrode is through the mediators (ETP3). Though we observed a direct redox activity for plastocyanin in our voltammograms, we do not eliminate the likeliness of plastocyanin dissolution from the thylakoid membrane. In such a situation, the observed redox activity could have been contributed by plastocyanin molecules adsorbed onto theMWNT.

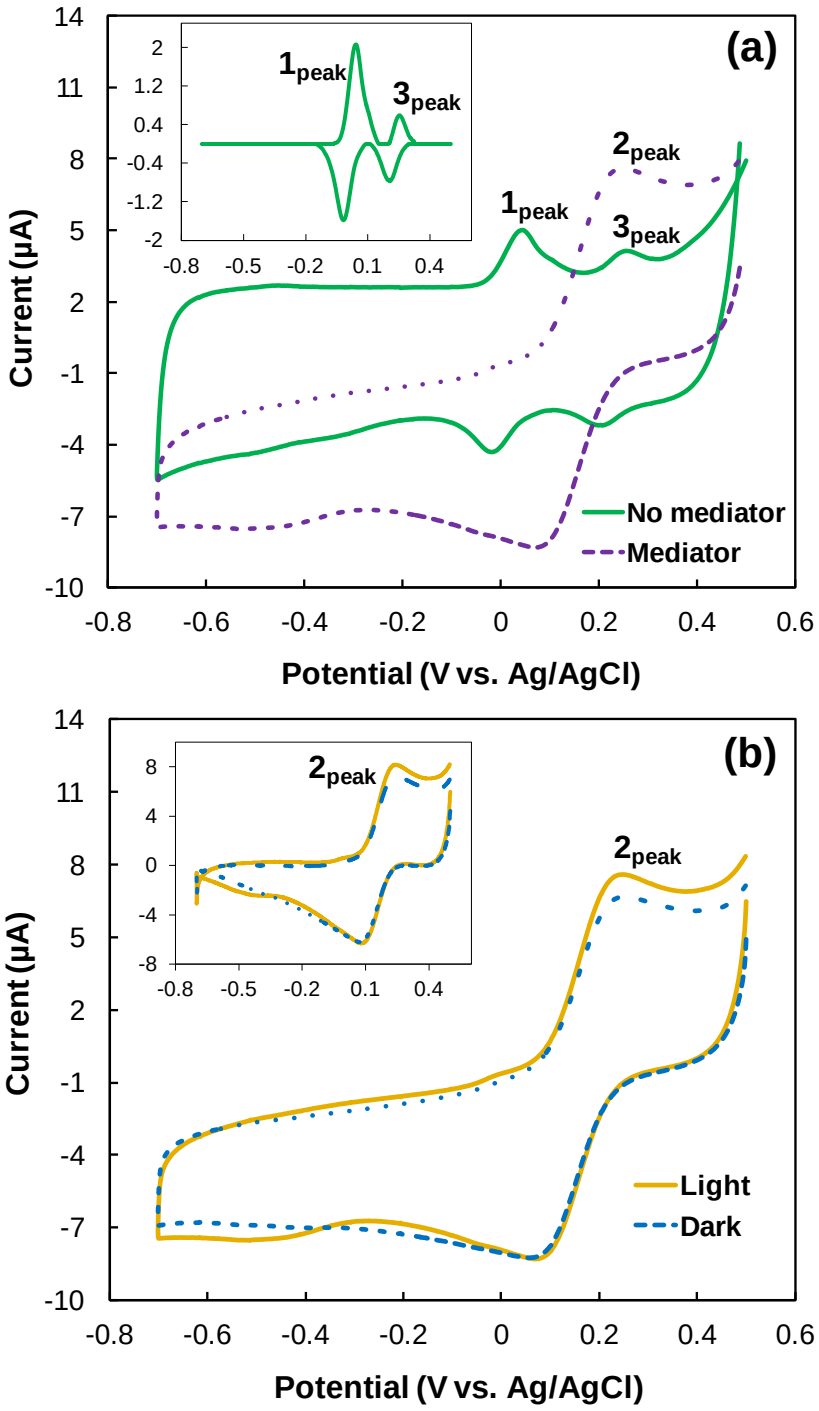

Figure 4.4. CV of Thylakoids: Cyclic voltammograms of thylakoid-MWNT composite modified electrode: (a) in presence and absence of 1.5 mM mediator, inset graph shows capacitance subtracted voltammogram (b) under light and dark conditions with 1.5 mM mediator, inset graph shows the background subtracted voltammograms. 1_{peak}, 2_{peak} and 3_{peak} represent the redox reactions of cyt b_6f, ferricyanide mediator and plastocyanin respectively.

Figure 4.4b show the oxygen evolution upon light illumination onMWNT-thylakoid bio-composite, where the E_{pc} at -0.4 V and E_{pa} at 0.3 V vs. Ag/AgCl represent oxygen reduction and ferricyanide oxidation reactions respectively. Upon illumination there is a small increase in the peak currents by 1.0 (I_{pa}) and 0.2 (I_{pc}) µA for both the reactions respectively. The increase in cathodic current in presence of light was due to the evolution of oxygen from the PSII induced water splitting reaction by thylakoid-MWNT matrix. Similarly, the increase in anodic current corresponds to the increase in concentration of ferrocyanide produced as a result of ferricyanide reduction by *cyt* b_6f upon illumination. This increase in anodic current must be proportional to the electron flux in ETP3. The results also suggest that the use of mediators could be favorable for high photo-current generation through ETP3. This phenomenon can be verified by the photo-activity analysis discussed in a later section.

CHAPTER 5

PHOTO-ACTIVITY OF THYLAKOID-MWNT COMPOSITES

The photo-electrochemical activity of thylakoid composites were evaluated using open circuit potential (OCP), potentiostatic current-time analysis, photo inhibition and AC impedance measurements.

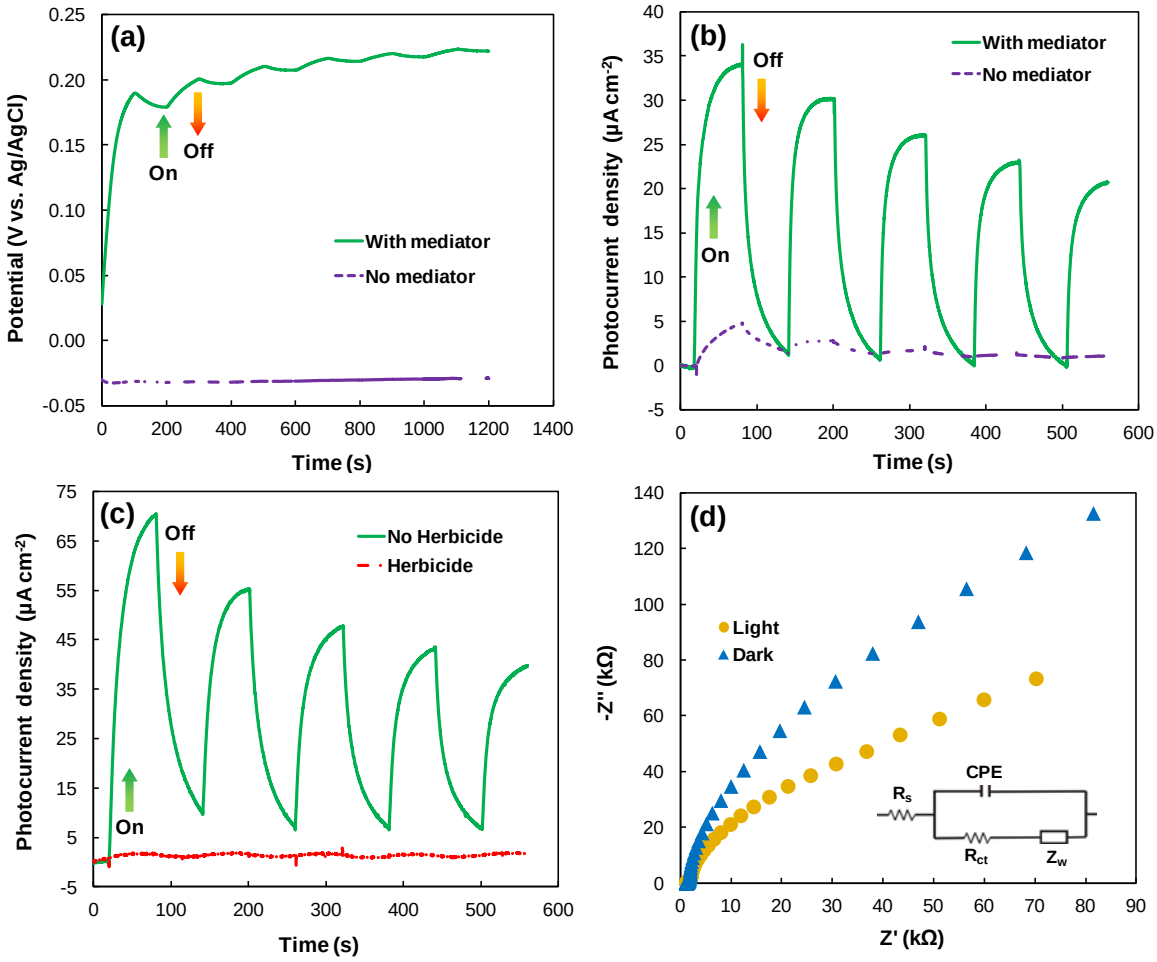

Figure 5.1. Electrochemical Studies: (a) Open circuit potentials of thylakoid-MWNT composite. (b) Photo-current response at a fixed potential of 0.2 V for thylakoid-MWNT composite in the presence and absence of 1.5 mM mediator. (c) Comparison of the photo-current response of unexposed and DCMU herbicide exposed electrodes. In (a-c), ↑ and ↓ represents light on and off conditions respectively. (d) Nyquist plots (Z' vs. –Z") \ under light and dark conditions. Inset in (d) shows the equivalent circuit model used to fit the Nyquist data.

5.1 Open Circuit Potential

Figure 5.1a compares the open circuit potentials of unmodified and thylakoid-MWNT modified electrodes. In the absence of $Fe(CN)_6]^{3-/4-}$ mediator, thylakoid-MWNT composites showed an OCP of about -0.05 V. The value of this OCP is dictated by the mixed potential caused by a variety of thylakoid membrane proteins whose individual redox potentials range from -1.3 to 1.0 V vs. SHE[141]. The addition of $[Fe(CN)_6]^{3-/4-}$ mediator increases the OCP of the composite to approximately +0.2 V. Upon changing the illumination conditions between light and dark over several light on-light off cycles, a clear variation in the open circuit potential was observed, indicative of photo-electrochemical activity. The variation was as high as 90 mV during the first on-off cycle, which eventually subsided during subsequent cycles consistent with the attainment of an equilibrium condition over time and protein bereavement due to photoinhibition over time during light exposure. On the other hand, the control electrode (MWNT without thylakoid modification) showed no variation in OCP between light and dark conditions (Figure 5.2a), confirming that the photo-electrochemical activity observed in the composites was caused by thylakoids and not the mediators.

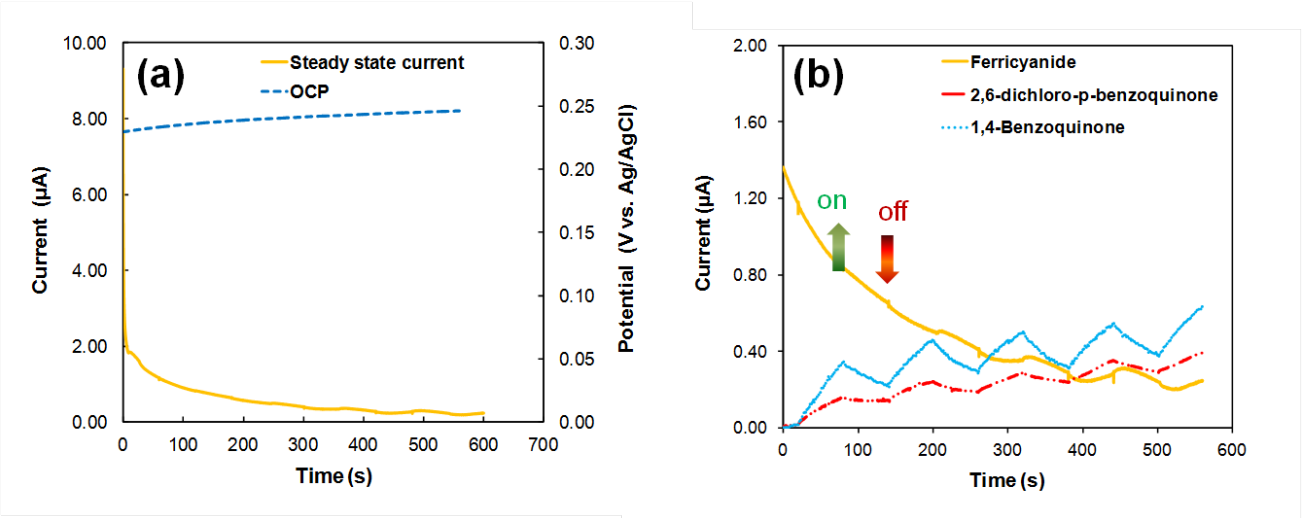

Figure 5.2. Mediator Activity: (a) Open circuit potential and current versus time forMWNT control electrode without thylakoids in the presence of 1.5 mM ferricyanide during light on-light off cycles. (b) Photo-electrochemical activity of 2,6-dichloro-p-benzoquinone (1.5 mM) and 1,4-benzoquinone (50 mM) mediators onMWNT modified electrodes without thylakoids. Ferricyanide data is also shown for comparison.

5.2 Potentiostatic Polarization

The photo-current activity of the thylakoid-MWNT composite was evaluated at constant anode potential of 0.2 V and the variation of anode current with time was evaluated during light on-light off cycles. As shown in Figure 5.1b, a noticeable photo-activity was observed for the composite even in the absence of mediator, with clear variations in current between light and dark conditions. This is a direct evidence of direct electron transfer (ETP1 and ETP2) in our composites and suggests for the first time that photosynthetic electrochemical systems could be developed without a mediator. The photo-current activity however was significantly enhanced (by ~50 fold) by the addition of $Fe(CN)_6]^{3-/4-}$ mediator as seen in Figure 5.1b, primarily because of the facilitated electron transfer indicated by ETP3 in Figure 4.1. For comparison, the control electrode

(MWNT without thylakoid modification) was also tested under similar conditions in the presence of mediator. No significant photo-activity was observed for $Fe(CN)_6]^{3-/4-}$ mediator in the absence of thylakoids (Figure 5.2). The maximum photocurrent densities in our experiments ranged from 34 to 68 μA cm^{-2} which stabilized steady values of 23 to 38 μA cm^{-2} after a few on-off cycles. These values were one to two orders of magnitude higher than the previously reported values for PSII based electrochemical cell[33] and bio-hydrogen production cell[101].

5.3 Steady State Analysis

When light was illuminated a large increase in anodic current was observed due to ferrocyanide oxidation at the electrode surface. This would require a continuous ferricyanide reduction by thylakoid membrane proteins in the presence of light. Over time the current generation stabilized to a constant value at approximately 0.675 μA (Figure 5.3a). This indicates that the observed decrease in photocurrent overtime during different light on-off cycles was due to transience in the mediator diffusion, which reaches steady state. The observed phenomenon could partly be due to the establishment of steady diffusion gradients in the system. Initially there was a high concentration of mediator present at the electrode-solution interface. Upon illumination, the redox couple undergoes transition from ferricyanide to ferrocyanide and which results in a decreased concentration of the ferricyanide at the interface. This slows down electron transfer to the electrode until it reaches concentration equilibrium upon which a steady photocurrent was observed. In the absence of light (Figure 5.3b), the current stabilized to approximately 0.8 nA of anodic current. As we can see

from the figures, over time the currents from both experiments reach the same steady value. This suggests that the decrease in the photocurrent over time was partly due to the transience in mediator diffusion. However a loss of photo-chemical activity or composite dissolution from the electrode surface over time can neither be verified nor confirmed based on our experimental results.

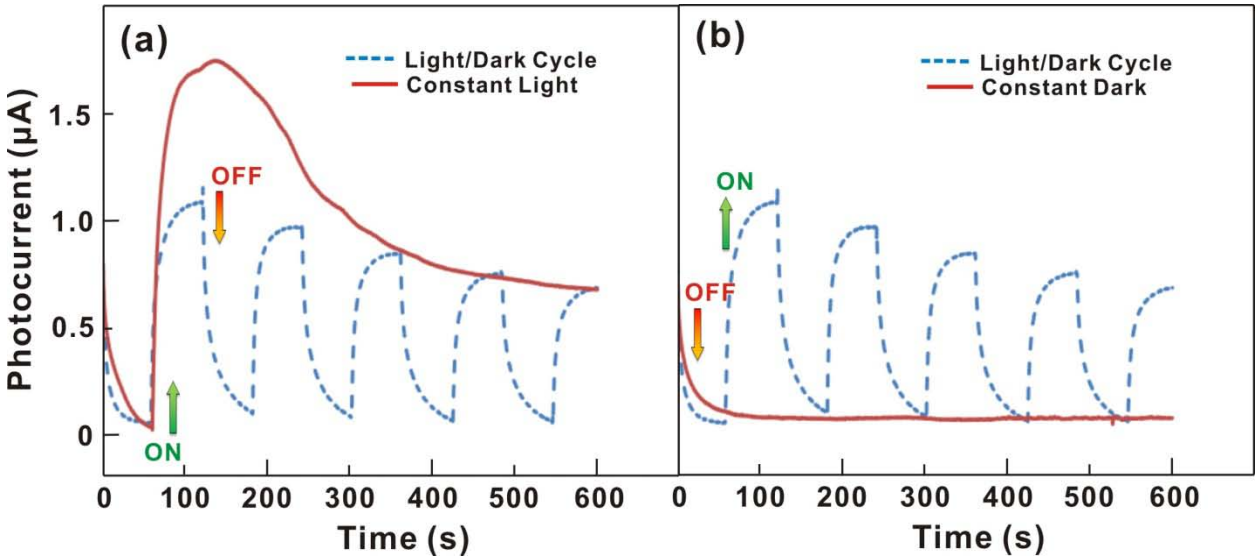

Figure 5.3. Constant Condition Current: Photocurrent analysis of thylakoid-MWNT modified gold electrode in constant light (a) and constant dark (b) conditions.

5.4 Optimization of Composite Composition

The plots of current versus time at fixed anode potentials were used as a guiding tool for optimizing the composition as well as the immobilization conditions preparing the thylakoid-MWNT composite electrode (Figure 5.4). The parameters optimized were thylakoid immobilization time (10.4a) and concentration (10.4b), mediator concentration (10.4c), and the anode operating potential (10.4d). The results showed the photocurrent was directly proportional to thylakoid concentration, however only a maximum of 0.44 μg cm^{-2} of thylakoids could be immobilized on our electrode due to size limitations.

Similarly, we noticed that incubation durations (for immobilization of thylakoids onMWNT matrix) beyond 1 h did not result in a significant increase in photocurrents. The photocurrent was also proportional to the mediator concentration, but the percent decrease of photocurrent per duty cycle varied. The optimized mediator concentration obtained was 1.5 mM, where the photocurrent was 0.9 µA for the first cycle while still maintaining stability through multiple cycles. The anode potential was also optimized at 0.2 V to observe noticeable photo-activity.

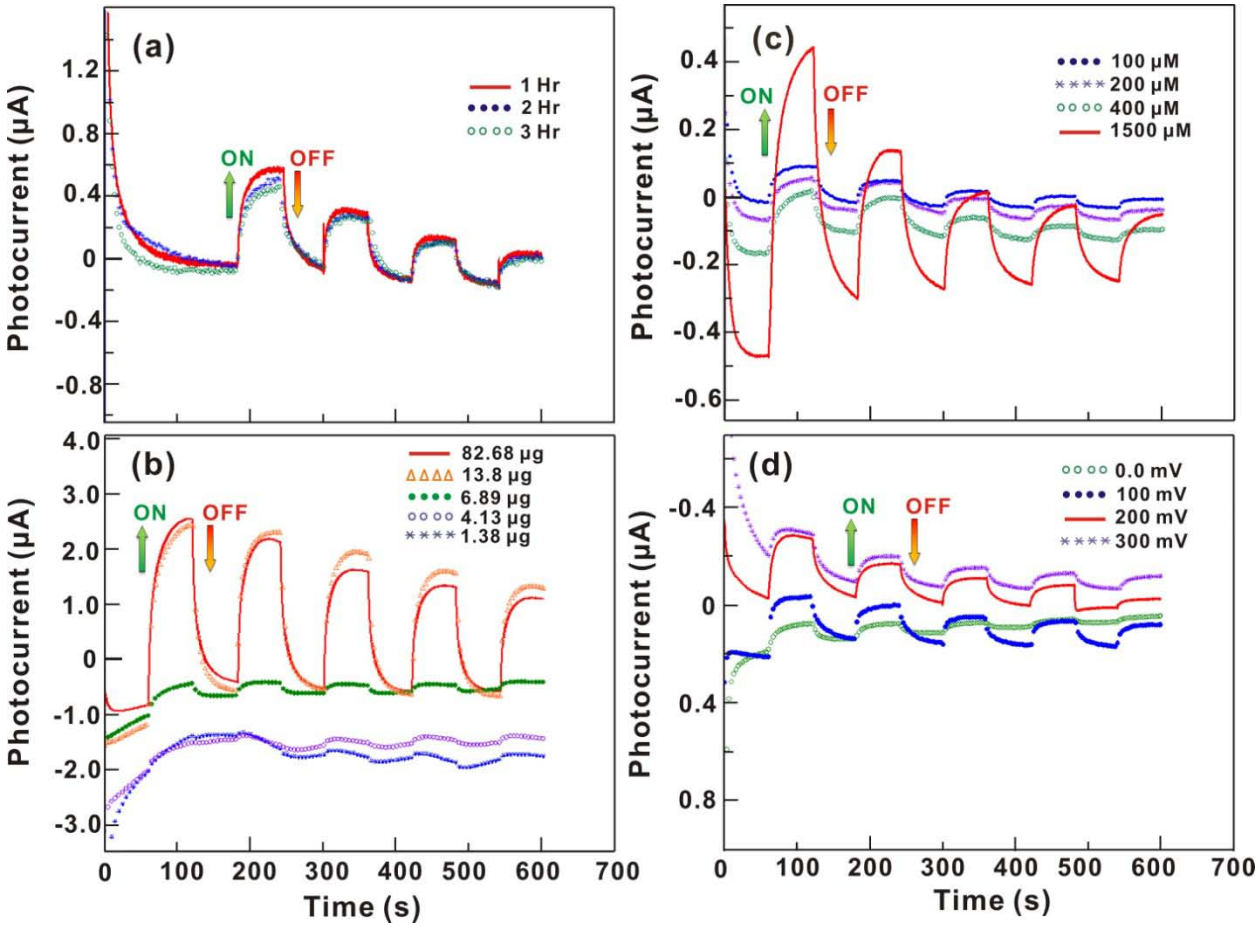

Figure 5.4. Optimization of Electrochemical Cell: Photocurrent analysis of (a) thylakoid immobilization time, (b) chlorophyll loading, (c) mediator concentration and (d) applied potential. ↑ represents light condition and ↓ represents dark. An applied potential of 0.2 V, 1 hr thylakoid immobilization time, and 1.5 mM mediator concentration were the most favorable conditions for this technique.

To understand if there is a significant advantage associated with immobilizing thylakoids for photo-electrochemical redox activity, we compared the immobilized thylakoids with that of thylakoids suspended in solution in the presence of mediator. Figure 5.5a reveals that the immobilized thylakoids exhibited a fairly stable and reproducible photo-current activity over several duty cycles, whereas the thylakoids suspended in solution showed a gradual loss in the photocurrent activity with less reproducibility. Moreover besides having a high concentration of thylakoids in solution (up to 400 times more chlorophyll content), the photocurrents were significantly lower than that for immobilized thylakoids. This is expected as the electron flux due to mediators for immobilized thylakoids is high because of the proximity of the surface bound proteins to the electrode reducing the diffusion distance for mediators. It can also be noticed that although high concentration of suspended thylakoids increases the photo currents, the trend is reversed at exceedingly high thylakoid concentrations due to the issues of high turbidity and low light penetration in the electrolyte. The cyclic voltammograms (Figure 5.5b) showed redox activities for immobilized thylakoids arising from the direct interaction of surface bound proteins with the electrode. For the case of thylakoids suspended in the solution there was no such redox activity. Therefore the immobilization method is vital for enhanced electron transfer and high photocurrents.

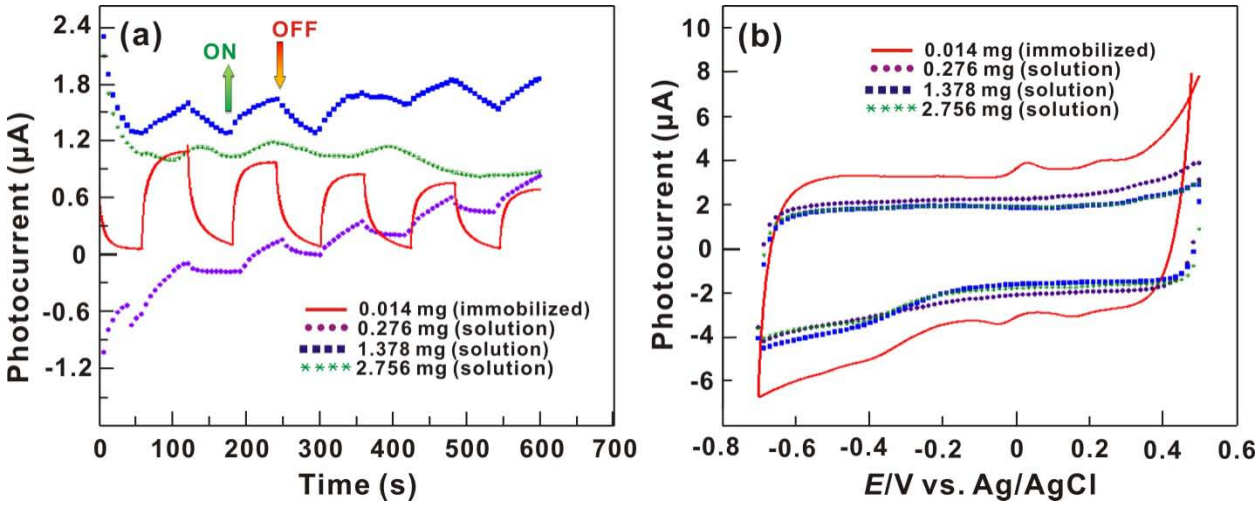

Figure 5.5. Solution vs. Immobilized Thylakoid Membranes: Immobilization technique vs. free thylakoids in solution (in mg mL^{-1}) (a) photocurrent curve analysis (↑ represents light condition and ↓ represents dark), and (b) cyclic voltammograms at the same conditions.

5.5 Protein Identification

In order to determine that the mediator was not interfering with absorbance activity of the thylakoids, an action spectrum was conducted with thylakoids in an 80% acetone solution compared with the $[Fe(CN)_6]^{3-/4-}$ mediator as shown in Figure 5.6 . The peak at 673 nm indicates absorbance via chlorophyll a. The graph with only mediator does not contain a chlorophyll peak, indicating that the mediator does not compete with chlorophyll absorbance. Also, the graph containing both thylakoids and mediator still contains the 664 nm chlorophyll peak, indicating that chlorophyll can still absorb light in the presence of the mediator.

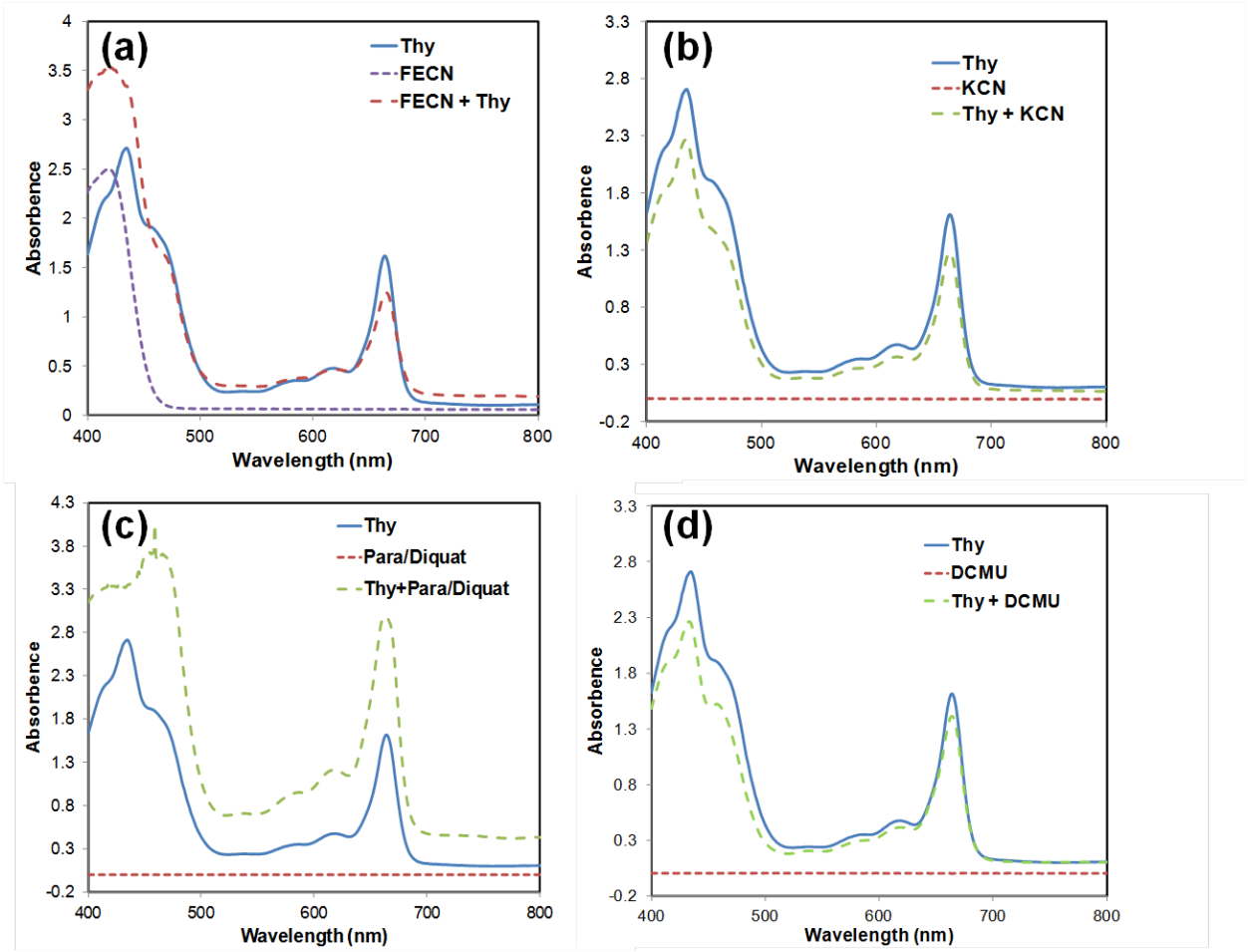

Figure 5.6. Action Spectrums: Action spectrum of thylakoid membranes with exposure to (a) ferricyanide mediator, (b) KCN, (c) para/diquat herbicide and (d) DCMU herbicide.

To confirm the identified plastocyanin peak, KCN (10mM) was added to the thylakoid solution prior to immobilization. KCN is thought to inhibit the plastocyanin protein during linear photosynthesis by removing the function of the copper unit at high concentrations (> 10mM) and at high pH values (>7.5). [53] The CVs are shown in Figure 5.7 where the identified plastocyanin peak is dramatically reduced, however the cyt b_6f peak is only slightly reduced. This indicates that the peak at ~200mV is plastocyanin. The reduction of the cyt b6f peak could be due to the absence of an electron acceptor from the cyt b6f

transfer site, causing the electrons to remain in the excited state and the inability for the molecule to dissipate its excited energy. The excited electron could react with oxygen to form oxygen singlets which results in lipid peroxidation over time.[51]

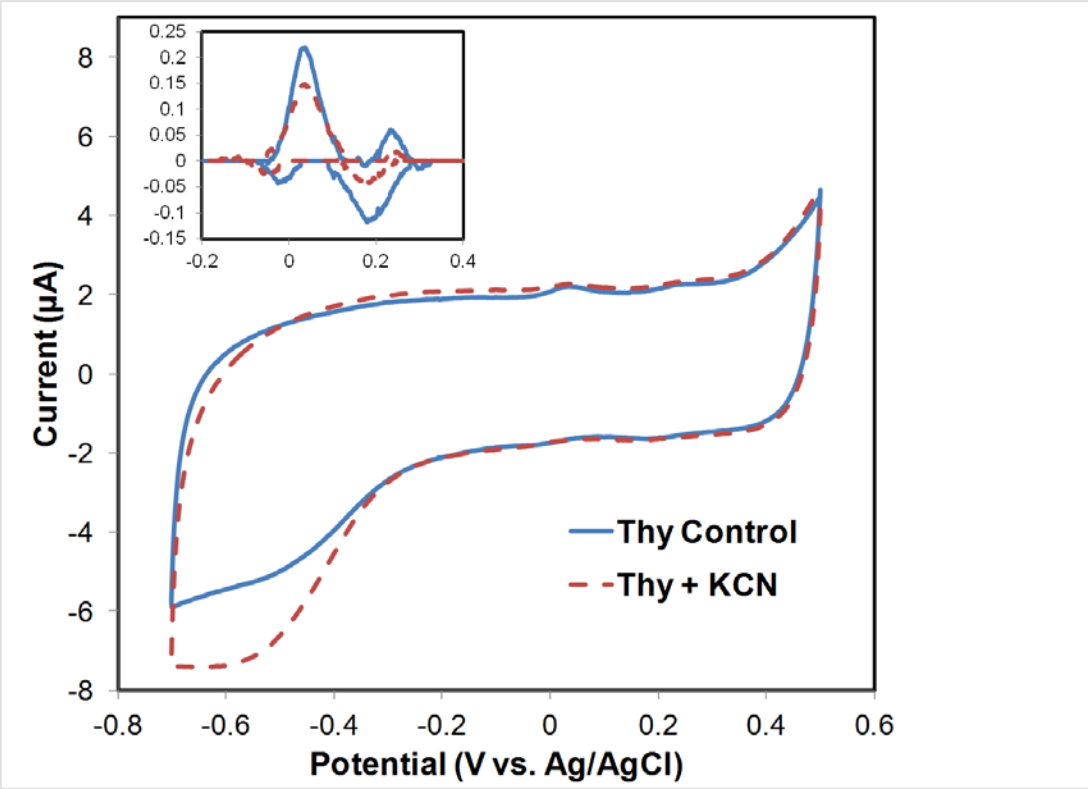

Figure 5.7. CV of KCN Exposed Thylakoids: CV of the effects of KCN (10mM) on thylakoids.

During amperometric analysis after one hour of thylakoid exposure to KCN (Figure 5.8a), higher anodic current is noticed when compared to controlled thylakoids not exposed to KCN. This indicates that more of the electrons can flow to the electrode without the completion of plastocyanin. When KCN is not present, electrons can flow from cyt b6f to plastocyanin or to the mediator, so inhibiting plastocyanin allows increased photocurrent generation. However,

thylakoids exposed to KCN for 15 hr have very little photocurrent activity compared to control thylakoids as shown in (Figure 5.8b). This indicates that KCN is detrimental to thylakoids over time, either due to a lack of an electron acceptor which inhibits energy to be released, or through lipid peroxidation due to oxygen singlets formed when oxygen is used as a replacement electron acceptor.

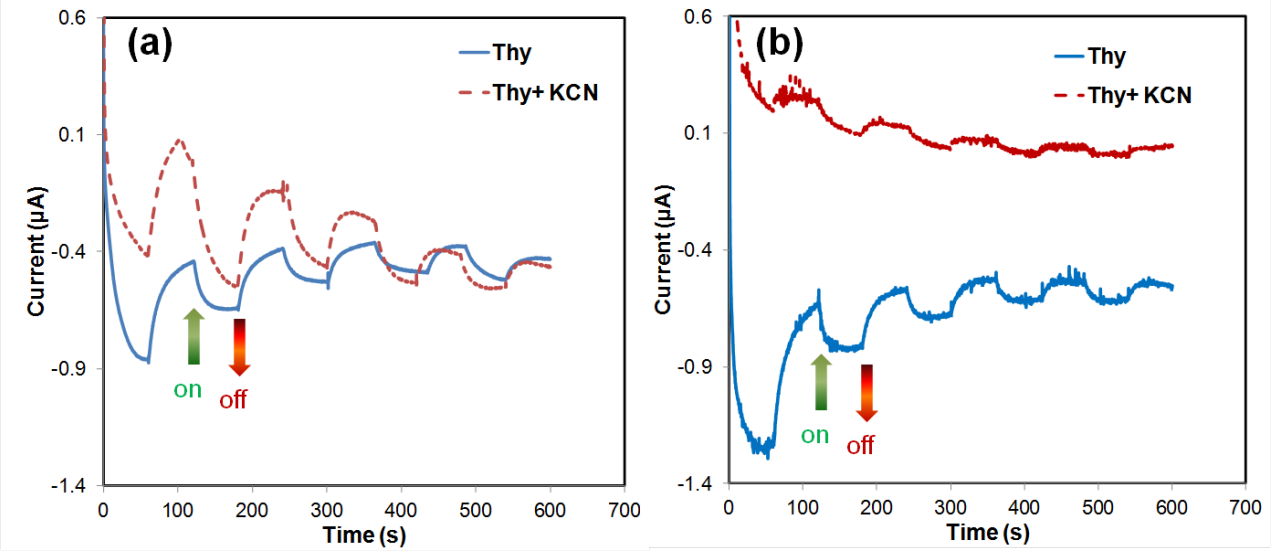

Figure 5.8. Photoactivity of KCN Exposed Thylakoids: Effects of KCN (10mM) on thylakoids: (a) the it-curve of thylakoids exposed and unexposed to KCN after 1 hr and (b) after 15 hours of exposure.

Thylakoids were also exposed to 250 µg ml^{-1} solution of paraquat/diquat solution to determine if the electron source could be from PSI instead of PSII. Paraquat and diquat are PSI inhibitors in the bipyridillum family, paraquat acts as a competitor to FD for the electron flow from the PSI F_a/F_b protein. F_a/F_b has a redox potential of -560 mv so it can easily pass electrons to FD at a redox potential of approximately -510 mv. Paraquat has a redox potential of -446 mv so it becomes more favorable for electron transfer. The reduced form of

paraquat is very reactive and will reduce oxygen to superoxide to regenerate the paraquat oxidized form. [51] Superoxide is destructive to plants, causing protein death. In Figure 5.9, current generation is similar to that of the control system. This indicates that the original electron source is from PSII. Since $[Fe(CN)_6]^{3-/4-}$ mediator accepts electrons prior to the PSI protein, the effects of the paraquat/diquat mixture is not seen during the experiment. However, it is possible that paraquat acts as a mediator as well which can shuttle electrons from PSI to oxygen or the electrode surface. As mentioned earlier, reactive also oxygen can form hydrogen peroxide which is able to react with the electrode.

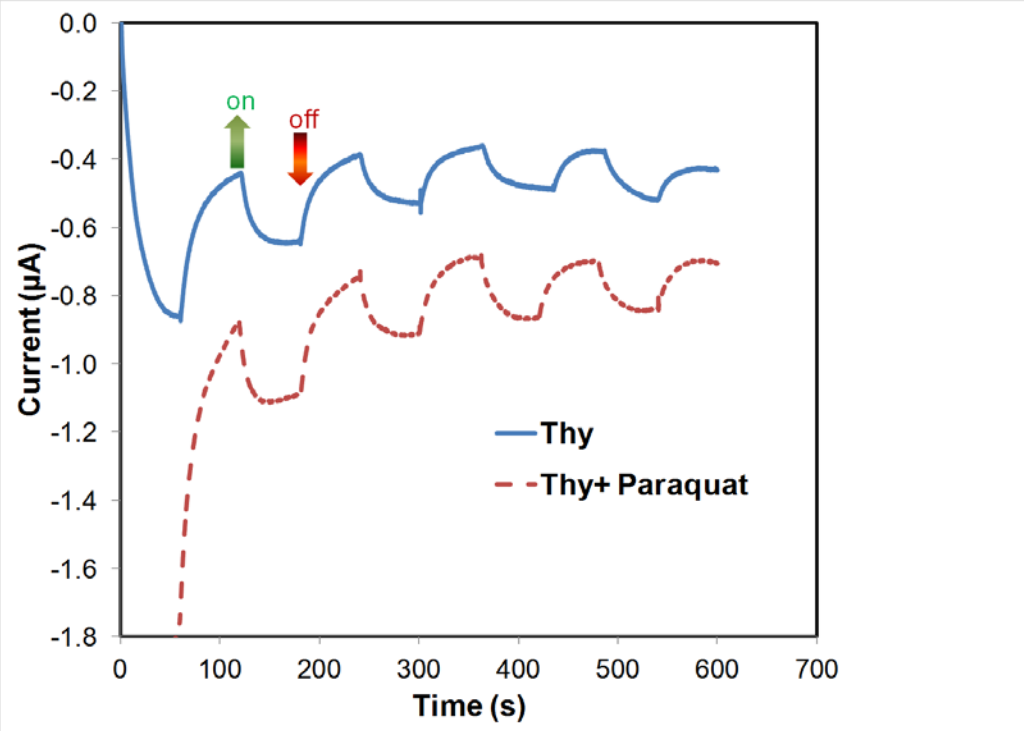

Figure 5.9. **Photoactivity of Paraquat/Diquat Exposed Thylakoids:** Effect of paraquat on photocurrent generation on thylakoid modified electrodes.

5.6 Photocurrent Stability

The decrease in the amplitude of photo-currents over continuous light on-off cycles observed in Figure 5.1b was partly due to the transience in mediator diffusion between thylakoid and electrode before the attainment of a steady state. This has been confirmed in a separate set of experiments where the thylakoid-MWNT composite electrodes were tested under different duty cycles (different ratios of $Time_{on}/Time_{off}$) as well as under continuous light on and continuous light off (dark) conditions (Figure 5.3). The standard operating conditions used in the experiments were based on an optimization over a narrow range of thylakoid loadings, immobilization duration, mediator concentrations and anode potentials (Figure 5.4). We also have confirmed that the immobilized thylakoids possess significant advantages for photo-current generation over free-thylakoids suspended in solution (Figure 5.5). However the experimental conditions were not meticulously optimized to enhance photo-currents and any variation in the composite composition should result in a significant change in photo-activity. Pursuing this optimization in any further detail is beyond the scope of this publication.

In addition, the thylakoid modified electrodes showed sensitivity to light intensity as shown in Figure 5.10. Initially the system was in darkness with the addition of high intensity light at time 60 s. Upon illumination, current up to approximately 2.6μA was observed. At time 540 s, the light intensity was decreased to medium intensity The corresponding current stabilized at approximately 1.9μA. When light intensity was decreased again to approximately

a lesser value, the photocurrent decreased to less than 0.9µA. This demonstrates the need for high intensity solar light in order to optimize current generation. Therefore, photosynthetic power sources will require implementation in regions with ample amounts of sunlight.

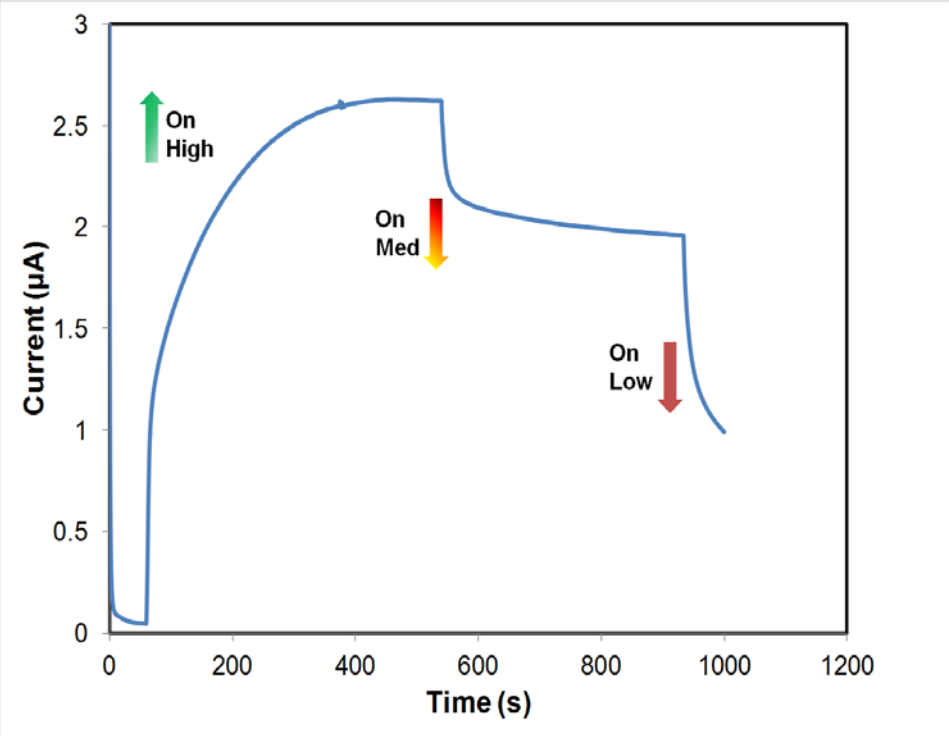

Figure 5.10.**Light Intensity Sensitivity of Thylakoids**: Effect of light intensity on thylakoid-modified electrodes. High light intensity was turned on at 60 s, medium intensity at 540 s and low light at 920 (s).

5.7 Electron Source

In order to confirm that the light-induced water splitting reaction is the actual electron source for the observed photo-currents in our composites, controlled electron transfer-inhibition studies were performed using DMCU as an inhibitor. DCMU is a herbicide that specifically blocks the electron transfer site of PSII, severing the electron transfer from PSII to the subsequent proteins in the bio-energetic pathway.[145] As shown in Figure 5.11, potentiostatic tests at 0.2 V

on thylakoid composites showed that when DCMU was used, the photocurrent was drastically reduced during the light on-light off tests.

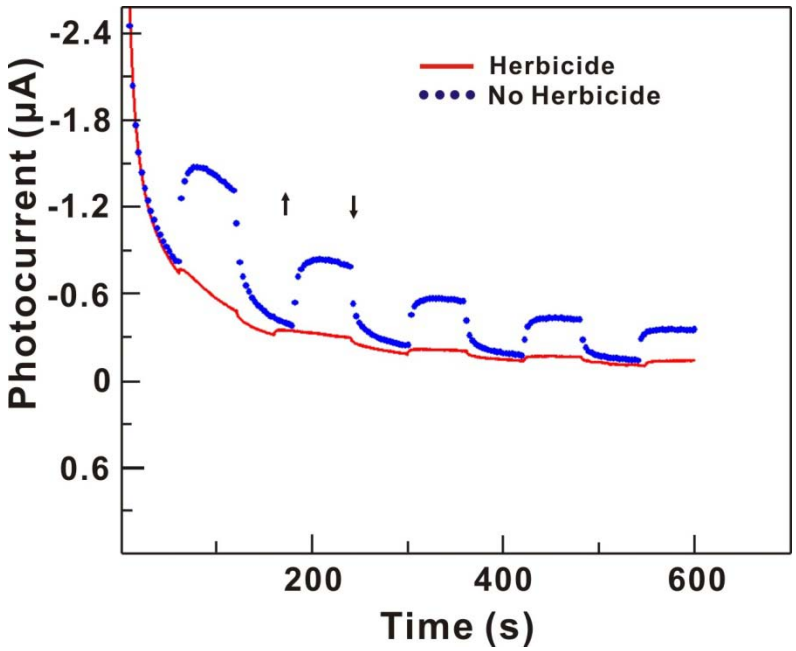

Figure 5.11. Photocurrent Activity of DCMU Exposed Thylakoids: Comparison of the current-time response of the unexposed and DCMU herbicide exposed thylakoid-MWNT modified electrodes under light and dark conditions.↑ represents light on and ↓ represents light off (dark).

More interestingly the cyclic voltammograms of DCMU exposed thylakoids (Figure 5.12) showed retention of redox electro-activity by both *cyt* b_6f and plastocyanin. This clearly indicates that the redox activities of the thylakoid membrane proteins and their direct electron transfer properties were not affected by the herbicide. These results also reiterate our inference that the source of electrons for the observed photo-currents, originate from PSII and that it is an integral part of the photosynthetic linear electron transport chain in our thylakoid modified electrodes.

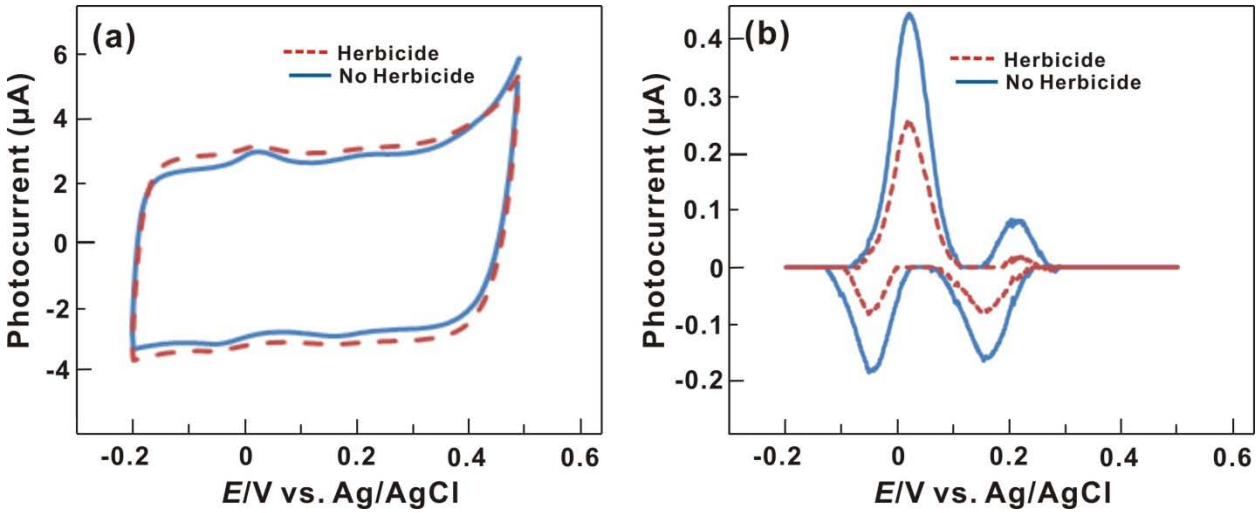

Figure 5.12. CV of DCMU Exposed Thylakoids (a) Cyclic voltammogram comparison of thylakoid-MWNT modified gold electrode with thylakoids exposed to DCMU herbicide with (b) background subtraction. Upon the addition of the herbicide, redox activities of cyt-b_6f and plastocyanin were reduced but not completely eliminated.

5.8 AC Impedance

AC impedance studies were also carried out on thylakoid-MWNT composite modified electrodes under light and dark in the presence of mediator to look at the individual resistances that influence the photo-current generation. The Nyquist plots (-Z'' vs. Z') of the impedance data and the equivalent electrical circuit (to which the data was fitted for parametric analysis) are given in Figure 5.1d. R_s represents electrolyte resistance, R_{ct} is charge transfer resistance, CPE is a constant phase element between the electrolyte solution and the modified electrode, and lastly Z_w represents the Warburg impedance due to the diffusion of mediator. The shape of the Nyquist profiles show a clear difference in the impedance between light and dark condition, with the composites showing lower impedance for charge transfer under the illuminated condition. The fitted values for R_{ct} were 87 and 317 kΩ under light and dark respectively. The results suggest

an enhanced electron transfer through lowered charge-transfer impedance for photo current in the presence of light.

CHAPTER 6

THYLAKOID-LACCASE PHOTOSYNTHETIC ELECTROCHEMICAL CELL

A rudimentary design photosynthetic electrochemical cell as shown in Figure 6.1, was constructed using the thylakoid-CNT modified anode and a laccase-CNT modified cathode. The molecular tethering method of immobilizing laccase onMWNT for bio-electrocatalytic oxygen reduction has been well established[135-137]. The polarization curves showed a maximum current density of ~70 μA/cm^2 and a maximum power density of 5.3 μW/cm^2. The power density values were comparable to the ones reported for PSII electrochemical cell using bilirubin oxidase cathode[33]. The marginally lower values in our system can be attributed to the low catalyst loading (because thylakoids are much bigger than PSII molecules) on our electrode, the high ohmic resistance of our buffer electrolyte, and the interference caused by ferricyanide on the cathode. These limitations can be overcome in a membrane less fuel cell. The primitive cell setup used here was constructed solely to demonstrate light to electricity conversion and was not optimized in any way to enhance power production.

This cell set-up could be beneficial to bacterial electrochemical cells due to having water as the input fuel source versus other more expensive or limited fuel sources. However, this system is limited to areas of strong solar emissions. The efficiency of this system is 0.17% which is significantly lower than that of solar panels at approximately 15% and current polymer based cells have reached an efficiency of approximately 6%. [89] Therefore improvement methods are needed before commercialization is possible. One way of increasing the

efficiency of the system is by decreasing the distance between the anode and cathode ends of the cell. Also, a more efficient mediator or the development of a mediator less system to allow for direct electron transfer will improve the overall efficiency.

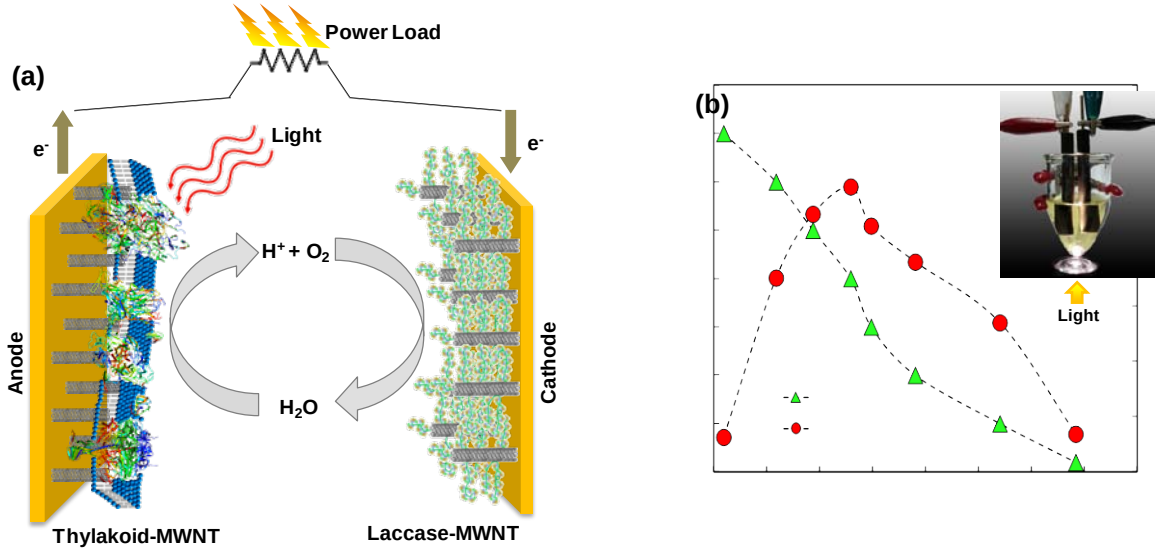

Figure 6.1 Full Electrochemical Cell with Thylakoids and Laccase. (a) Schematic representation of a photo-electrochemical cell containing thylakoid-MWNT based photo-anode and laccase-MWNT based biocathode. (b) Steady state polarization and power density of the photo-electrochemical cell. Picture of the simple photo-electrochemical cell setup is shown in the inset.

CHAPTER 7

MATERIALS AND METHODS

7.1 Materials and Apparatus

MWNT, 10 nm diameter and 1 to 2 μm length (Dropsens, Spain) was used as the immobilization support and electron carrier. 1-pyrenebutanoic acid succinimidyl ester (PBSE) (Anaspec Inc., Fremont, CA) was used as the molecular tethering agent. Potassium ferricyanide, redox mediator, and *N,N*-dimethyl formamide (DMF), solvent used for reagent preparation, were purchased from Acros Organics, Geel, Belgium. 3-(3,4-Dichlorophenyl)-1,1-dimethylurea (DCMU) was purchased from Tokyo Chemical Industry, Tokyo, Japan. Laccase from *Trametes versicolor* (Sigma, St. Louis, MO) was the enzyme used in the cathode. KCN was purchased from Fisher Scientific Co LLC (Hanover, IL). Paraquat/Diquat was purchased from Ultra Scientific (North Kingstown, RI). Tricine (OmniPur, Darmstadt, Germany), sorbitol (EMD Chemicals Inc, Darmstadt, Germany), ethylenediaminetetraacetic acid (EDTA) (VWR International LLC, West Chester, PA), and potassium hydroxide (Mallinckrodt Baker, Inc, Phillipsburg, NJ) were used for preparing buffer solutions. All these buffer solutions were prepared using nanopure distilled water (ddH_2O). And all electrolyte solutions were purged for 30 min with N_2 to remove any dissolved O_2. The pH 6.8, 0.1 M phosphate buffer electrolyte for fuel cell was prepared using monobasic and dibasic potassium phosphates (VWR, Suwanee, GA). All the experiments were conducted at 25 ± 2 ºC.

Bare and modified gold electrodes were used as working electrodes in a three electrode electrochemical cell setup with a platinum wire counter electrode and a silver-silver chloride (Ag/AgCl) reference electrode (CH Instruments Inc, Austin).MWNTs were dispersed in DMF using an ultrasonic homogenizer (Omni International Kennesaw, GA) and XP-Pro ultrasonic cleaner, Sharptek, China. For the thylakoid isolation process, a Beckman Coulter Avanti J-E, Brea, CA, centrifuge was used. Oxygen evolution activity was monitored via a Clark-type O_2 electrode (symphony Dissolved Oxygen Probe, VWR International, Atlanta, GA). The photo-electrochemical studies by cyclic voltammetry (CV), current vs. time (i-t curve, steady state current) and electrochemical impedance spectroscopy studies were conducted using CHI-920c model potentiostat (CH Instruments Inc, Austin, TX). The light source for photo-electrochemical studies was from Fiber-Lite model 190 (Dolan-Jenner Industries, MA) with 'high' intensity setting (80 mW cm^{-2}). Surface morphology of the immobilized thylakoids was studied using a scanning electron microscope (SEM) (FEI Inspect F FEG-SEM, Hillsboro, Oregon), atomic force microscope (AFM) (Multimode Nanoscope IIIa, Digital Instruments/Veeco Metrology Group, Ford, PA) and a UV-Visible spectrophotometer (UV-Vis) (Varian Cary 50 Bio, Sparta, NJ). Action spectrums were conducted via a Genesys 10S UV-Vis spectrophotometer (Thermo Scientific, Suwanee, GA).

7.2 Methods

Slurries ofMWNT were prepared by dispersing 1 mg mL^{-1} ofMWNTs in 10 mM DMF by 10 min ultra sonication using an ultrasonic probe at the power

output of 20 watts. The dispersion was sonicated again for 1 h in a bath sonic cleaner. The obtainedMWNT dispersion was used as it is for electrode modifications.

Thylakoids were isolated from *Spinacia oleracea* (spinach) leaves using the procedure given in literature[138], during which the chlorophyll concentration was determined (2.8 mg mL^{-1}) using UV-Vis spectroscopy (see appendix A). The isolated thylakoids were in the form of a pellet and was stored in the dark at -80° C. The DCMU exposed thylakoids were prepared by suspending thylakoids in 0.1 mM DCMU solution and incubated on ice for 30 min.

Prior to thylakoid modification, gold electrodes (0.02 cm^2) were polished with 0.05 µm alumina slurry. The polished electrode was rinsed and ultrasonicated in ddH_2O for 8 min. Then the electrode was modified with 4 µL ofMWNT dispersion and then dried at 70° C. 10 µM PBSE was drop casted on theMWNT modified electrode and incubated for 15 min in ice bath, and then it was washed in DMF to remove the loosely bounded PBSE followed by tricine buffer to neutralize the pH of the electrode surface. Then, 5 µL of thylakoid suspended solution was drop casted on the electrode surface (0.44 µg cm^{-2} chlorophyll concentration) and allowed to immobilize for 1 h in the dark in an ice bath, and then washed with tricine buffer prior to experimentation.

The fuel cell was constructed using thylakoid-MWNT composite modified anode and laccase-MWNT composite modified cathode. The electrodes were held inside a glass vial containing 0.1 M phosphate buffer solution (pH 6.8) as

electrolyte. No oxygen was bubbled during the experiment and the oxygen available in the electrolyte was reduced to water at the cathode.

7.3 Electrochemical Techniques

Cyclic voltammetry (CV) is a potentiodynamic electrochemical measuring technique where the potential of the working electrode varies in a linear fashion versus time. Once the potential reaches a set point, the potential is inverted and follows a reverse linear pathway. This process can be repeated a number of times. The voltammogram displays current at the working electrode versus applied potential voltage. The ramping of the potential is known as the scan rate and it is measured in V/s. Since voltage is relative, the potential is applied between the working and reference electrode. The current generation is measured between the counter and the working electrode.

The analytes along the working electrode will be reduced or oxidized depending on the direction of the scan. If the oxidation and reduction peaks are similar in shape, the reaction is reversible. The scan rate can vary the size of the peaks due to the diffusion limitation of the redox species to the electrode surface. The current peak should be proportional to the square root of the scan rate according to Cottrell's equation.

Amperometric i-t curves apply a constant potential along the working electrode surface and records the current generated. The output graph displays current versus time. To identify the ideal potential setting, Open circuit potential (OCP), or sometimes called Open-circuit voltage, experiments were used to calculate the potential of a system versus time. It monitors the difference in

electrical potential between two terminals of a device that is not connected to a circuit.

Another electrochemical technique used was electrical impedance. Impedance is a measure of the resistance of a circuit during the passage of a current when voltage is applied. An alternating current is applied to the circuit and a complex ratio of the voltage to current is generated. Unlike normal resistance with just magnitude, impedance contains both magnitude and phase against an alternating current; therefore resistance is impedance with a zero phase angle.

CHAPTER 8

INVESTIGATION OF PHOTOSYSTEM II

PSII was isolated from the spinach in an attempt to enhance the photosynthetic energy transfer through selective immobilization of PSII complexes on the electrode using the procedure described in Appendix C. Using the smaller PSII protein from the thylakoid membranes will allow more proteins to be immobilized per surface area and allow only electron transfer from high energy states from the PSII active site (950 mV vs. Ag/AgCl).

8.1 Cyclic Voltammetry

Cyclic voltammetry was used to study redox activity of the unmodified and PSII-MWNT composite electrodes and to identify the possible redox potentials. The electrodes were cycled between -0.7 to 0.5 V vs. Ag/AgCl at a scan rate of 0.02 V s^{-1}. Figure 8.1 compares the cyclic voltammograms of PSII-MWNT composites in the presence and absence of the mediator. The formal potential (E^0) values for the peak was at approximately 0.2 V vs. Ag/AgCl as shown in figure 8.1. The peak was identified as plastocyanin as discussed earlier.

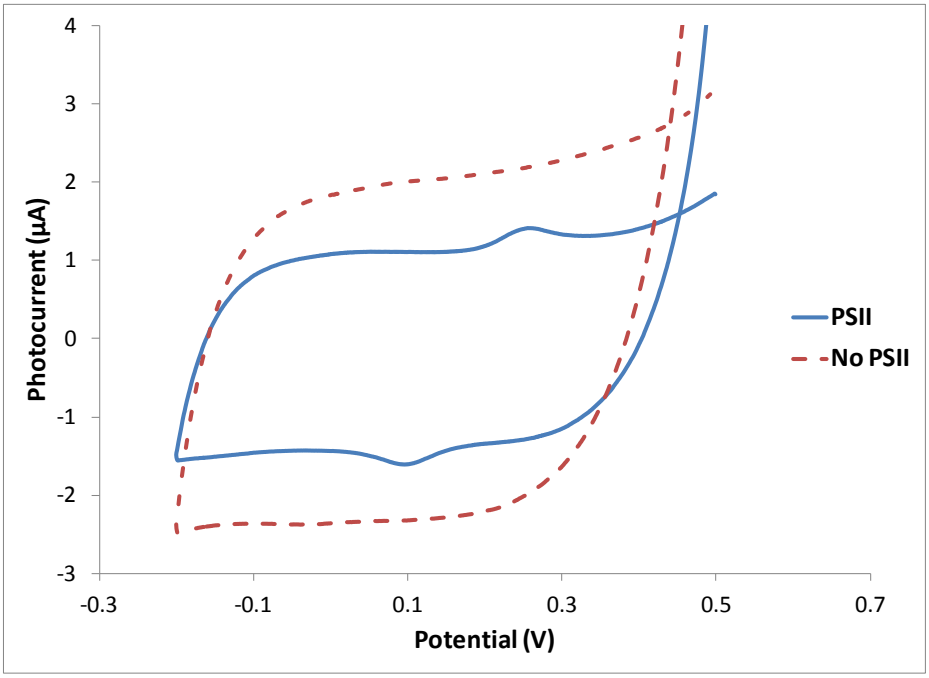

Figure 8.1 PSII CV: Cyclic voltammetry graph of PSII-modified electrodes vs. a control modified electrode lacking the PSII protein. A peak was identified at approximately 0.2 V vs. Ag/AgCl.

8.2 i-t Analysis

The photo-electrochemical activity of the thylakoid-MWNT composite was evaluated at constant anode potential of 0.2 V and the variation of anode current with time was evaluated during light on - light off cycles as shown in Figure 8.2.

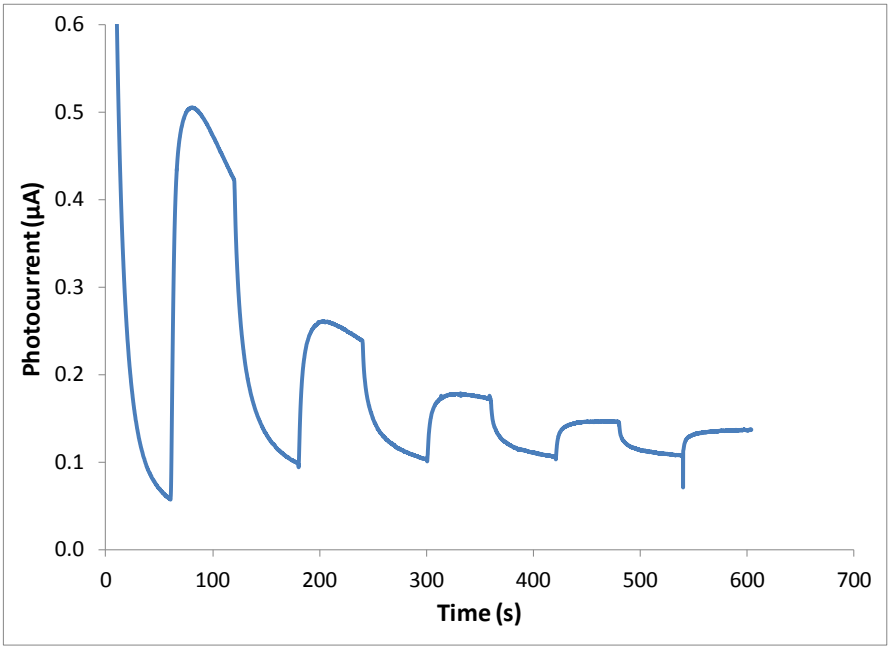

Figure 8.2 i-t Analysis of PSII: The it-curve of PSII-modified electrodes are shown with a maximum photocurrent reaching approximately 0.45μA and a steady state photocurrent of 0.07μA.

Light sensitivity to photocurrent was established using the believed to be isolated PSII proteins. The maximum photocurrent was approximately 0.45μA with a steady state photocurrent of 0.07μA. The photocurrent generation was sensitive to light intensity as shown in Figure 8.3.

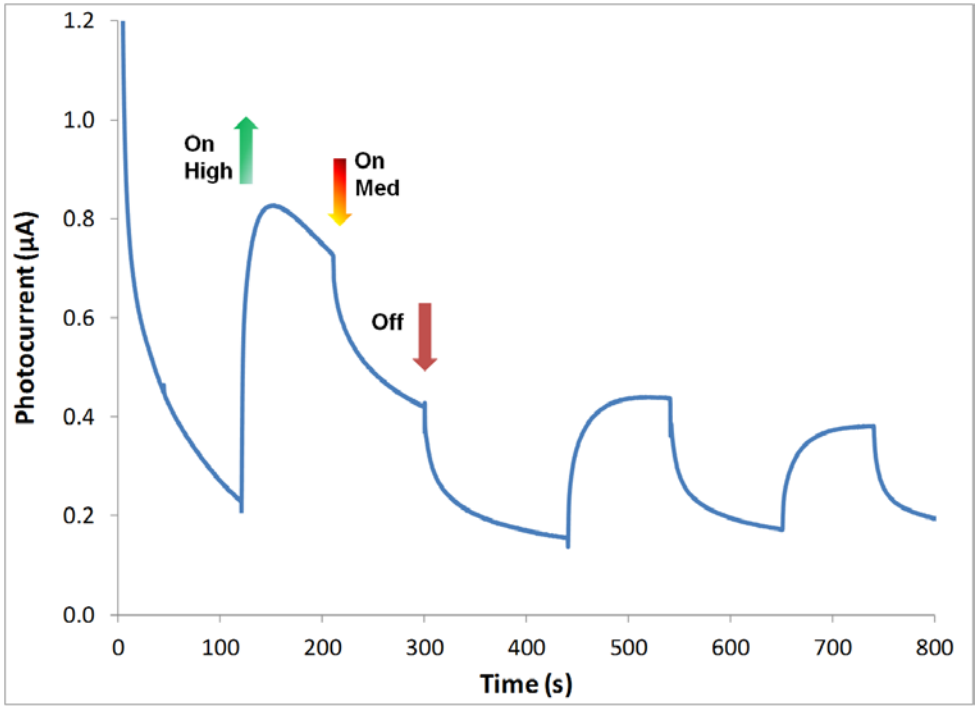

Figure 8.3.**Light Intensity Effect on PSII**: Effect of light intensity on PSII-modified electrodes. High light intensity was turned on at 120s as indicated by the green arrow, medium intensity at 200s indicated by the orange and yellow arrow and no light at 300s as shown by the red arrow. Light on and light off cycles followed.

8.3 Open Circuit Potential

OCP experiments were ran on the PSII-modified electrodes to identify potential shifts due to light exposure. Upon changing the illumination conditions between light and dark over several light on - light off cycles, a clear variation in the open circuit potential was observed, indicative of photo-electrochemical activity for the PSII-MWNT composite electrode. The variation was as high as 20 mV during the first on-off cycle, which eventually subsided during subsequent cycles consistent with the attainment of dynamic equilibrium over time. No such variation in OCP between light and dark was observed for the unmodifiedMWNT electrode (control) in Figure 8.4.

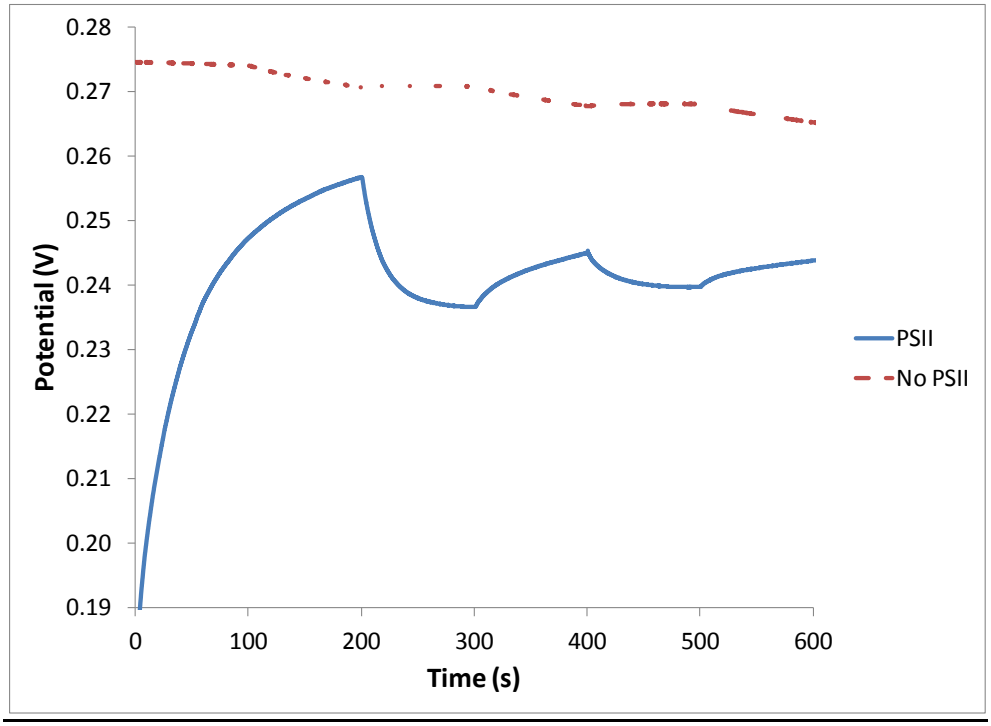

Figure 8.4. OCP of PSII-modified electrodes: (a) Open circuit potentials of unmodified (control) and thylakoid modifiedMWNT electrodes in the presence of 1.5 mM [Fe(CN)6]3-/4-.

8.4 PSII based Fuel Cell

A fuel cell type electrochemical cell was constructed using the PSII-MWNT composite anode and laccase-MWNT composite cathode and tested in an electrolyte solution (PBS buffer pH 6.8). The anode oxidizes water upon illuminated with light using PSII-MWNT composites as photo-biocatalysts, whereas the cathode reduces oxygen to regenerate water in the system using laccase as enzymatic bio-electrocatalyst. The use of lacsase for bio-electrocatalytic oxygen reduction in biological fuel cells has been well established[135-137]. The molecular tethering approach used for thylakoid immobilization was also used for laccase immobilization onMWNT at the cathode. Photocurrent of the system was monitored in various light on and light

off conditions as show in Figure 8.5. They system reached a maximum photocurrent generation of 6.19nA and a steady state photocurrent of 1.1nA during each 60s duty cycle.

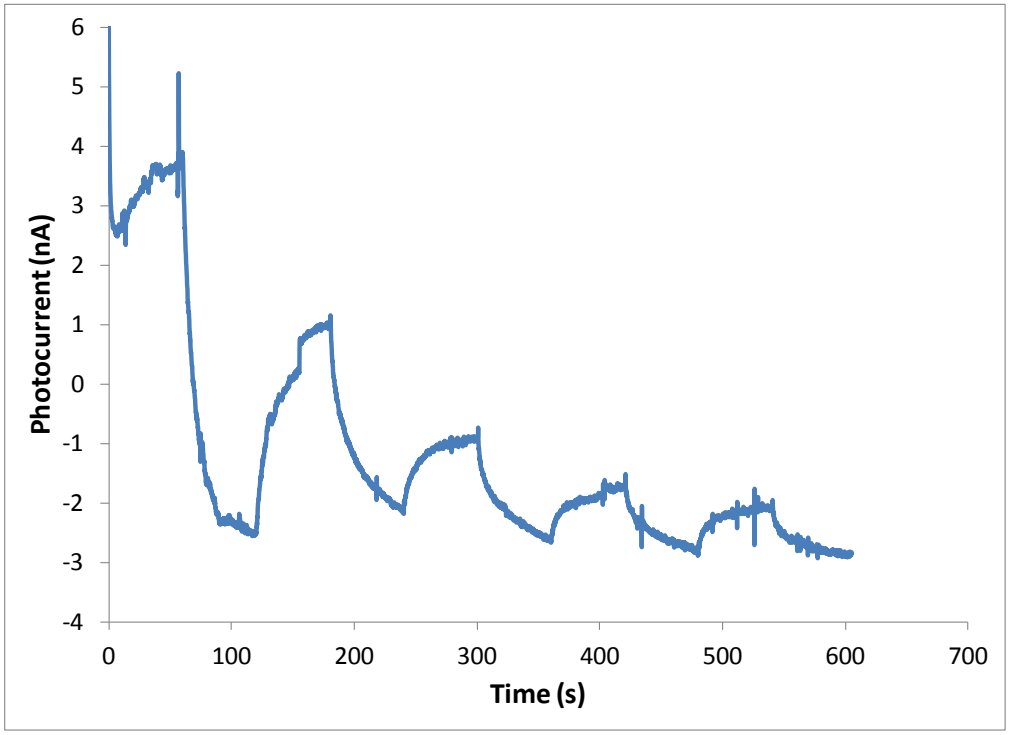

Figure 8.5 PSII Full Cell Duty Cycle: Photocurrent generation using a PSII and laccase enzyme full cell.

8.5 SDS Page

A sodium dodecyl sulfate polyacrylamide gel electrophoresis (SDS-Page) was used to test purity of the PSII isolation process. It was found that the used procedure did not produce extremely pure PSII proteins and that the photoactivity of the PSII experiments performed could be due to impurities in the matrix. Figure 8.6 shows the SDS-Page results of both PSII and thylakoid isolations in killodalton (kD) units. The Dalton is a non-SI unit permitted for molecular mass. The column on the left indicates the molecular weight marker. The middle

column represents isolated PSII proteins and the column on the right represents isolated thylakoid membranes.

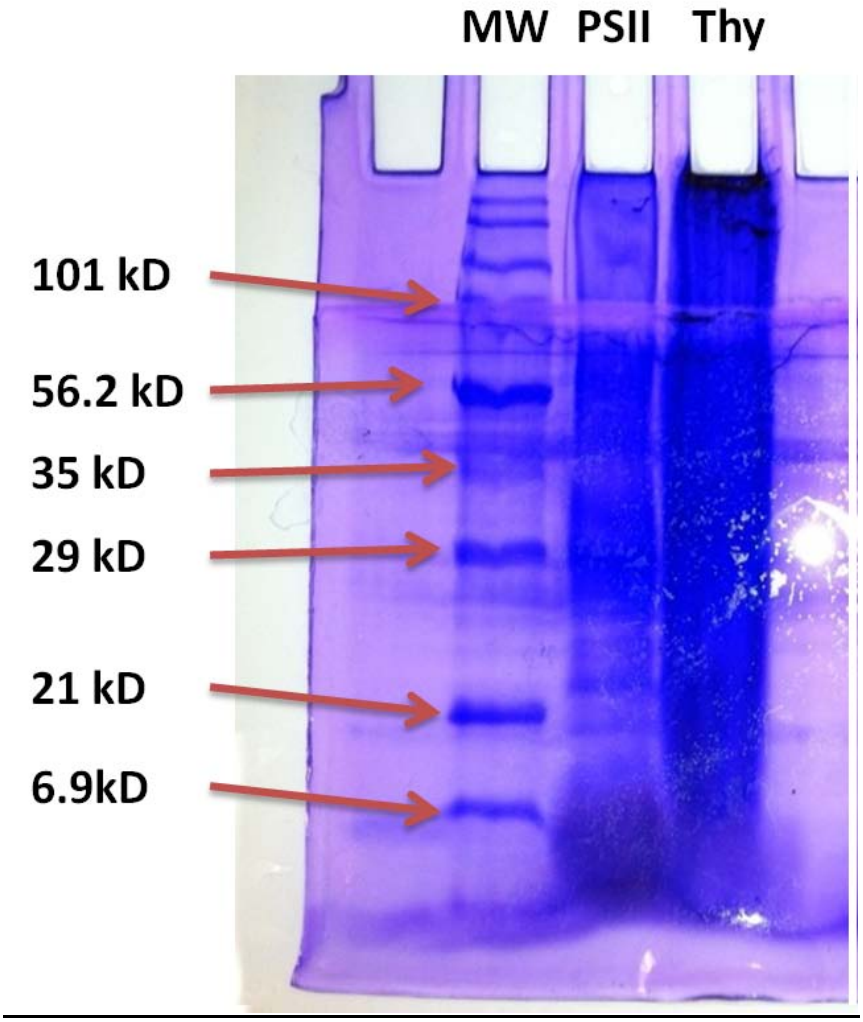

Figure 8.6 SDS-Page: SDS-Page of PSII proteins and thylakoid membranes

CHAPTER 9

CONCLUSION

We have demonstrated photo-current generation using natural photosynthetic sub-organelles and demonstrated its application for light to energy conversion in an electrochemical cell. The advantage of using thylakoid membranes as opposed isolated photosystem proteins lies in the utilization of direct electrochemical redox activities of membrane integral proteins of thylakoids. The thylakoid-MWNT composite electrode yielded a maximum current density of 68 $\mu A/cm^2$ and a steady state current density of 38 $\mu A/cm^2$. The photo-electrochemical cell delivered a maximum power output of 5.3 $\mu W/cm^2$. Future work must focus on understanding the toxicity of ferricyanide mediators and the development of a mediator-free system. A multi-fold improvement in the power density can be achieved by addressing system level issues through improved cell design. The bio-inspired technology offers the potential for green energy harvesting based on natural systems that have evolved over millions of years.

9.1 Acceptable Power Densities

The range of current densities for photosynthetic devices ranges from as little as a few hundred nanoamperes to nearly 400$\mu A\ cm^{-2}$. However, it is difficult to compare multiple devices due to variations in conditions and potential inputs. Each system requires a different overpotential input to adequately produce power, which will be a factor for overall net energy after processing. Also, surface area varies with each prototype. As mentioned earlier, increasing the surface area of the electrode will increase the number of immobilized organelles

which has a positive impact on power output. Many define current density using geometric surface area, which fails to allow a good comparison of devices when surface morphology is modified.

In the case of fuel production, for example hydrogen, the units are expressed in x mol H_2 mg_{Chl}^{-1} h^{-1}. Using chlorophyll as a standardizing agent is convenient; however chlorophyll content varies per species. PSI from spinach has three times as much chlorophyll than that of PSI from *Thermosynechococcus elongates*. Therefore, when looking at the rate of hydrogen production, it is not an exact comparison and the hydrogen output enhances by three when comparing per reaction center. [64] Currently the range of hydrogen production rate vary from a few hundred micromoles to 12.5 mmol mg_{chl}^{-1} h^{-1}, which is the highest reported to date via a sulfur deprived algae in suspension. Once immobilized, the algae saturated at approximately 10 mmol mg_{chl}^{-1} h^{-1}.[146]

9.2 Future Power Needs and Theoretical Limits

Today the world is using energy at an equivalent rate of 200 million barrels of oil per day. Energy is projected to grow at 76% from 2007 to 2030 at an average rate of 2.5% each year. That is 16,429 TWh to 28,930 TWh. [147] Photosynthesis operates at nearly 100% internal quantum efficiency, but the energy storage efficiency is in the range of ~27% in ideal conditions and 1-5% in harsh conditions. [148, 149] This is relatively low compared to the majority of current silicon solar panels operating around 15% efficiency with rates as high as 40% as mentioned earlier. Also, photosynthetic species usually only access the visible region of the light spectrum (from 400nm to 700nm) compared to silicon

PV cells that can extend light absorption in to the ultraviolet and near-infrared regions. Therefore photosynthetic organisms only use about half of the incident solar energy.[150-152] The theoretical limit for single-junction photovoltaic system is a conversion efficiency of ~32% at one-sun intensity and an AM1.5 spectral distribution based on the Shockley-Queisser limit.[150, 153] Due to the chlorophyll band-edge absorption and the structure of the photosynthetic pathway, there is a theoretical limit of 12% efficiency for glucose production from CO_2 and water based on free energy. [12, 154] However the conversion efficiency is further decreased due to energy loss in light absorptions, overpotentials, and respiration; making the theoretical yield 4.6% for C3 plants and 6.0% for C4 plants.[150, 151]

9.3 Potential Applications and Future Directions

The ultimate goal of this is to develop a system that splits water via solar energy into chemical energy that can be collected and applied. This system needs to have high quantum conversion efficiencies and large power density outputs to meet energy demands. Life expectancy and stability of the system needs to be comparable with current solar panels (20-40 years). Figure 9.1 shows the predicted amount of land needed for solar powered farms in order to meet energy demands in the U.S for 2/3 of the country, assuming 1/3 of the power is taken care of by roof top solar panels. The land space is approximately 1.7% of the entire U.S and will provide 3 TW of energy. Assuming the theoretical yield of photosynthetic energy is approximately 5% as mentioned earlier, and solar panels having an average conversion efficiency of 15%, the land mass

required for photosynthetic energy would triple (5.1%) to meet 2/3 of the U.S. energy demands. Other factors, like sun light availability, also come into play.

Figure 9.1. Solar Farm Land Required: Solar farm land requirement to meet 3 TW of solar energy to power the U.S. Adopted from reference 155. [155]

Photosynthetic power efficiencies have grown substantially over the past few decades. Harnessing photosynthetic energy in both photovoltaic and fuel cell based devices proves promising for the future, but there is definitely a long way to go. With the increase in the world population and energy demands, as well as a need for a clean energy source, photosynthetic energy becomes a potentially vital resource. There has been great progress in the field of understanding water oxidation in living organisms and the possible application of using these organisms in energy systems. Genetic modification of organisms to increase stability and production rates could be the next best step to identifying the true capabilities of these living systems. Although mimicking the oxygen evolving complex is still trivial, with the complete structure of PSII in higher order plants still unknown, artificial photosynthesis could supply a more stable catalyst. This system will potentially not require self-repair machinery and will be unaffected by photoinhibition.

There is much research ahead in the field of photosynthetic energy. As we learn more about the stature and capabilities of how nature conducts photosynthesis, we come closer to finding ways to harness energy in a similarly clean way. Photosynthetic energy conversion has the ability to one day be used as remote sensors, small scale battery systems and even a fuel that can replace oil. In the near future, new techniques of optimizing stabilization and high quantum efficiencies must be developed to create a system that can compete with current solar energy sources. Isolation of proteins currently poses a time consuming and inefficient cost to utilizing photosynthetic energy sources. Therefore, a more probable near future solution will be based on photosynthetic bacterium or algae sources. This allows renewable energy without the need to isolate and develop stabilization methods for proteins. Currently cyanobacteria and green algae are the most promising natural sources for this type of application. In conclusion, all of these sources are still very unpredictable since environmental conditions and variations in climate are not controllable. Still the research and current understandings of these systems have improved dramatically over the past decade, and new advances in this field are expected in the near future.

REFERENCES

1. Lubitz, W., Reijerse, E.J. & Messinger, J. Solar water-splitting into H2 and O2: design principles of photosystem II and hydrogenases. *Energy & Environmental Science* **1**, 15-31 (2008).
2. Habjanec, D. in http://interestingenergyfacts.blogspot.com/2009/09/fossil-fuels-facts.html2010).
3. Lebedev, N. et al. Conductive Wiring of Immobilized Photosynthetic Reaction Center to Electrode by Cytochrome c. *Journal of the American Chemical Society* **128**, 12044-12045 (2006).
4. Carpentier, R. & Mimeault, M. The photosynthetic partial reactions involved in photoelectrochemical current generation by thylakoid membranes. *Biotechnology Letters* **9**, 111-116 (1987).
5. Esper, B., Badura, A. & Rögner, M. Photosynthesis as a power supply for (bio-)hydrogen production. *Trends in plant science* **11**, 543-549 (2006).
6. Hall, D. & KRISHNA, R. Immobilized photosynthetic membranes and cells for the production of fuels and chemicals. *Chimica oggi* **7**, 41-47 (1989).
7. Lam, K.B., Irwin, E.F., Healy, K.E. & Lin, L. Bioelectrocatalytic self-assembled thylakoids for micro-power and sensing applications. *Sensors and Actuators B: Chemical* **117**, 480-487 (2006).
8. Das, R. et al. Integration of Photosynthetic Protein Molecular Complexes in Solid-State Electronic Devices. *Nano Letters* **4**, 1079-1083 (2004).
9. Fourmond, V., Lagoutte, B., Sétif, P., Leibl, W. & Demaille, C. Electrochemical Study of a Reconstituted Photosynthetic Electron-Transfer Chain. *Journal of the American Chemical Society* **129**, 9201-9209 (2007).
10. Badura, A. et al. Photo-Induced Electron Transfer Between Photosystem 2 via Cross-linked Redox Hydrogels. *Electroanalysis* **20**, 1043-1047 (2008).
11. Ramasamy, R.P., Luckarift, H.R., Ivnitski, D.M., Atanassov, P.B. & Johnson, G.R. High electrocatalytic activity of tethered multicopper oxidase–carbon nanotube conjugates. *Chemical Communications* **46**, 6045-6047 (2010).
12. Blankenship, R.E. Molecular Mechanisms of Photosynthesis. (Blackwell Science, Oxford, U.K.; 2002).
13. Lewis, N.S. Artificial photosynthesis. *American Scientist* **83**, 534-541 (1995).
14. Sun, L., Hammarstrom, L., Akermark, B. & Styring, S. Towards artificial photosynthesis: ruthenium-manganese chemistry for energy production. *Chemical Society Reviews* **30** (2001).
15. Meyer, T.J. Chemical approaches to artificial photosynthesis. *Accounts of Chemical Research* **22**, 163-170 (1989).
16. Iwuchukwu, I.J. et al. Self-organized photosynthetic nanoparticle for cell-free hydrogen production. *Nat Nano* **5**, 73-79 (2010).
17. Ptak, A., Dudkowiak, A. & Frgckowiak, D. Photoelectrical properties of green bacteria cells and cell fragments located in electrochemical cell. *Journal of Photochemistry and Photobiology A: Chemistry* **115**, 63-68 (1998).
18. Wasielewski, M.R. Photoinduced electron transfer in supramolecular systems for artificial photosynthesis. *Chemical Reviews* **92**, 435-461 (1992).

19. Wasielewski, M.R. Self-Assembly Strategies for Integrating Light Harvesting and Charge Separation in Artificial Photosynthetic Systems. *Accounts of Chemical Research* **42**, 1910-1921 (2009).
20. Rybtchinski, B., Sinks, L.E. & Wasielewski, M.R. Combining Light-Harvesting and Charge Separation in a Self-Assembled Artificial Photosynthetic System Based on Perylenediimide Chromophores. *Journal of the American Chemical Society* **126**, 12268-12269 (2004).
21. Bard, A.J. & Fox, M.A. Artificial Photosynthesis: Solar Splitting of Water to Hydrogen and Oxygen. *Accounts of Chemical Research* **28**, 141-145 (1995).
22. Bhardwaj, R., Pan, R.L. & Gross, E.L. in Photosynthesis VI. Photosynthesis and Productivity, Photosynthesis and Environment. (ed. G. Akoyunoglou) 719-728 (Balaban International Science Services, Philadelphia; 1981).
23. Pan, R.L., Bhardwaj, R. & Gross, E.L. A Photosynthetic Photoelectrochemical Cell using Flavin Mononucleotides as the Electron Acceptor *Photochemistry and Photobiology* **35**, 655-664 (1982).
24. Sanderson, D., Pan, R. & Gross, E. Studies of a photosynthetic photoelectrochemical cell using various electrodes. *Applied Biochemistry and Biotechnology* **8**, 395-405 (1983).
25. Lam, K.B., Johnson, E.A., Chiao, M. & Lin, L. A MEMS Photosynthetic Electrochemical Cell Powered by Subcellular Plant Photosystems. *J Microelectromech S* **15**, 1243-1250 (2006).
26. Okano, M., T. lida, H. Shinohara, H. Kobayashi, and T. Mitamura Water photolysis by a photoelectrochemical cell using an immobilized chloroplasts-methyl viologen system. *Agricultural and Biological Chemistry* **48**, 1977-1983 (1984).
27. Lemieux, S. & Carpentier, R. Properties of a photosystem II preparation in a photoelectrochemical cell. *Journal of Photochemistry and Photobiology B: Biology* **2**, 221-231 (1988).
28. Katz, E.Y., Shkuropatov, A.Y. & Shuvalov, V.A. Electrochemical approach to the development of a photoelectrode on the basis of photosynthetic reaction centers. *Journal of Electroanalytical Chemistry and Interfacial Electrochemistry* **298**, 239-247 (1990).
29. Abe, K., Ishii, A., Hirano, M. & Rusling, J.F. Photoactivity Characteristics of a Biodevice Using Primary Photosynthetic Reaction Centers. *Electroanalysis* **17**, 2266-2272 (2005).
30. Tsujimuraa, S., Wadanob, A., Kanoa, K. & Ikedaa, T. Photosynthetic bioelectrochemical cell utilizing cyanobacteria and water-generating oxidase. *Enzyme and Microbial Technology* **29**, 225-231 (2001).
31. Vittadello , M. et al. Photoelectron Generation by Photosystem II Core Complexes Tethered to Gold Surfaces. *ChemSusChem* **3**, 471-475 (2010).
32. Noji, T. et al. Photosystem II–Gold Nanoparticle Conjugate as a Nanodevice for the Development of Artificial Light-Driven Water-Splitting Systems. *The Journal of Physical Chemistry Letters* **2**, 2448-2452 (2011).
33. Yehezkeli, O. et al. Integrated photosystem II-based photo-bioelectrochemical cells. *Nat Commun* **3**, 742 (2012).

34. Meunier, C.F., Van Cutsem, P., Kwon, Y.-U. & Su, B.-L. Thylakoids entrapped within porous silica gel: towards living matter able to convert energy. *Journal of Materials Chemistry* **19**, 1535-1542 (2009).
35. Guskov, A. et al. Cyanobacterial photosystem II at 2.9-A resolution and the role of quinones, lipids, channels and chloride. *Nat Struct Mol Biol* **16**, 334-342 (2009).
36. Renger, T. & Schlodder, E. Optical properties, excitation energy and primary charge transfer in photosystem II: theory meets experiment. *J Photochem Photobiol B* **104**, 126-141 (2011).
37. Zinth, W. & Wachtveitl, J. The First Picoseconds in Bacterial Photosynthesis—Ultrafast Electron Transfer for the Efficient Conversion of Light Energy. *ChemPhysChem* **6**, 871-880 (2005).
38. Konermann, L. & Holzwarth, A.R. Analysis of the Absorption Spectrum of Photosystem II Reaction Centers: Temperature Dependence, Pigment Assignment, and Inhomogeneous Broadening†. *Biochemistry* **35**, 829-842 (1996).
39. Germano, M. et al. Pigment Organization and Their Interactions in Reaction Centers of Photosystem II: Optical Spectroscopy at 6 K of Reaction Centers with Modified Pheophytin Composition†. *Biochemistry* **40**, 11472-11482 (2001).
40. Durrant, J.R. et al. A multimer model for P680, the primary electron donor of photosystem II. *Proceedings of the National Academy of Sciences* **92**, 4798-4802 (1995).
41. Svensson, B. et al. A Model for the Photosystem II Reaction Center Core Including the Structure of the Primary Donor P680†,‡. *Biochemistry* **35**, 14486-14502 (1996).
42. Bendall D.S., M.R.S. Cyclic photophosphorylation and electron transport. *Biochimica et Biophysica Acta - Bioenergetics* **1229**, 23-38 (1995).
43. DalCorso, G. et al. A Complex Containing PGRL1 and PGR5 Is Involved in the Switch between Linear and Cyclic Electron Flow in Arabidopsis. *Cell* **132**, 273-285 (2008).
44. Nakayama, M., Akashi, T. & Hase, T. Plant sulfite reductase: molecular structure, catalytic function and interaction with ferredoxin. *Journal of Inorganic Biochemistry* **82**, 27-32 (2000).
45. Knaff, D.B. & Hirasawa, M. Ferredoxin-dependent chloroplast enzymes. *Biochimica et Biophysica Acta (BBA) - Bioenergetics* **1056**, 93-125 (1991).
46. Shanklin J., C.E.B. Desaturation and related modifications of fatty acids. *Annual Review of Plant Biology* **49**, 611-641 (1998).
47. Jacobs, J., Pudollek, S., Hemschemeier, A. & Happe, T. A novel, anaerobically induced ferredoxin in Chlamydomonas reinhardtii. *FEBS Letters* **583**, 325-329 (2009).
48. Terauchi A.M., L.S.-F., Zaffagnini M., Tappa S., Hirasawa M., Tripathy J.N., Knaff D.B., Merchant S.S. Pattern of expression and substrate specificity of chloroplast ferredoxins from Chlamydomonas reinhardtii. *Journal of Biological Chemistry* **284**, 25867-25878 (2009).
49. Hanke, G.T. & Hase, T. Variable Photosynthetic Roles of Two Leaf-type Ferredoxins in Arabidopsis, as Revealed by RNA Interference†. *Photochemistry and Photobiology* **84**, 1302-1309 (2008).

50. Tharayil-Santhakumar, N. in Plant & Soil Sciences (University of Massachusetts, Amherst, MA; 2004).
51. Fuerst, E.P.a.N., M.A. Interaction of herbicides with photosynthetic electron transport. *Weed Science* **39**, 458-464 (1991).
52. DUYSENs LNH, H.S. Mechanisms of two photochemical reactions in algae as studied by means of fluorescence. *In Studies in Microalgae and Photosynthetic Bacteria (Japan Society of Plant Physiologists)*, 353-372 (1963).
53. Ouitrakul, R. & Izawa, S. Electron transport and photophosphorylation in chloroplasts as a function of the electron acceptor. II. Acceptor-specific inhibition by KCN. *Biochimica et Biophysica Acta (BBA) - Bioenergetics* **305**, 105-118 (1973).
54. Roberts, A.G. & Kramer, D.M. Inhibitor "double occupancy" in the Q(o) pocket of the chloroplast cytochrome b6f complex. *Biochemistry* **40**, 13407-13412 (2001).
55. Roberts, A.G., Bowman, M.K. & Kramer, D.M. The inhibitor DBMIB provides insight into the functional architecture of the Qo site in the cytochrome b6f complex. *Biochemistry* **43**, 7707-7716 (2004).
56. Larom, S., Salama, F., Schuster, G. & Adir, N. Engineering of an alternative electron transfer path in photosystem II. *Proceedings of the National Academy of Sciences* **107**, 9650-9655 (2010).
57. Ulas, G.z. & Brudvig, G.W. Redirecting Electron Transfer in Photosystem II from Water to Redox-Active Metal Complexes. *Journal of the American Chemical Society* **133**, 13260-13263 (2011).
58. Shibamoto, T., Kato, Y., Sugiura, M. & Watanabe, T. Redox Potential of the Primary Plastoquinone Electron Acceptor QA in Photosystem II from Thermosynechococcus elongatus Determined by Spectroelectrochemistry. *Biochemistry* **48**, 10682-10684 (2009).
59. Robinson, H.H. & Crofts, A.R. Kinetics of the oxidation—reduction reactions of the photosystem II quinone acceptor complex, and the pathway for deactivation. *FEBS Letters* **153**, 221-226 (1983).
60. Fultz, M.L. & Durst, R.A. Mediator compounds for the electrochemical study of biological redox systems: a compilation. *Analytica Chimica Acta* **140**, 1-18 (1982).
61. Szentrimay, R., Yeh, P. & Kuwana, T. in Electrochemical Studies of Biological Systems, Vol. 38 143-169 (AMERICAN CHEMICAL SOCIETY, 1977).
62. V. T. Taniguchi, N.S.-S., F. C. Anson and H. B. Gray Thermodynamics of metalloprotein electron transfer reactions. *Pure and Appied Chemistry* **52**, 2275-2281 (1980).
63. Acharya, K., Zazubovich, V., Reppert, M. & Jankowiak, R. Primary Electron Donor(s) in Isolated Reaction Center of Photosystem II from Chlamydomonas reinhardtii. *The Journal of Physical Chemistry B* **116**, 4860-4870 (2012).
64. Krassen, H., Ott, S. & Heberle, J. In vitro hydrogen production-using energy from the sun. *Physical Chemistry Chemical Physics* **13**, 47-57 (2011).
65. Jacobson, M.Z., Colella, W.G. & Golden, D.M. Cleaning the Air and Improving Health with Hydrogen Fuel-Cell Vehicles. *Science* **308**, 1901-1905 (2005).

66. Vignais, P.M. & Colbeau, A. Molecular biology of microbial hydrogenases. *Curr Issues Mol Biol* **6**, 159-188 (2004).
67. Lyon, E.J. et al. UV-A/blue-light inactivation of the 'metal-free' hydrogenase (Hmd) from methanogenic archaea. *Eur J Biochem* **271**, 195-204 (2004).
68. Happe, T., Hemschemeier, A., Winkler, M. & Kaminski, A. Hydrogenases in green algae: do they save the algae's life and solve our energy problems? *Trends Plant Sci* **7**, 246-250 (2002).
69. Girbal, L. et al. Homologous and heterologous overexpression in Clostridium acetobutylicum and characterization of purified clostridial and algal Fe-only hydrogenases with high specific activities. *Appl Environ Microbiol* **71**, 2777-2781 (2005).
70. Ghirardi, M.L. et al. Hydrogenases and Hydrogen Photoproduction in Oxygenic Photosynthetic Organisms*. *Annual Review of Plant Biology* **58**, 71-91 (2007).
71. Vignais, P.M., Billoud, B. & Meyer, J. Classification and phylogeny of hydrogenases. *Fems Microbiol. Rev.* **25**, 455-501 (2001).
72. Mishra, J., Kumar, N., Ghosh, A.K. & Das, D. Isolation and molecular characterization of hydrogenase gene from a high rate of hydrogen-producing bacterial strain Enterobacter cloacae IIT-BT 08. *International Journal of Hydrogen Energy* **27**, 1475-1479 (2002).
73. Seibert, M., Vol. 2012National Renewable Energy Laboratory, Golden, CO; 2009).
74. Rosen, B.A. et al. Ionic liquid-mediated selective conversion of CO(2) to CO at low overpotentials. *Science* **334**, 643-644 (2011).
75. Rakowski Dubois, M. & Dubois, D.L. Development of Molecular Electrocatalysts for CO2 Reduction and H2 Production/Oxidation. *Accounts of Chemical Research* **42**, 1974-1982 (2009).
76. Hollinger, A.S. et al. Nanoporous separator and low fuel concentration to minimize crossover in direct methanol laminar flow fuel cells. *Journal of Power Sources* **195**, 3523-3528 (2010).
77. Stewart, W.D.P. Some Aspects of Structure and Function in N Fixing Cyanobacteria. *Annual Review of Microbiology* **34**, 497-536 (1980).
78. Fay, P. Photostimulation of nitrogen fixation in Anabaena cylindrica. *Biochimica et Biophysica Acta (BBA) - Bioenergetics* **216**, 353-356 (1970).
79. Lambert, G.R. & Smith, G.D. THE HYDROGEN METABOLISM OF CYANOBACTERIA (BLUE-GREEN ALGAE). *Biological Reviews* **56**, 589-660 (1981).
80. Kumar D., K.H.D. Effect of monochromatic lights on nitrogen fixation and hydrogen evolution in the isolated heterocysts of Anabaena sp. strain CA. *International Journal of Hydrogen Energy* **16**, 397-401 (1991).
81. Das, D. & Veziroğlu, T.N. Hydrogen production by biological processes: a survey of literature. *International Journal of Hydrogen Energy* **26**, 13-28 (2001).
82. S. Sarker, K.D.P., A.K. Kashyap Hydrogen photoproduction by filamentous non-heterocystous cyanobacterium Pleatonemaboryanna and simultaneous release of ammonia. *Int J Hydrogen Energy* **16**, 397-401 (1992).
83. Lambert, G.R. & Smith, G.D. Hydrogen metabolism by filamentous cyanobacteria. *Archives of Biochemistry and Biophysics* **205**, 36-50 (1980).

84. Melnicki, M.R. et al. Sustained h2 production driven by photosynthetic water splitting in a unicellular cyanobacterium. *MBio* **3**, 00197-00112 (2012).
85. Grimme, R.A., Lubner, C.E., Bryant, D.A. & Golbeck, J.H. Photosystem I/Molecular Wire/Metal Nanoparticle Bioconjugates for the Photocatalytic Production of H2. *Journal of the American Chemical Society* **130**, 6308-6309 (2008).
86. Hanna, M.C. & Nozik, A.J. Solar conversion efficiency of photovoltaic and photoelectrolysis cells with carrier multiplication absorbers. *Journal of Applied Physics* **100**, 074510 (2006).
87. Li, G. et al. High-efficiency solution processable polymer photovoltaic cells by self-organization of polymer blends. *Nat Mater* **4**, 864-868 (2005).
88. Sista, S. et al. Highly Efficient Tandem Polymer Photovoltaic Cells. *Advanced Materials* **22**, 380-383 (2010).
89. Guo, X. et al. Ultrathin and efficient flexible polymer photovoltaic cells based on stable indium-free multilayer transparent electrodes. *Journal of Materials Chemistry* **22**, 17176-17182 (2012).
90. Powles, S.B. Photoinhibition of Photosynthesis Induced by Visible Light. *Annual Review of Plant Physiology* **35**, 15-44 (1984).
91. Vauthey, S., Santoso, S., Gong, H., Watson, N. & Zhang, S. Molecular self-assembly of surfactant-like peptides to form nanotubes and nanovesicles. *Proceedings of the National Academy of Sciences* **99**, 5355-5360 (2002).
92. Zhao, X. et al. Designer short peptide surfactants stabilize G protein-coupled receptor bovine rhodopsin. *Proceedings of the National Academy of Sciences* **103**, 17707-17712 (2006).
93. Terasaki, N. et al. Fabrication of novel photosystem I–gold nanoparticle hybrids and their photocurrent enhancement. *Thin Solid Films* **499**, 153-156 (2006).
94. Ciesielski, P.N. et al. Functionalized Nanoporous Gold Leaf Electrode Films for the Immobilization of Photosystem I. *ACS Nano* **2**, 2465-2472 (2008).
95. Kavakka, J.S. et al. Noncovalent attachment of pyro-pheophorbide a to a carbon nanotube. *Chemical Communications*, 519-521 (2007).
96. Armstrong, F.A., Hill, H.A.O. & Walton, N.J. Reactions of electron-transfer proteins at electrodes. *Quarterly Reviews of Biophysics* **18**, 261-322 (1985).
97. Yuji Furukawa1, T.M.a.K.M. Design principle and prototyping of a direct photosynthetic/metabolic biofuel cell (DPMFC) *Journal of Micromechanics and Microengineering* **16**, S220 (2006).
98. Nakamura, C., Hasegawa, M., Yasuda, Y. & Miyake, J. Self-assembling photosynthetic reaction centers on electrodes for current generation. *Applied Biochemistry and Biotechnology* **84-86**, 401-408 (2000).
99. Trammell, S.A. et al. Effects of Distance and Driving Force on Photoinduced Electron Transfer between Photosynthetic Reaction Centers and Gold Electrodes. *The Journal of Physical Chemistry C* **111**, 17122-17130 (2007).
100. Trammell, S.A., Spano, A., Price, R. & Lebedev, N. Effect of protein orientation on electron transfer between photosynthetic reaction centers and carbon electrodes. *Biosensors and Bioelectronics* **21**, 1023-1028 (2006).

101. Badura, A. et al. Light-Driven Water Splitting for (Bio-)Hydrogen Production: Photosystem 2 as the Central Part of a Bioelectrochemical Device. *Photochemistry and Photobiology* **82**, 1385-1390 (2006).
102. Liu, J., Lauterbach, R., Paulsen, H. & Knoll, W. Immobilization of Light-Harvesting Chlorophyll a/b Complex (LHCIIb) Studied by Surface Plasmon Field-Enhanced Fluorescence Spectroscopy. *Langmuir* **24**, 9661-9667 (2008).
103. Malik, S. et al. A self-assembling self-repairing microbial photoelectrochemical solar cell. *Energy & Environmental Science* **2**, 292-298 (2009).
104. Carpentier, R., Lemieux, S., Mimeault, M., Purcell, M. & Goetze, D.C. A photoelectrochemical cell using immobilized photosynthetic membranes. *Journal of Electroanalytical Chemistry and Interfacial Electrochemistry* **276**, 391-401 (1989).
105. Salin, M. *Physiol. Plant* **72**, 439 (1987).
106. Guilbault, G.G. & Lubrano, G.J. An enzyme electrode for the amperometric determination of glucose. *Analytica Chimica Acta* **64**, 439-455 (1973).
107. Goldsmith, J.O. & Boxer, S.G. Rapid isolation of bacterial photosynthetic reaction centers with an engineered poly-histidine tag. *Biochimica et Biophysica Acta (BBA) - Bioenergetics* **1276**, 171-175 (1996).
108. Trammell, S.A., Wang, L., Zullo, J.M., Shashidhar, R. & Lebedev, N. Orientated binding of photosynthetic reaction centers on gold using Ni□NTA self-assembled monolayers. *Biosensors and Bioelectronics* **19**, 1649-1655 (2004).
109. Bedford, N.M., Winget, G.D., Punnamaraju, S. & Steckl, A.J. Immobilization of Stable Thylakoid Vesicles in Conductive Nanofibers by Electrospinning. *Biomacromolecules* **12**, 778-784 (2011).
110. Mershin, A. et al. Self-assembled photosystem-I biophotovoltaics on nanostructured TiO2 and ZnO. *Sci. Rep.* **2** (2012).
111. Boghossian, A.A., Ham, M.-H., Choi, J.H. & Strano, M.S. Biomimetic strategies for solar energy conversion: a technical perspective. *Energy & Environmental Science* **4**, 3834-3843 (2011).
112. Enami, I. et al. Total immobilization of the extrinsic 33 kDa protein in spinach Photosystem II membrane preparations. Protein stoichiometry and stabilization of oxygen evolution. *Biochimica et Biophysica Acta (BBA) - Bioenergetics* **1060**, 224-232 (1991).
113. de Wijn R, v.G.H. Kinetics of electron transfer from Q(a) to Q(b) in photosystem II. *Biochemistry* **40**, 11912-11922 (2001).
114. Badura, A. et al. Photo-induced electron transfer between photosystem 2 via cross-linked redox hydrogels. *Electroanalysis* **20**, 1043-1047 (2008).
115. Badura, A. et al. Light-driven water splitting for (bio-)hydrogen production: photosystern 2 as the central part of a bioelectrochemical device. *Photochemistry and Photobiology* **82**, 1385-1390 (2006).
116. Lam, K.B., Johnson, E.A., Chiao, M., Lin, L. A MEMS Photosynthetic Electrochemical Cell Powered by Subcellular Plant Photosystems *Journal of Microelectromechanical Systems* **15**, 1243-1250 (2006).
117. McDermott, G. et al. Crystal structure of an integral membrane light-harvesting complex from photosynthetic bacteria. *Nature* **374**, 517-521 (1995).

118. Sanders, J.K.M. Porphyrin Handbook, Vol. 3. (Academic Press, New York; 2000).
119. Iengo, E., Zangrando, E. & Alessio, E. Cover Picture: Discrete Supramolecular Assemblies of Porphyrins Mediated by Coordination Compounds (Eur. J. Inorg. Chem. 13/2003). *European Journal of Inorganic Chemistry* **2003**, 2361-2361 (2003).
120. Fujishima, A. & Honda, K. Electrochemical Photolysis of Water at a Semiconductor Electrode. *Nature* **238**, 37-38 (1972).
121. Licht, S. et al. Over 18% solar energy conversion to generation of hydrogen fuel; theory and experiment for efficient solar water splitting. *International Journal of Hydrogen Energy* **26**, 653-659 (2001).
122. Maeda, K. et al. Photocatalyst releasing hydrogen from water. *Nature* **440**, 295 (2006).
123. Puntoriero, F. et al. Photoinduced water oxidation using dendrimeric Ru(II) complexes as photosensitizers. *Coordination Chemistry Reviews* **255**, 2594-2601 (2011).
124. Zong, R. & Thummel, R.P. A New Family of Ru Complexes for Water Oxidation. *Journal of the American Chemical Society* **127**, 12802-12803 (2005).
125. Kanan, M.W. & Nocera, D.G. In Situ Formation of an Oxygen-Evolving Catalyst in Neutral Water Containing Phosphate and Co2+. *Science* **321**, 1072-1075 (2008).
126. Joya, K.S. & de Groot, H.J.M. Biomimetic molecular water splitting catalysts for hydrogen generation. *International Journal of Hydrogen Energy* **37**, 8787-8799 (2012).
127. Lai, Y.-H. et al. Facile assembly of an efficient CoOx water oxidation electrocatalyst from Co-containing polyoxotitanate nanocages. *Chemical Communications* (2013).
128. Esswein, A.J., Surendranath, Y., Reece, S.Y. & Nocera, D.G. Highly active cobalt phosphate and borate based oxygen evolving catalysts operating in neutral and natural waters. *Energy & Environmental Science* **4**, 499-504 (2011).
129. Liu, H., Cheng, S. & Logan, B.E. Power Generation in Fed-Batch Microbial Fuel Cells as a Function of Ionic Strength, Temperature, and Reactor Configuration. *Environmental Science & Technology* **39**, 5488-5493 (2005).
130. Ringeisen, B.R. et al. High Power Density from a Miniature Microbial Fuel Cell Using Shewanella oneidensis DSP10. *Environmental Science & Technology* **40**, 2629-2634 (2006).
131. Moon, H., Chang, I.S. & Kim, B.H. Continuous electricity production from artificial wastewater using a mediator-less microbial fuel cell. *Bioresour Technol* **97**, 621-627 (2006).
132. Liu, H. & Logan, B.E. Electricity Generation Using an Air-Cathode Single Chamber Microbial Fuel Cell in the Presence and Absence of a Proton Exchange Membrane. *Environmental Science & Technology* **38**, 4040-4046 (2004).
133. Fan, Y., Hu, H. & Liu, H. Enhanced Coulombic efficiency and power density of air-cathode microbial fuel cells with an improved cell configuration. *Journal of Power Sources* **171**, 348-354 (2007).

134. Masamoto, K., Itoh, S. & Nishimura, M. Salt-induced pH changes in spinach chloroplast suspension. Changes in surface potential and surface pH of thylakoid membranes. *Biochimica et Biophysica Acta (BBA) - Bioenergetics* **591**, 142-152 (1980).
135. Ramasamy, R.P., Luckarift, H.R., Ivnitski, D.M., Atanassov, P.B. & Johnson, G.R. High electrocatalytic activity of tethered multicopper oxidase-carbon nanotube conjugates. *Chemical Communications* **46**, 6045-6047 (2010).
136. Parimi, N.S., Umasankar, Y., Atanassov, P. & Ramasamy, R.P. Kinetic and Mechanistic Parameters of Laccase Catalyzed Direct Electrochemical Oxygen Reduction Reaction. *ACS Catalysis* **2**, 38-44 (2011).
137. Lau, C. et al. Design of Carbon Nanotube-Based Gas-Diffusion Cathode for O2 Reduction by Multicopper Oxidases. *Advanced energy materials* **2**, 162-168 (2012).
138. Carpentier, R. Photosynthesis Research Protocols, Vol. 274. (Humana Press, Totowa, N.J; 2004).
139. Walker, D. the Use of the Oxygen Electrode and Fluorescence Probes in Simple Measurements of Photosynthesis. (Sheffield, UK; 1990).
140. Semenova, G.A. The thylakoid membrane in a wide pH range. *Journal of Plant Physiology* **159**, 613-625 (2002).
141. Bartlett, P.N. Bioelectrochemistry Fundamentals, Experimental Techniques and Applications. (John Wiley & Sons, Ltd, UK; 2008).
142. Richard, M. & Pedro, J.A. Identification of a g = 1.90 high-potential iron-sulfur protein in chloroplasts. *Biochem Bioph Res Co* **63**, 1157-1160 (1975).
143. Sanderson, D.G., Anderson, L.B. & Gross, E.L. Determination of the redox potential and diffusion coefficient of the protein plastocyanin using optically transparent filar electrodes. *Biochimica et Biophysica Acta (BBA) - Bioenergetics* **852**, 269-278 (1986).
144. Shie, J.-W., Yogeswaran, U. & Chen, S.-M. Electroanalytical properties of cytochrome c by direct electrochemistry on multi-walled carbon nanotubes incorporated with DNA biocomposite film. *Talanta* **74**, 1659-1669 (2008).
145. Duysens, L.N.M. 3-(3,4-Dichlorophenyl)-1,1-dimethylurea (DCMU) Inhibition of System II and Light-Induced Regulatory Changes in Energy Transfer Efficiency. *Biophys J* **12**, 858-863 (1972).
146. Ghirardi, M.L. (ed. U.S.D.o.E. National Renewable Energy Laboratory)2011).
147. , Vol. 2012. (ed. W.N. Association)2012).
148. Zhu, X.G., Long, S.P. & Ort, D.R. What is the maximum efficiency with which photosynthesis can convert solar energy into biomass? *Curr. Opin. Biotechnol.* **19**, 153-159 (2008).
149. Brudvig, G.F.M.a.G.W. Energy Conversion in Photosynthesis: A Paradigm for Solar Fuel Production. *Annu. Rev. Condens.Matter Phys* **2**, 303-327 (2011).
150. Blankenship, R.E. et al. Comparing Photosynthetic and Photovoltaic Efficiencies and Recognizing the Potential for Improvement. *Science* **332**, 805-809 (2011).
151. Zhu, X.-G., Long, S.P. & Ort, D.R. Improving Photosynthetic Efficiency for Greater Yield. *Annual Review of Plant Biology* **61**, 235-261 (2010).
152. Bolton, J.R. & Hall, D.O. Photochemical Conversion and Storage of Solar Energy. *Annual Review of Energy* **4**, 353-401 (1979).

153. Shockley, W. & Queisser, H.J. DETAILED BALANCE LIMIT OF EFFICIENCY OF P-N JUNCTION SOLAR CELLS. *Journal of Applied Physics* **32**, 510-& (1961).
154. Walker, D.A. Biofuels, facts, fantasy, and feasibility. *J. Appl. Phycol.* **21**, 509-517 (2009).
155. Lewis, N., Vol. 2012Caltech, The Lewis Group; 2004).

APPENDEX A

CHLOROPHYLL CONCENTRATION CALCUATION

The chlorophyll concentration was calculated by applying the data from UV-Vis spectrum in equation (E1),

$$chlorophyll\left(\frac{mg}{mL}\right) = \frac{8.02 \times A663 + 20.2 \times A645}{10} \quad \rightarrow \text{(E1)}$$

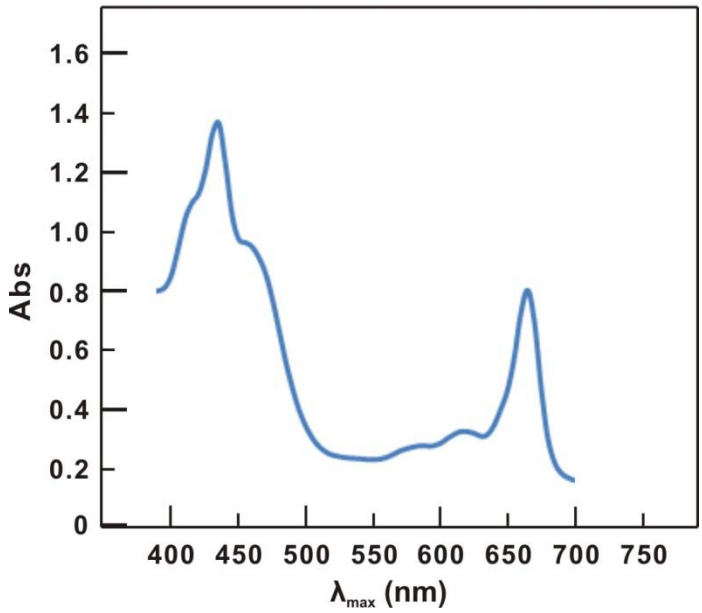

Figure A1. *UV-Vis spectrum of thylakoid membranes to calculate chlorophyll concentration.*

APPENDEX B

THYLAKOID ISOLATION PROCEDURE

The isolation of thylakoids membranes are shown in the following procedure up until step 9. The rest of the procedure is for the isolation of PSI proteins.

App B.1 Solutions and Buffers

Buffer A: (Homogenization buffer) 50mM Tricine/KOH pH 7.8, 0.4M Sorbitol

Buffer B: (Resuspension buffer) 20mM Tricine/KOH pH 7.8, 5mM EDTA, 50mM Sorbitol

Buffer C: 20mM Tricine/KOH pH 7.8

Buffer D: 1.0 M sucrose, 20mM Tricine/ KOH pH 7.8, Triton X-100 at 0.04% m/v

Buffer E: 0.1M sucrose, 20mM Tricine/ KOH pH 7.8, Triton X-100 at 0.04% m/v

Buffer F: 0.5 M sucrose, 20mM Tricine/KOH pH 7.8

1M $MgCl_2$

2M KCl

App B.2 Preparations of Solutions

1. Solution Preparation Stock:

   To prepare a stock solution of 0.5M Tricine/KOH pH 7.8, dissolve 44.8g of Tricine (179.2g/mol) in 300mL of ddH_2O. Adjust pH to 7.8 using 4M KOH solution and add ddH_2O to final volume of 500mL.

To prepare a stock solution of 2M Sorbitol, dissolve 182.17g of Sorbitol (182.173g/mol) in 300mL ddH_2O and bring to final volume of 500mL using ddH_2O.

Solutions:

Buffer A: Mix 100mL of stock Tricine with 200mL of stock Sorbitol, dilute with ddH_2O to final volume of 1000mL.

Buffer B: Dissolve 0.292g EDTA (292.25g/mol) in 100mL ddH_2O, add 8mL of stock Tricine and 5mL stock sorbitol. Adjust volume to 200mL using ddH2O.

Buffer C: Mix 8mL of stock Tricine with 192mL of ddH_2O.

Buffer D: To prepare 100mL, dissolve 34.23g (342.2992g/mol) sucrose in 50mL ddH_2O, add 4mL 0.5M Tricine stock, add 0.380mL Triton X-100 from 10.5% m/v stock and adjust up 100mL to volume using ddH_2O.

Buffer E: To prepare 100mL, dissolve 3.42g (342.2992g/mol) sucrose in 50mL ddH_2O, add 4 mL 0.5M Tricine stock, add 0.380mL Triton X-100 from 10.5% m/v stock and adjust up 100mL to volume using ddH_2O.

Note: Do not vortex anything!

Triton X-100 is purchased as a 10.5% (w/v) solution in ddH_2O. Use as received. If different stock concentration is purchased adjust all calculations and formulas appropriately.

1M $MgCl_2$: To prepare 100mL; mix 9.52g (95.211g/mol) $MgCl_2$ in 75mL ddH_2O and bring up to volume using ddH_2O.

2M KCl: To prepare 100mL mix 14.9g (74.543g/mol) KCl in 75mL of ddH_2O and bring up to volume using ddH_2O.

App B.3 Preparation of Thylakoids

Note:

- Experiments should be conducted in dark conditions
- Buffers should be stored in ice box

1. Take 400g of Spinach Leaves and wash with cold distilled water.
2. Put into chilled distilled water and put into dark at 4ºC for at least 2h.
3. Chop leaves in food processor.
4. Homogenize with blender using Buffer A per 1.5ml to 1g of spinach. (600ml for 400g of spinach). Note: Do not blend for longer than 30s.
5. Collect in Erlenmeyer flasks with high contact surface area to keep it cold. Filter through four layers of cheese cloth (VWR) & Mira cloth (calbio). From step 6 to 9 carryout at 4ºC (cold room)

6. Centrifuge the supernatant at 10,000g for 20 min.
7. Discard supernatant and suspend pellet in the minimum volume of Buffer B (100 ml in total). Use a Potter Homogenizer to ensure particles are broken up; also use a paint brush to re-suspend.
8. Determine chlorophyll concentration and divide suspension into 60mg (chlorophyll) aliquots. Use syringe for pipetting (very tough).
9. Centrifuge at 10,000g for 20min. Discard the supernatant. Cover with aluminum foil and store at -80ºC.

App B.4 Isolation of LHCII

1. Use paint brush and punch homogenizer, re-suspend 160mg sample in cold Buffer C (less than 50 to 60ml, don't dilute it too much) using Potter Homogenizer. Note: Use the minimum amount of Buffer C.
2. Adjust chlorophyll content to 0.8 mg/ml. (Dilute by adding Buffer C in aluminum foiled conical flask). Triton works better between 0.8-1.0 mg/ml chlorophyll.

   Note: In step 2, make 1mg/ml and add triton to further dilute it to 0.8-1.0 mg/ml final concentration.
3. Add Triton to final concentration of 0.9% w/v.
4. Slow stir on ice for 45min until the clouds disappear.
5. At this time prepare the sucrose gradient in ultra-centrifuge tubes (centrifuge withstand 300,000g) using the gradient marker by combining Buffers D and E.

6. Centrifuge at 30,000g 45min and discard the pellet (follow step 4), supernatant must have all protein in solubilized form.
7. Layer on a sucrose gradient of 0.1-1.0M sucrose (top to bottom) with sucrose gradient exceeding two times the volume of LHCII solution.
8. Centrifuge at 60,000rmp for 5h using the Beckman Ti70 rotor in the ultra-centrifuge. (265,000g).
9. Carefully remove the LHCII band without disturbing the pellet on the bottom of the tube. If the LHCII band is very close to pellet, leave a small amount of the lower portion of the band behind in order to keep LHCII pure. (use 18 gauge needle syringe to suck out)
10. Add $MgCl_2$ to final concentration of 25mM and then quickly add KCl to final concentration of 150mM.
11. Then stir for 25 min at room temperature.
12. Layer suspension on Buffer F and centrifuge at 30,000g for 40 min.
13. Discard the supernatant. Note: At this step the pellet may be frozen for a short period of time for later re-suspension.
14. Wash the pellet with either
    a. 0.6% Beta Octyl Glucoside (BOG,) 10mM Tris/HCl pH 7.8 or
    b. 0.01% Dodecyl maltoside (DM,) 10mM Tris/HCl pH 7.8.

    Note: It is crucial to use the smallest possible volume to wash the pellet and less than 1mL should always be sued. This step washes out excess Mg and K and makes for easier solubilization later, using too

much buffer or doing for too long may lead to the protein not precipitating in the next step.

15. Immediately centrifuge at 5,000rpm in the microcentrifuge for 5 min.
16. Discard Supernatant and resuspend pellet in the desired detergent buffer
    a. 1.8% BOG, 10mM Tris/HCl pH 7.8 or
    b. 1.5% DM Tris/HCl pH 7.8.

App B.5 Formulas

Formula 1.1: Chlorophyll content Calculation (using Arnon formulas)

(10ul Solution in 1mL 80% Acetone)

Chl(mg/mL) = [8.02 x A663) + (20.2 x A 645)] / 10

Formula 2: Chlorophyll Content Adjustment

X = [(Current Conc.)(Current Vol) – (0.8)(Current Vol)] / 0.8

Where X = Desired vol of the Buffer currently being used to adjust concentration of chlorophyll.

Formula 3: Triton Conc. Adjustment

X = [(Desired Percentage)(Current Vol)] / (10.5- Desired Percentage)

Where X= Desired Vol of Triton X 100 (10.5%) Note: Stock concentration may vary from 10.5% w/v please use appropriate amount in formula.

(1M)(X) = (0.025M)(X + Current Vol)

This simplifies to:

Formula 4.1

X $MgCl_2$ = (2.56 x 10-2) (Current vol)

KCl:

(2M)(X) = (0.15M)(X + Current Vol)

This simplifies to:

Formula 4.2

X KCl = (8.11 x 10-2) (Current Vol)

App B.6 Calculations

Step 2:

Formula 1.1: Chlorophyll Conc. Calculation

Chl (mg/mL) = [(8.02 x A663) + (20.2 x A645)]/10

A663	A645

Chl mg/ml = _____

X=[(Current Conc.)(Current Vol) – (0.8)(Current Vol)] / 0.8

Current Volume:_____ml

Volume Buffer C added: _____ml

Step 3:

X= [(Desired Percentage)(Current Volume)] / (10.5 – Desired Percentage)

Current Volume: _____ml

Volume Triton X-100 added: _____ml

Step 10:

X $MgCl_2$ = (2.56 x 10-2) (Current Volume)

Current Volume: _____ml

Volume $MgCl_2$ added:_____ml

X KCl = (8.11 x 10-2) (Current Vol)

Current Volume: _____ml

Volume MgCl2 added: _____ml

Analysis of Protein

Final Volume: _____ml

Note: Take 2-4 reading and use average to calculate final volumes

A645	A646.6	A663	A663.3	A750

Using Porra et al. 1989

Chl (mg/ml) = [(7.34 x A663.6) + (17.76 x A646.6)] / 10

Total Chl Concentration: _____mg/ml

Chl a = [(12.25) A663.3 – (2.55) A646.6] / 10 =

_____mg/ml

Chl b = [(20.31) A646.6 – (4.91) A663.3] / 10 =

_____mg/ml

(Chl a)/ (Chl b) = _____
Protein (mg/ml) = ((Chl Concentration (mg/ml)) * 120,000) / (899.5 * 42) =
_____mg/ml

APPENDIX C:

PSII ISOLATION PROCEDURE

PS II Purification

Use HEPES buffer instead of TRIS for PS II.

10X HEPES pH 7.5

Dissolve 119 g HEPES in 800 ml distilled water.

Adjust pH to 7.5 with NaOH and then adjust volume to 1 liter.

1 M $MgCl_2$ Stock

Dissolve 20.33 g $MgCl_2 \bullet 6H_2O$ in distilled water and dilute to 100 ml.

Grinding Buffer for Chloroplast prep from spinach

0.3 M sucrose

50 mM HEPES, pH 7.5

100 mM NaCl

2 mM sodium ascorbate

For 1 liter:

100 ml 10X HEPES pH 7.5

5.84 g NaCl or 50 ml of 2 M NaCl

150 ml of 2 M sucrose or 102.6 g sucrose

Add distilled water to 1 liter

Add 0.396 g sodium ascorbate (or 0.352 g ascorbic acid and check pH) immediately before use.

BBY Resuspension Buffer (add detergent as required for each step)

Final concentrations

5 mM $MgCl_2$

15 mM NaCl

20 mM HEPES pH 7.5

For 1 liter:

5 ml 1 M $MgCl_2$ stock solution

7.5 ml 2 M NaCl stock solution

40 ml 500 mM HEPES pH 7.5 stock solution

Distilled water to 1 liter

For 100 ml:

0.5 ml 1 M $MgCl_2$ stock solution

0.75 ml 2 M NaCl stock solution

4 ml of 500 mM HEPES pH 7.5 stock solution

Distilled water to 1 liter

For 1 liter:

1.0165 g $MgCl_2$•6H2O

0.8766 g NaCl

4.76 g HEPES

Dissolve in 900 ml distilled water, then adjust pH to 7.5 with NaOH.

Add distilled water to final volume of 1 liter.

BBY Storage Buffer

Final concentrations

0.40 M sucrose

5 mM $MgCl_2$

15 mM NaCl

20 mM HEPES pH 7.5

For 1 liter:

200 ml of 2 M sucrose

5 ml 1 M $MgCl_2$ stock solution

7.5 M 2 M NaCl stock solution

40 ml 500 mM HEPES pH 7.5 stock solution

Distilled water to 1 liter

For 100 ml:

20 ml of 2 M sucrose

0.5 ml 1 M $MgCl_2$ stock solution

0.75 ml 2 M NaCl stock solution

4 ml of 500 mM HEPES pH 7.5 stock solution

Distilled water to 100 ml

Isolation Method

Make 100X sodium ascorbate (200 mM) by dissolving 0.0396 g in 1 ml water.

Weigh spinach leaves.

Wash spinach leaves in ice water.

Shake off water.

Add 2 mM sodium ascorbate to grinding buffer (0.0396 g per 100 ml)

Homogenize spinach leaves in 3 ml/g of grinding buffer.

Filter through 4 layers of cheese cloth or Miracloth.

Centrifuge at 300 g for 5 min in JLA 10.5 rotor to pellet cellular debris.

Centrifuge supernatant at 12,000 g for 15 min in JLA 10.5 rotor to pellet chloroplasts.

Collect green top of pellet with brush and resuspend in 0.1 ml/g spinach of resuspension buffer to which 2 mM ascorbate has been added (0.10-0.3 ml/g spinach).

Determine chlorophyll concentration.

Calculate amount of detergent to add for Triton X-100 solubilization at 25 mg Triton/mg chl. Use Calbiochem Triton X100 protein grade 10% (check bottle for exact concentration).

Add Triton and incubate for 30 min on ice with occasional gentle mixing.

Collect PSII membranes by centrifuging at 25,000 g for 30 min in JLA 25.5 rotor.

Resuspend in resuspension buffer containing 2 mM ascorbate at 2 mg/ml chl.

Add 5 mg/mg chl of Triton X-100, mix, and centrifuge immediately at 25,000 g for 30 min in JLA 25.5 rotor.

Resuspend in storage buffer at 0.1 ml/g spinach and store at -80ºC.

Grinding Buffer for Chloroplast prep from spinach

0.3 M sucrose

50 mM HEPES, pH 7.5

100 mM NaCl

2 mM sodium ascorbate

BBY Resuspension Buffer (add detergent as required for each step)

Final concentrations

5 mM $MgCl_2$

15 mM NaCl

20 mM HEPES pH 7.5

BBY Storage Buffer

Final concentrations

0.40 M sucrose

5 mM $MgCl_2$

15 mM NaCl

20 mM HEPES pH 7.5

BBY Original Recipe

Berthold, D. A., Babcock, G. T., Yocum, C. F. (1981) FEBS Lett. 134(2), 231-234. A highly resolved, oxygen-evolving photosystem II preparation from spinach thylakoid membranes.

Spinach thylakoids (2 mg/ml) were suspended in 5 mM MgCl2, 15 mM NaCl, 20 mM HEPES pH 7.5 then incubated with 25 mg/mg chl of Triton X-100 at 4ºC for 30 min, followed by centrifugation at 40,000 X g for 30 min. The pellet from the centrifugation was resuspended in the same buffer (2 mg chl/ml) with 5mg/mg chl of Triton X-100 and recentrifuged immediately at 40,000 X g for 30 min. The pellet was resuspended and stored in 0.4M sucrose, 5 mM MgCl2, 15 mM NaCl,, and 20 mM HEPES pH 7.5 at -35ºC.

Ono & Inoue Modified BBY Recipe

Ono, T. A., Inoue, Y. (1983) FEBS Lett. 164(2), 255-260. Mn-preserving extraction of 33-, 24- and 16-kDa proteins from O2-evolving PS II particles by divalent salt-washing.

Thylakoid membranes were resuspended at 2 mg chl/ml in 300 mM sorbitol, 10 mM NaCl, 5 mM MgCl2, and 40 mM MES pH 6.5 and incubated with 25 mg/mg chl Triton X-100 for 5 min at 4ºC, followed by centrifugation at 35,000 X g for 20

min. The precipitate was resuspended in the same buffer without Triton X-100 and centrifuged at 7000 X g for 15 min. The pelleted PS II particles were resuspended in the same medium and stored at -80ºC.